531

A STUDY OF
SOME THIN TRANSITION METAL OXIDE FILMS.

A THESIS PRESENTED FOR THE DEGREE OF
DOCTOR OF PHILOSOPHY.

BY

BENABDELLAH YAGOUBI.

Physics Department
Brunel University
Uxbridge, Middlesex
England

October, 1989.

ACKNOWLEDGEMENTS.

I wish to express my sincere gratitude and appreciation to my supervisor, Professor C. A. Hogarth for his encouragement and constant guidance throughout this study.

I would like to take the advantage of this opportunity to thank the Algerian government for the financial contribution towards the accomplishment of this work.

I would also like to thank the physics department and E.T.C centre technical staff for their technical assistance.

My gratitude also to my colleagues for their valuable discussions.

ABSTRACT

This thesis analyses the effect of varying the compositions of co-evaporated V_2O_5/TeO_2, WO_3/CeO_2, SiO/TeO_2 and WO_3/TeO_2 amorphous thin films on their electrical and optical properties. Some information about the electronic properties of these oxides may be obtained by comparison of the results. In the oxide systems containing transition metal ions the expression for hopping energy at low temperatures contains a term due to the hopping energy of polarons in addition to that due to the disorder. In the dielectric SiO/TeO_2 thin films the distortion of the molecule is thought to be quite weak and thus the carriers do not form polarons. They would move by hopping at the band edge at low temperatures and by excitation to a mobility edge at high temperatures.

The electrical conductivity of V_2O_5/TeO_2 amorphous thin films is discussed in the light of the Mott(1968) theory. The optical absorption edge was found to obey the direct forbidden transitions equation $\alpha\hbar\omega=B(\hbar\omega-E_{opt})^{3/2}$.

The frequency-squared dependence of the conductivity of WO_3/CeO_2 thin films (high content of CeO_2) in the frequency region where the capacitance is constant is associated with the lead resistance according to Street *et al* (1971). The optical energy gap of the films varies with the composition in same way as in doped crystalline semiconductors. The value of the optical

WO_3/CeO_2 was calculated using the Davis and Mott (1970) formula for non-direct optical transitions.

The capacitance of SiO/TeO_2 thin films is found to be almost independent of frequency as well as of temperature. This is due to a strong ionic bonding which characterises a good insulator. The optical absorption edge of SiO/TeO_2 is found to be sharper than that of WO_3/CeO_2 and very similar to that found in most crystalline solids. The value of the optical energy gap is calculated using the same formula as in WO_3/CeO_2. The systematic change of the optical gap with composition is observed only in a limited range of compositions.

The a.c electrical properties of WO_3/TeO_2 amorphous thin films are described using the Springett(1974) and Elliott(1977) models. The optical absorption edge of WO_3/TeO_2 is found to lead to new arguments about the origin of the Urbach edges.

The a.c electrical conductivity shows a frequency dependence of the form $\sigma_{a.c} \propto \omega^s$ in all samples studied in the present work. The mechanism of conduction at low temperatures with the index s varying from 0.5 to 1 is thought to be due to hopping of electrons between localized states in the gap.
At high fields the d.c current shows a non-linear dependence on the applied electric field. This is thought to be due to either space charge or Schottky effects in the oxides containing

transition metal ions. In SiO/TeO_2 dielectric films, the non-linear dependence of current on the electric field is thought to be due to either the Poole-Frenkel effect or at slightly lower fields it could be due to impurities.

Content

-Acknowledgements

-Abstract.

-Chapter 1	Intrduction.	4
-chapter 2	Electronic properties of amorphous semiconductors.	7
-2.1	Anderson localisation and metal-nonmetal transition.	7
-2.2	Cohen-Fritzsche-Ovshinsky model(C.F.O).	8
-2.3	Davis-Mott model.	9
-2.4	Marshall and Owen model.	10
-2.5	Electrical properties of amorphous semiconductors.	11
-2.5.1	Metal-insulator contact.	11
	A) Neutral contacts.	13
	B) Blocking contacts.	13
	C) Ohmic contacs.	14
-2.5.2	D.C conductivity.	14
	A) Band conduction.	14
	B) Thermally assisted tunneling.	15
	C) Tunnelling conduction near the Fermi level.	16
-2.5.3	Impurity conduction.	16
-2.5.4	Conduction at high field.	17
	A) Space-charge limited current	17

B) Schottky and Poole-Frenkel effects. 19
-2.5.5 A.C conduction. 21
-2.5.6 Ionic conduction. 22

-Chapter 3 Optical properties of amorphous semiconductors. 25

-3.1 Introduction. 25
-3.2 Optical absorption edge. 25
-3.3 Low optical absorption. 27

-Chapter 4 Experimental Work. 29

-4.1 Vacuum evaporation system. 29
-4.2 Sources of evaporation. 30
-4.3 Substrate cleaning. 30
-4.4 Evaporation procedure. 31
-4.5 Thickness measurements. 32
-4.6 Electrical measurements. 34
-4.6.1 D.C measurements. 35
-4.6.2 A.C measurements. 36
-4.7 Optical measurements. 37
-4.8 Electron diffraction study. 38

-Chapter 5 Results and discussion of electrical and optical properties of V_2O_5/TeO_2 thin films.

-5.1 Introduction. 39
-5.2 D.C conduction. 39
-5.3 A.C conduction. 45
-5.4 Optical absorption edge of V_2O_5/TeO_2 thin films. 62
-5.4.1 Introduction. 62
-5.4.2 Results and discussion of V_2O_5/TeO_2 optical absorption edge. 62
-5.3 Electron microscope study of V_2O_5/TeO_2 thin films. 68

-Chapter 6 Results and discussion of WO_3/CeO_2 thin films 71

-6.1 Introduction. 71
-6.2 A.C and D.C electrical conduction in WO_3/CeO_2 thin films. 72
-6.3 Optical absorption edge of WO_3/CeO_2 thin films. 86
-6.4 Electron microscope study of WO_3/CeO_2. 93

-Chapter 7 Results and discussion of SiO/TeO_2 thin films. 95

-7.1 Introduction. 95
-7.2 A.C and D.C electrical conductions of SiO/TeO_2. 95
-7.3 Optical absorption edge of SiO/TeO_2 thin films. 113

-7.3.1 Introduction. 113

-7.3.2 Results and discussion of the absorption edge of SiO/TeO_2 thin films. 113

-7.4 Electron microscope study of SiO/TeO_2. 119

-Chapter 8 Results and discussion of WO_3/TeO_2 thin films. 122

-8.1 A.C conduction mechanism in WO_3/TeO_2 thin films. 122

-8.2 Optical absorption edge of WO_3/TeO_2. 133

-8.2.1 Introduction. 133

-8.2.2 Optical absorption edge of WO_3 thin film. 133

-8.2.3 Effect of inhomogeneities on the optical absorption edge of WO_3/TeO_2 thin films. 135

-8.3 Electron microscope study of WO_3/TeO_2 thin films. 139

-Chapter 9 Summary and conclusion. 142

-References. 148

CHAPTER 1- Introduction

Thin film studies have advanced many new areas of research in solid state physics and chemistry. Thin films of thickness less than 1μm are well known by their applications in microelectronics. They can be used as capacitors, protective coatings, temperature and pressure sensors, thermistors and insulating layers. Thin films are also used in optics as antireflection coatings, highly reflecting mirrors, beam splitters, filters, polarisers and in integrated optics.

Amorphous materials in the form of glasses form a distinctive class [Morey, (1954)] because of their preparation in bulk form by quenching them from the liquid phase, whereas thin amorphous films can be formed by various physical and chemical methods such as thermal evaporation. The characteristics of thin films depend mostly on the preparation technique used and their behaviour may differ from that of the corresponding bulk material. The properties and uses of thin films have been discussed in detail by Anderson(1966), Dupuy and Cachard(1976) and by Coutts and Kazmerski(1978).

In the present work, all films are prepared by vacuum evaporation. Most workers agreed that films prepared by this technique present a high state of disorder which can be observed by the electron microscopy and electron diffraction techniques. The theoretical and the experimental aspects of these techniques have been reviewed by Hirsch *et al* (1965). These techniques show

that amorphous films do not exhibit the sharp reflections associated with crystalline materials, but instead, exhibit a few broad haloes indicating that the atoms are randomly arranged and consequently, in order to describe the properties of these thin films, a theory of fully disordered systems is needed.

The theory of amorphous materials has been developed over the last decades largely through the efforts of Mott (1967-1968), (1972a), Austin (1969) and Cutler (1969) who synthesized Anderson's (1958) work. Anderson (1958) considered an electron moving through a medium in which the potential energy varies randomly from point to point and once this randomness exceeds a certain critical amount, all the states become localized. This is the Anderson (1958) transition. Mott (1967) pointed out that if the disorder is not great enough to create localization throughout the whole band, it will nonetheless lead to localized states in the band tail which is separated from the band of extended states by a sharply defined energy E_c. Thus, the process of electrical conduction changes from extended to localized states, hence band models, to provide the density of states $g(E)$ and the mobility $\mu(E)$ as a function of energy, are needed. These models are described in Chapter 2.

A limited amount of work has been carried out on the electrical and optical properties of V_2O_5/TeO_2 glasses by Flynn and Owen(1981). The A.C electrical and optical properties of this mixture in the form of thin evaporated films had not previously been studied. Al-Ani and Hogarth(1984) have studied the optical

absorption edge of WO_3/TeO_2 glasses with WO_3 content less than 50%. In the present work we study the electrical and optical properties of this mixture with compositions of WO_3 greater than 50%.

The electrical and optical properties of amorphous SiO, V_2O_5, TeO_2, CeO_2 and WO_3 thin films have been studied mainly by Hogarth and Ilyas(1983), Bidadi and Hogarth(1975), Al-Ani and Hogarth(1984) and Razzaq and Hogarth(1988).

CHAPTER 2 - ELECTRONIC PROPERTIES OF AMORPHOUS SEMICONDUCTORS

2-1. ANDERSON LOCALISATION AND METAL-NONMETAL TRANSITION.

Anderson (1958) considered an electron moving through a medium in which the potential energy is random [Fig(2.1)], and once this randomness exceeds a certain amount all the states become localized. This is Anderson's transition (1958). Therefore, if at zero temperature, a degenerate electron gas is in a non-periodic field and if the states at the Fermi energy are localized in the Anderson sense, then the material is not a metallic conductor and the conductivity tends to zero with temperature [Mott and Twose(1961)]. The material which exhibits this behaviour is known as a Fermi glass.

A simple example of a metal-nonmetal transition due to localization of states is given by the phenomenon of impurity conduction in doped semiconductors discovered by Hung and Gliessman (1950). One of the metallic state characteristics is the non-thermally activated electrical conductivity, that is E_F lies above E_C; if it lies below then it is in a nonmetallic state. This can be done by changing the composition of the material or by varying other parameters such as pressure. hence a metal-nonmetal transition is predicted.

Mott(1970) introduced the concept of minimum metallic conductivity defined as the minimum conductivity just before the

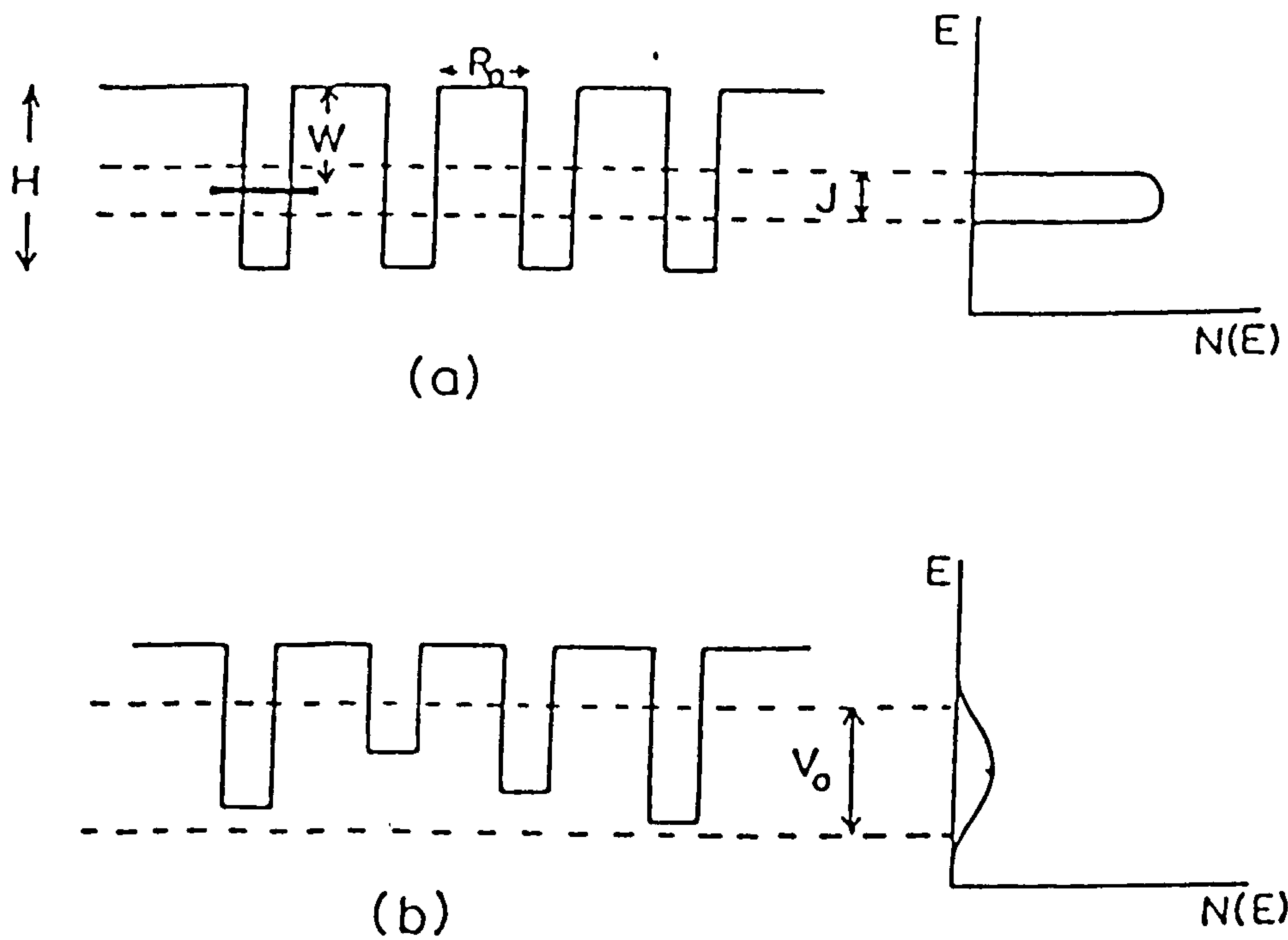

Fig. 2.1. (*a*) Without and (*b*) with the random potential energy V. J is the band width in the absence of V. The density of states $N(E)$ is shown in both cases.

H is a potential well, W is a well occupied by an electron, J is the band width in the absence of V and R_0 is the distance between nearest neighbours [Mott(1970)].

Anderson transition sets in. It should be noted that an Anderson transition, unlike the Mott transition, does not depend on the electron-electron interaction.

2-2. COHEN-FRITZSCHE-OVSHINSKY MODEL(C.F.O)

Cohen *et al* (1969) described a band model which can be applied to covalent amorphous alloys.This model is based on the assumption that in these materials, the co-ordination environment adjusts to satisfy the valence requirements of each atom [Mott (1967)]. This leads to the existence of a valence band of extended states and thus it is obvious that to generate carriers, an energy is needed to break the valence bonds. This energy is roughly equal to the energy gap separating the conduction and the valence bands. The existence of this energy gap is supported by some experimental results on the transmission of infrared light by these alloys [Frerichs(1953) and Kolomiets(1964)] and by the thermal activation energy needed for the electrical conductivity of these materials. However, there is evidence for existence of localized states in the gap given by some photoconductivity [Andriesh and Kolomiets(1963)] and recombination-radiation [Kolomiets *et al* (1968)] measurements. These localized states are supposed to be due to the fluctuations in potential on the atomic scale caused by the compositional disorder in the structure. The localized states which extend from the valence and conduction bands overlap. This means that some electrons may fall from the top of the valence band tail into the

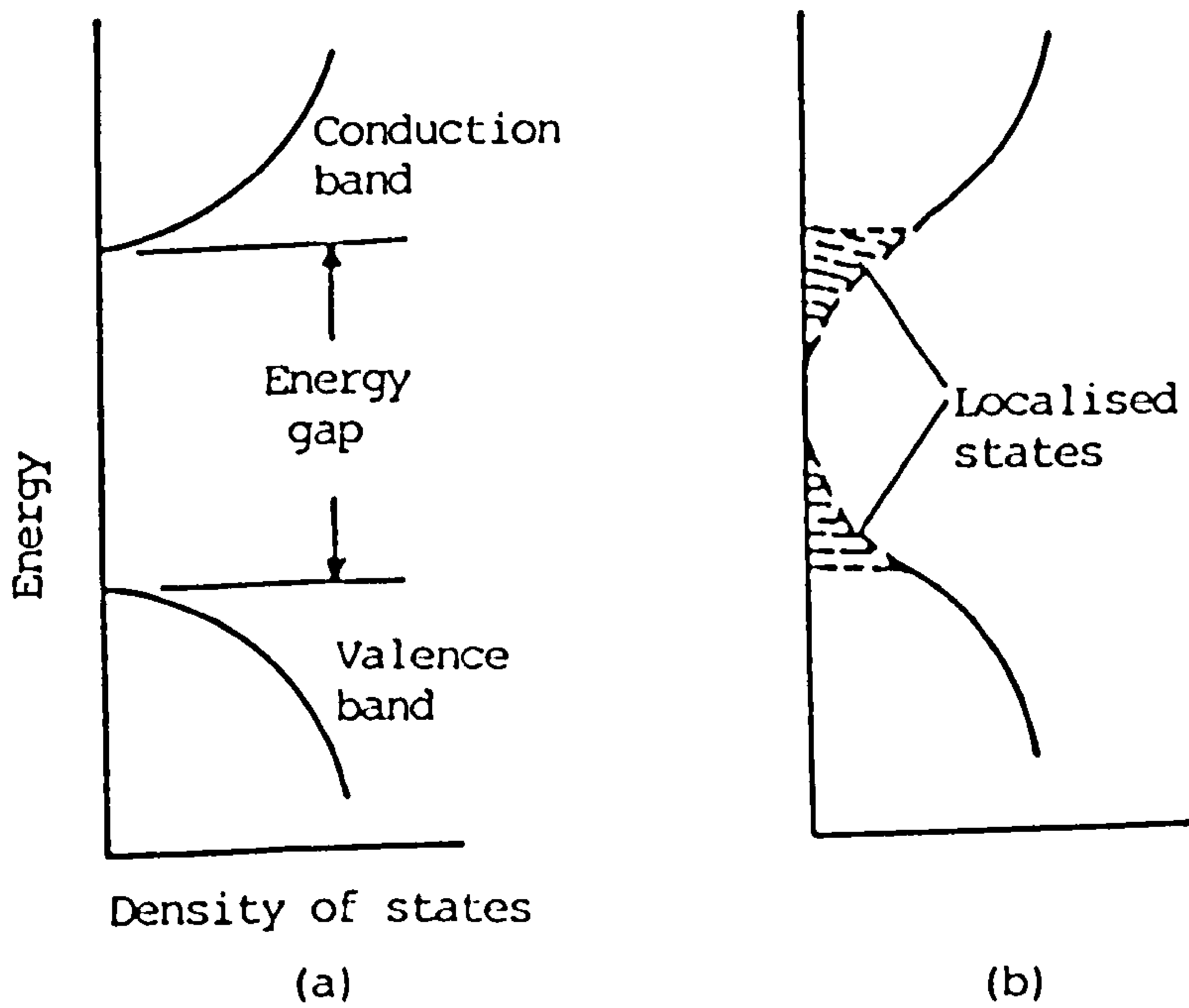

Energy band diagram of
(a) crystalline insulator (b) amorphous insulator.

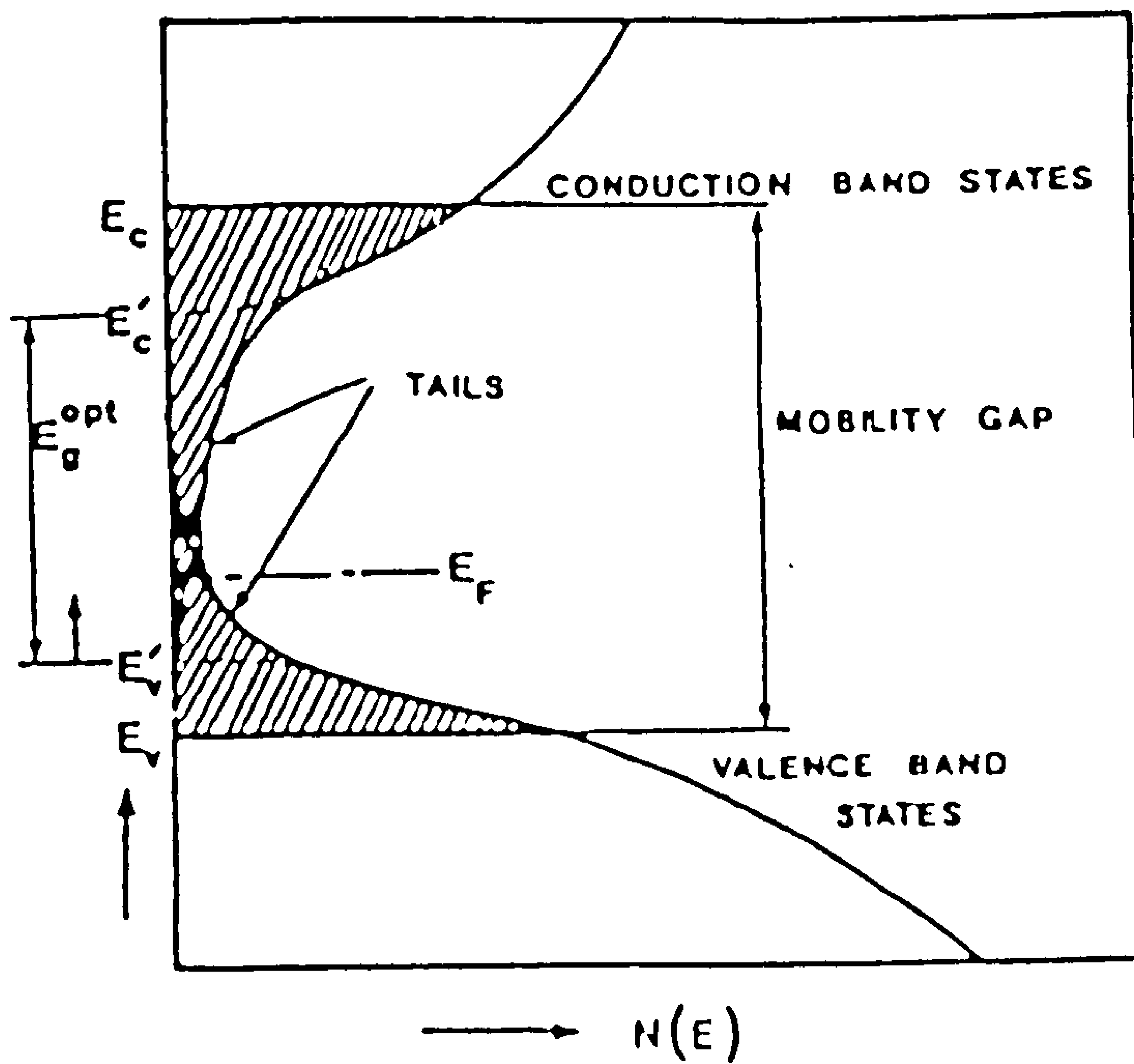

Fig. 2.2. Density of states N(E) as a function of energy E in an amorphous semiconductor according to Cohen et al, 1969, E_V and E_C are mobility edges.

lower conduction band tail. Therefore the Fermi level falls near the centre of the gap where the total density of states is near its minimum.

The empty valence band tail states below E_F and the occupied conduction band tail states above E_F are supposed to be charged and act as efficient trapping centres for electrons and holes respectively .

At the mobility edges E_V and E_C, the mechanism of the conduction changes from band conduction in extended states with finite mobility at T=0K to thermally–activated hopping conduction between localized gap states which vanishes at T=0K. Therefore the difference E_C-E_V=E_g is defined as the mobility gap which contains only localized states. Finally the features of this model are overlapping conduction and valence band tails of localized states and sharp mobility edges as indicated in Fig(2.2).

2-3. DAVIS-MOTT MODEL

The model shown in Fig (2.3) was suggested by Davis and Mott (1970). The definition given by C.F.O to the `mobility gap` is maintained in the Davis -Mott model. Two major modifications are introduced by these authors. The first is that there is a clear distinction between (a) the localized states which extend from the bottom of the conduction band to E_A and from the top of the valence band to E_B and are due to the lack of long-range order, and (b) those which are forming tails in the range E_F to E_A and E_B to E_F

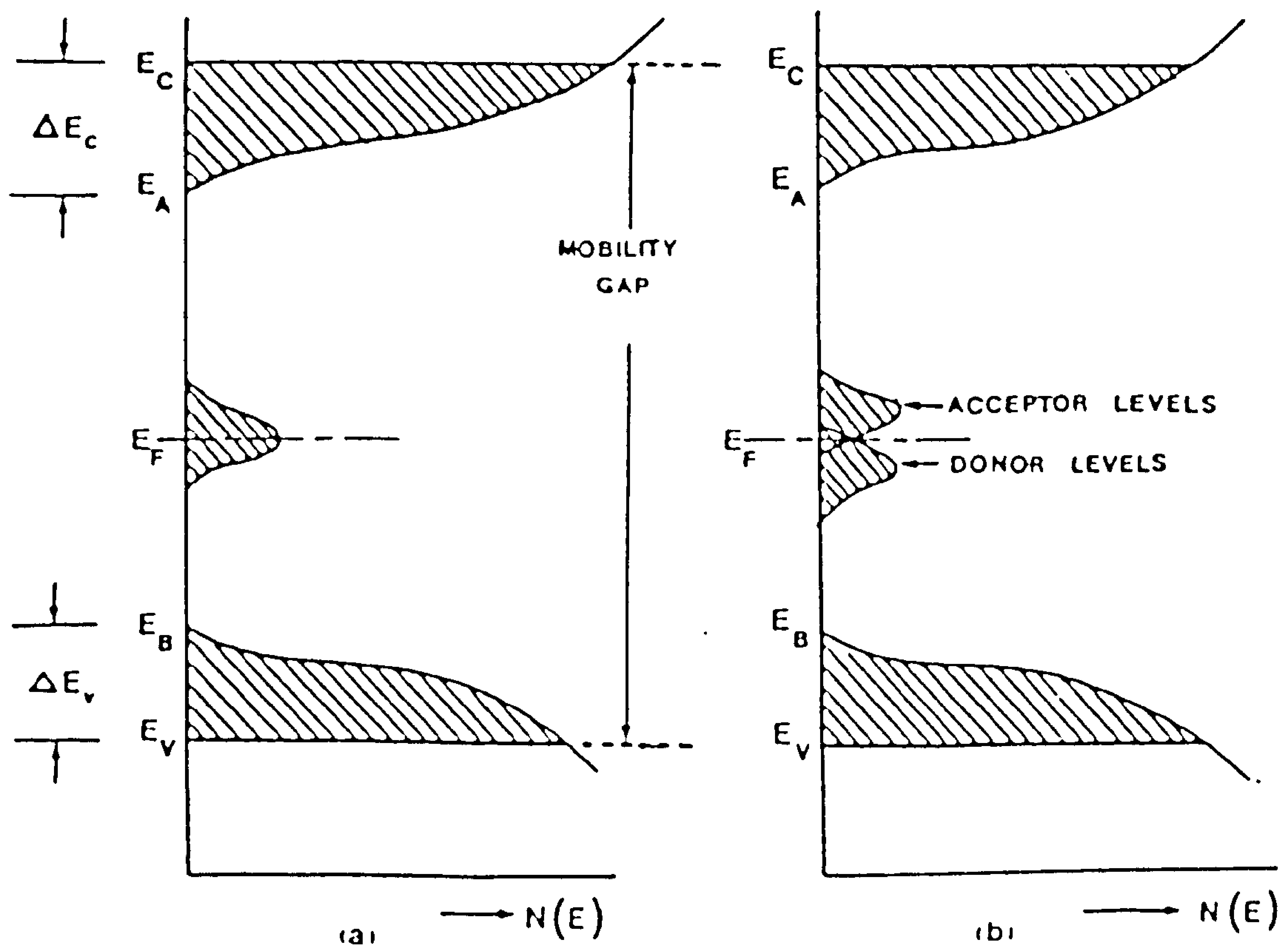

Fig. 2.3. Density of states N(E) as a function of energy in an amorphous semiconductor: (a) according to Davis and Mott (1970) and (b) with acceptor and donor states (modified Davis and Mott model).
Localised states are shown shaded.

with a low density of states and are due to defects. The second modification is the assumption of a band of compensated levels near the gap centre, supposed to be due to dangling bonds. This assumption was first made by Mott (1967) about amorphous germanium. Later many authors [Rockstad(1970), Owen(1967), Owen and Robertson (1970), Fagen and Fritzsche(1970a,b)] confirmed the existence of this band of states at the Fermi level. The density of states at the Fermi level can be estimated also by using the theoretical formula for the a.c conductivity given by Austin and Mott (1969).

The evidence for the existence of localized states due to the lack of long-range order may be given by some drift mobility measurements [Spear(1957, 1960)]. Hartke (1962) found approximately 10^{19} cm^{-3} electron traps just below the conduction band and $10^{21} cm^{-3}$ hole traps just above the valence band. These traps are identified in the Davis-Mott model as the localized states due to the lack of long-range order.

2-4. MARSHALL AND OWEN MODEL

The band model shown in Fig (2.4) was proposed by Marshall and Owen (1971). The experimental results of these authors on arsenic-triselenide show that the conduction at high field is due to the Poole-Frenkel effect, which means that a density of states acting as trapping centres, exists somewhere in the gap. In order to locate this density of states and to estimate its value, Marshall and Owen used the trap-limited drift mobility equation

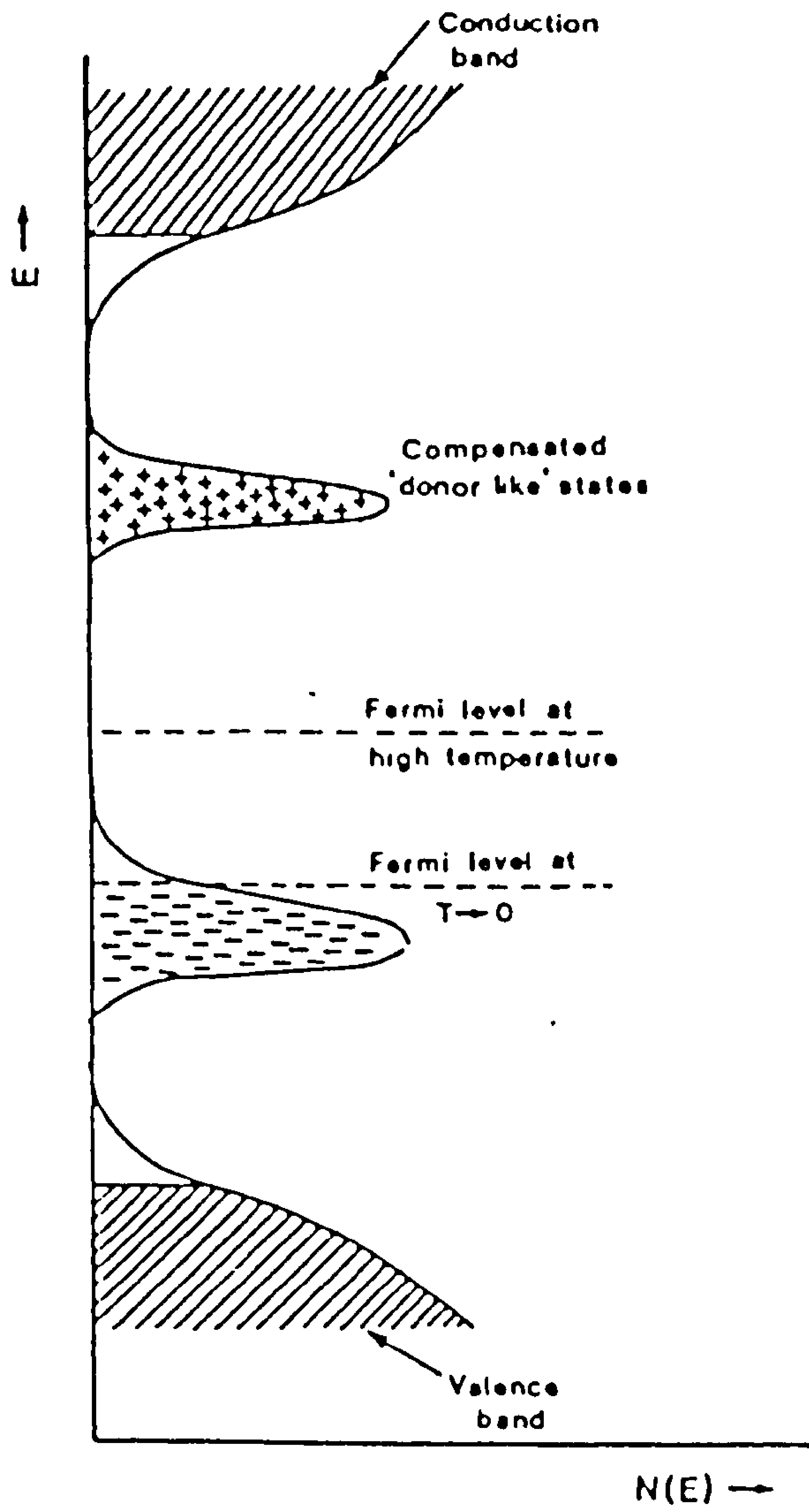

Fig. 2.4. Suggested band structure of vitreous As_2Se_3 according to Marshall and Owen (1971).

given by Lamb (1967) in a one-dimensional analysis and they found a large value of approximately $10^{25}m^{-3}$ which is of the order of the density of states in the valence band and it is located at about 0.43eV from the top of the valence band. These states are considered as acceptor-like. However it is known that chalcogenide glasses appear to be intrinsic semiconductors because the electrical energy gap is approximately equal to the optical energy gap. Therefore these authors had to assume the existence of a compensating set of donor-like states above the Fermi level and about the same density as the acceptors.

At low temperatures if the compensation is complete, the Fermi level will lie halfway between the two impurity bands. If this is not the case, then the Fermi level will move to one of the impurity bands which contains an excess of states and at high temperatures it will remain approximately symmetrically between the two impurity bands because the compensation is completed.

The localized state tails just above the valence and below the conduction bands similar to those of the Davis-Mott model are also present in the Marshall-Owen model

2-5. ELECTRICAL PROPERTIES OF AMORPHOUS SEMICONDUCTORS.

2-5-1. METAL-INSULATOR CONTACT.

When two materials with different Fermi levels are brought into

contact, free carriers will flow from one material into the other until an equilibrium condition is reached, that is, until the total free energy of both materials is a minimum. This means that until the Fermi levels of the two materials are aligned, the flow of the carriers from one material into the other will set up a negative space charge on one side and a positive space charge on the other side of the interface, creating a potential step which is referred to as the potential barrier. The role of the latter is to stop any further flow of current at equilibruim.

There are many contacts and the simplest one is the contact between a metal and a vacuum. The electrons in the metal must surmount a potential barrier before they can leave the metal and enter the vacuum.

The work function of the metal is defined as the difference between the Fermi energy of the electrons in the metal and the lowest energy level of the electrons in the vacuum.

$$\psi_m = \Phi - E_{Fm}.$$

where Φ is the difference in potential energy between the inside and the outside of the metal and E_{Fm} is the Fermi energy of the metal.

The work function of the nonmetallic materials (and non-degenerate extrinsic semiconductors) is defined by

$$\psi_s = X + E_c - E_{Fs}.$$

where X is the electron affinity, E_c is the bottom of the conduction band and E_{Fs} is the Fermi energy of the semiconductor (insulator). There are many types of electrical contact; the most common ones are discussed as in the following [Fig(2.5)].

A) NEUTRAL CONTACTS.

Neutral contact means that there is no space charge and no band bending so that both the conduction and the valence band edges will be flat, which means that the carrier concentration at the contact is equal to that in the bulk of the semiconductor. There are two possibilities to satisfy the condition of neutrality.

a) $\psi_m=\psi_s$; In this case the probability for electrons to flow from the metal to the semiconductor is the same as the probability for the electrons to flow in the reverse direction .

b) $\psi_m\neq\psi_s$; At low temperatures or with an electron-trapping level at distance sufficiently above E_F in wide band gap semiconductors (Simmons, 1971). Under such conditions the trapped space charge will be too small to influence the band edges.

B) BLOCKING CONTACTS.

When $\psi_m > \psi_s$, the electrons will not flow from the metal into the semiconductor, but they will flow in the reverse direcion. These types of contacts are known as a rectifying contacts because electrons can flow easily from the semiconductor to the metal

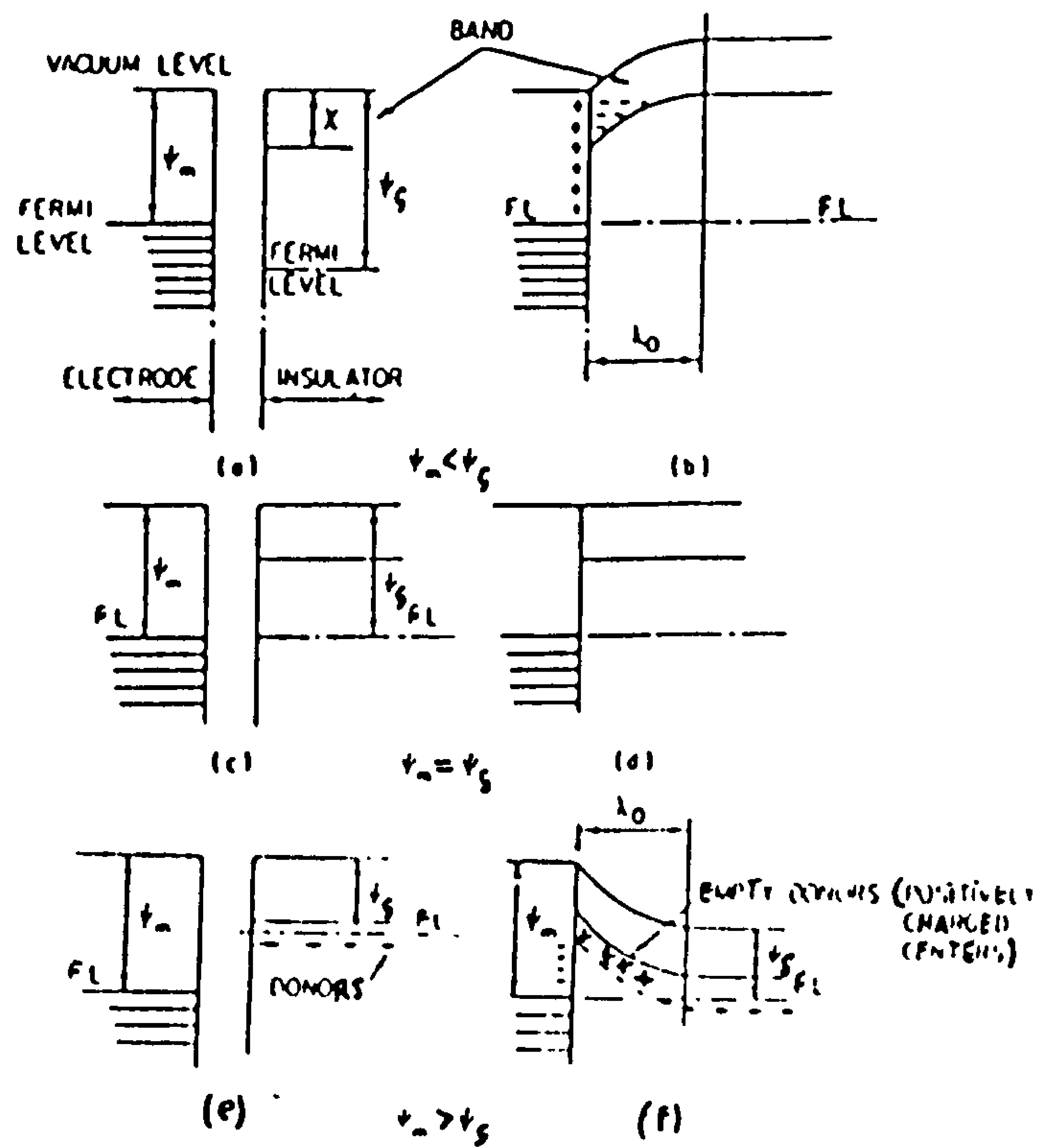

Fig. 2.5. Energy diagrams showing the requirements and type of contact of (a, b) ohmic contact; (c, d) neutral contact. (e, f) blocking contact

while in the reverse direction, the flow of electrons is limited only by the electrons which can surmount the Schottky barrier.

C) OHMIC CONTACTS.

In the case of metal-insulator (metal-intrinsic semiconductor) junctions, the contact is ohmic when $\psi_m < \psi_s$. At low fields the conduction is ohmic as long as the rate of the injecting carriers from the metal is less than or equal to that of the thermally-generated carriers in the semiconductor. The conduction becomes non-linear at high fields when the rate of the carrier injection exceeds that of the carrier generation in the semiconductor.

2-5-2. D.C CONDUCTIVITY .

According to the Davis-Mott model figure(2.3) of the density of states and of mobilities in an amorphous semiconductor there are three forms for the D.C conductivity;

A) BAND CONDUCTION.

The conduction in this band is due to electrons excited above E_c or holes below E_v and it is of the form (for electrons)

$$\sigma = \sigma_o \exp[-(E_C-E_F)/kT]. \quad (2.1)$$

The range $\Delta E_c = E_C - E_F$ is dependent on temperature. Davis and Mott(1970) assumed that ΔE_c varies linearly with temperature as $\Delta E_c = E(o) - \gamma T$.

Inserting this in equation (2.1) we obtain

$$\sigma = \sigma_o \exp(\gamma/k).\exp(-E(o)/kT).$$

The temperature coefficient γ can be estimated by using the thermopower S given by Cutler and Mott (1969)

$$S = k/e\ [\ E(o)/kT - \gamma/k + 1]\ .$$

B) THERMALLY ASSISTED TUNNELLING.

This mechanism of conduction involves the emission or absorption of phonons in addition to the activation energy needed to raise the carrier to the unoccupied state. This type of conduction is due to electrons excited to E_A or holes to E_B and it is given (for electrons) by the expression

$$\sigma = \sigma_1 \exp[-(E_A - E_F + \Delta H_1)/kT].$$

where ΔH_1 is hopping energy due to phonons.

C). TUNNELLING CONDUCTION NEAR THE FERMI LEVEL .

This conduction is of the form

$$\sigma = \sigma_2 \exp[-\Delta H_2/kT] .$$

This equation shows that a phonon with energy ΔH_2 has to be absorbed to raise an electron to the appropriate state. However, as the temperature is decreased, the number of phonons to be absorbed decreases and the equation given above cannot be applied. Mott (1969,1972b) derived another equation for this type of conduction

$$\sigma = C_o \exp[-(T_o/T)^{1/4}].$$

2-5-3. IMPURITY CONDUCTION

In their paper, Hung and Gliessman (1950) reported on the anomalous low temperature behaviour of the resistivity and the Hall coefficient of germanium. This behaviour was anomalous in that the resistivity and the Hall coefficient do not increase as the temperature is reduced. Hung (1950) pointed out that in the limit of low temperatures, conduction in the conduction band can be neglected and that all electrons are in the impurity band. This latter is formed by interaction between the impurity states at

high concentration. In this case these states are extended and carriers can move from one impurity state to another one in the impurity band without activation energy. On the other hand if the concentration is not high enough for a transition to the metallic state to have occurred (zero activation energy), but just enough to allow tunnelling to occur, then the process will involve an activation energy and the carriers could move by hopping from one impurity centre to another. However this type of conduction can be possible only in the presence of some other unoccupied states. Therefore the existence of some minority centres, to compensate the majority centres, becomes an essential feature of impurity conduction [Pollak and Geballe(1961), Mott and Twose (1961)].

2-5-4. CONDUCTION AT HIGH FIELD.

A). SPACE-CHARGE LIMITED CURRENT (S.C.L.C)

At low fields, ohmic conduction is dominant because the rate of injection of the free carrier density at the injecting contact does not exceed that of the free carrier generated density inside the semiconductor. This balance is maintained by dielectric relaxation. At high fields this balance ceases to be maintained and as a result accumulation of excess charge takes place at the contact region. This is known as ` space-charge limited current ` (S.C.L.C).

The characteristic current density and voltage of S.C.L.C. in a

perfect trap-free insulator is governed by the Mott and Gurney (1940) relation.

$$J_{fSCL} = (9/8)\ \varepsilon\mu V^2/d^3.$$

where V is the voltage across the sample, d its thickness, ε is the absolute permittivity and μ is the mobility.
The empty traps which are considered as charged can be neutralised by a certain density of charges from the region of the space-charge, which means that the presence of these traps reduces the S.C.L.C. In this case Rose (1955) found the following relation

$$J_{fS.C.L.C} = (9/8)\varepsilon\mu\Theta V^2/d^3.$$

where $\Theta = (N_c/N_t)\ e^{-E_t/kT}$

N_t is the density of shallow traps occupying an energy level E_t in the gap and N_c is the effective density of states in the conduction band .
There are four discrete regions of space charge ;
(a) Ohmic region, (b) a region governed by a modified Mott and Gurney law due to the traps, (c) a trap-filled-limited region and (d) a trap-free Mott and Gurney law region. These regions are shown in Fig (2.7). A more detailed account of the S.C.L.C effect is given by Lampert (1964).

B) SCHOTTKY AND POOLE-FRENKEL EFFECTS.

When a high field is applied across a metal-insulator interface, a relation of the form $\ln(I) \propto \beta V^{1/2}$ may be observed and it is due to either Schottky or Poole-Frenkel effects because both effects have similar mechanisms which is lowering the height of a potential barrier so that carriers can pass over it. However there is a significant difference between these two effects which lies in the origin of this potential barrier.

In the case of the Schottky effect, the resultant potential energy due to the combination of the applied electric field and the image force is given by

$$W(x) = W_o - (e^2/16\pi\varepsilon x) - eFx. \qquad (2)$$

where W_o is the barrier height at the metal-insulator interface, F is the applied field, ε is the absolute permittivity.

The maximum of W(x) is given by

$$\frac{\delta w}{\delta x} = 0$$

This gives the abscissa x_m of the maximum of equation(2)

$$x_m = (e/16\pi\varepsilon F)^{1/2}.$$

Inserting this value in eq.(2) we obtain the maximum $W(x_m)$ of the barrier height.

$$W(x_m) = W_o - (e^3 F/4\pi\varepsilon)^{1/2}.$$

$$= W_o - \Delta W_S.$$

The height of the barrier is reduced by

$$\Delta W_S = \beta_S . F^{1/2}.$$

where $\beta_S = (e^3/4\pi\varepsilon)^{1/2}$ is the Schottky barrier lowering coefficient. The current density of the Schottky emission at temperature T over the potential barrier W is given by the Richardson-Schottky law

$$J = A^* T^2 \exp(-W/kT) \qquad (3)$$

where A^* is the Richardson-Schottky constant and $W = W_o - \Delta W_S$. Inserting this value of W in eq. (3) we obtain

$$J = A^* T^2 \exp(-W_o/kT). \exp(\beta_S F^{1/2}/kT)$$

In the case of the Poole-Frenkel effect the electron is trapped by a coulombic trapping centre probably arising from impurities or defects. Therefore, the distance from the trapping centre to the

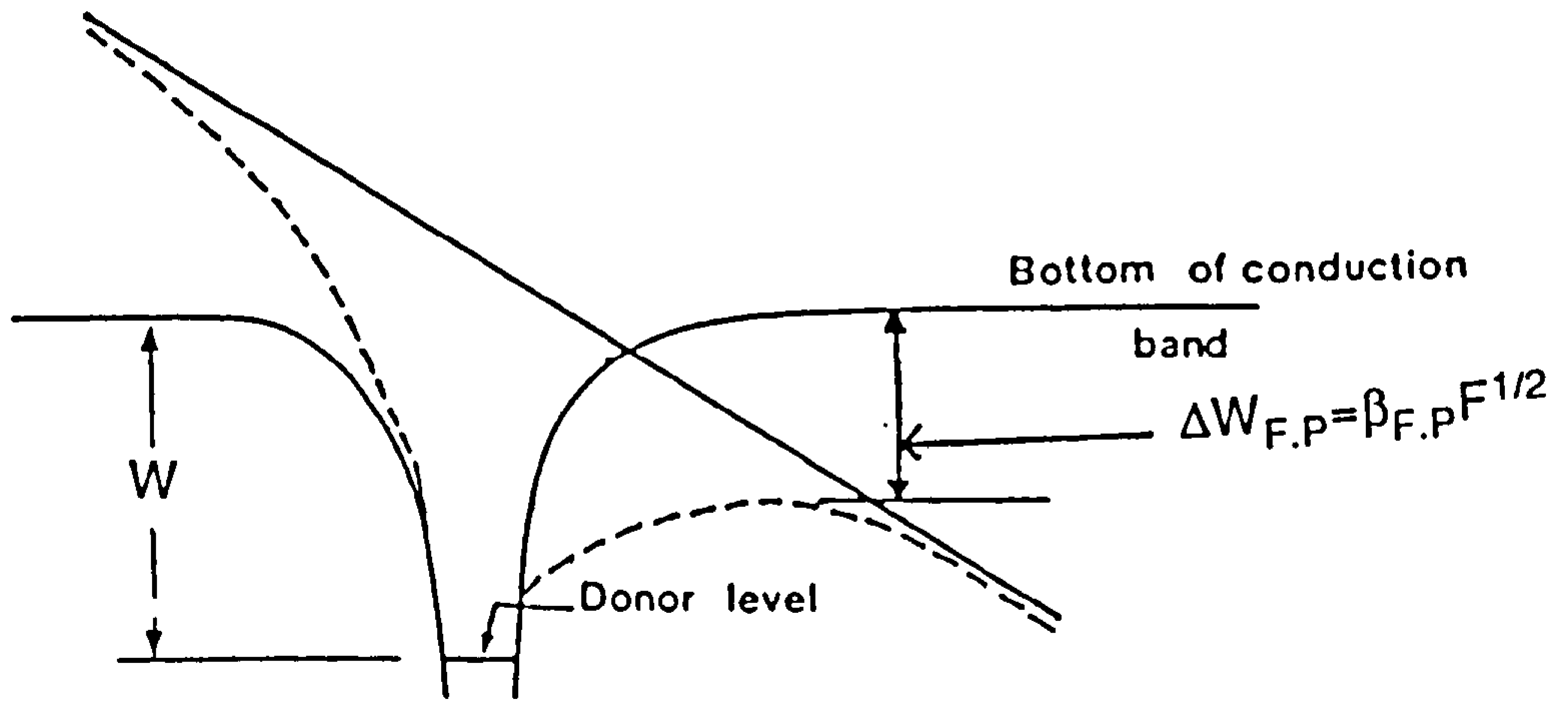

Fig. 2.6. Poole-Frenkel effect at a donor centre.

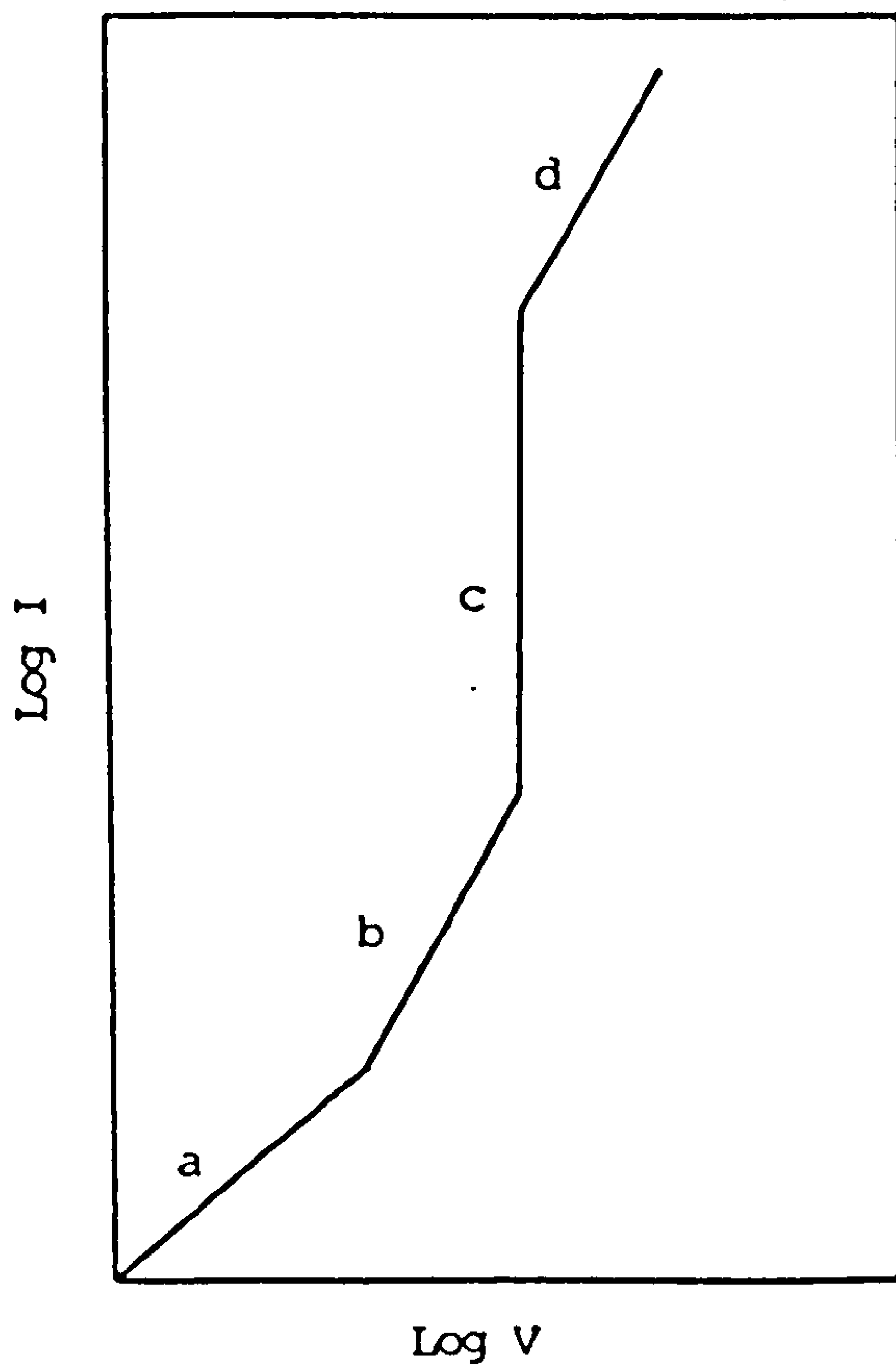

Fig. 2.7. I-V characteristics for SCLC of an insulator containing shallow traps.

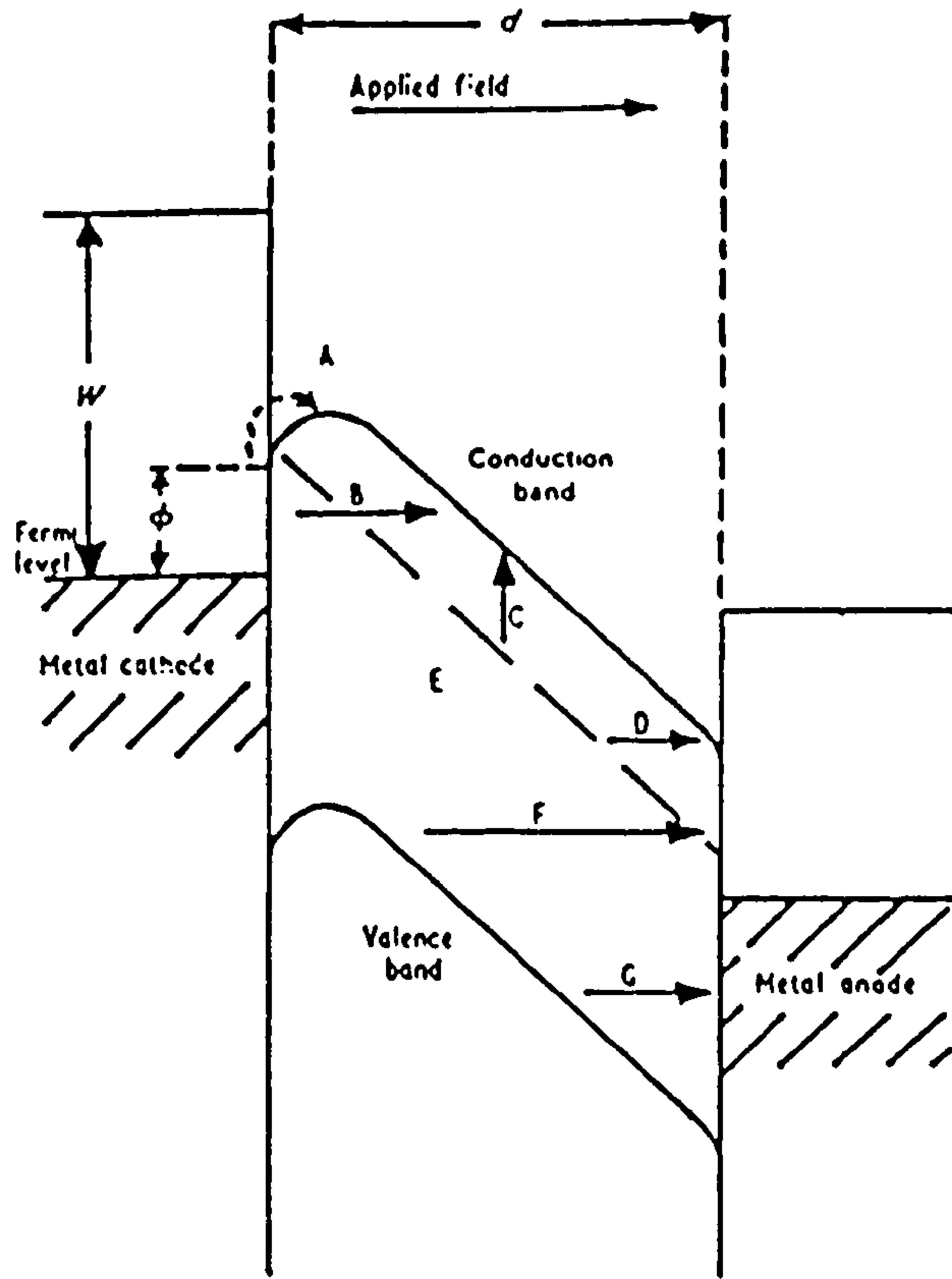

The energy band diagram of an MIM structure showing the possible conduction processes under high field conditions.

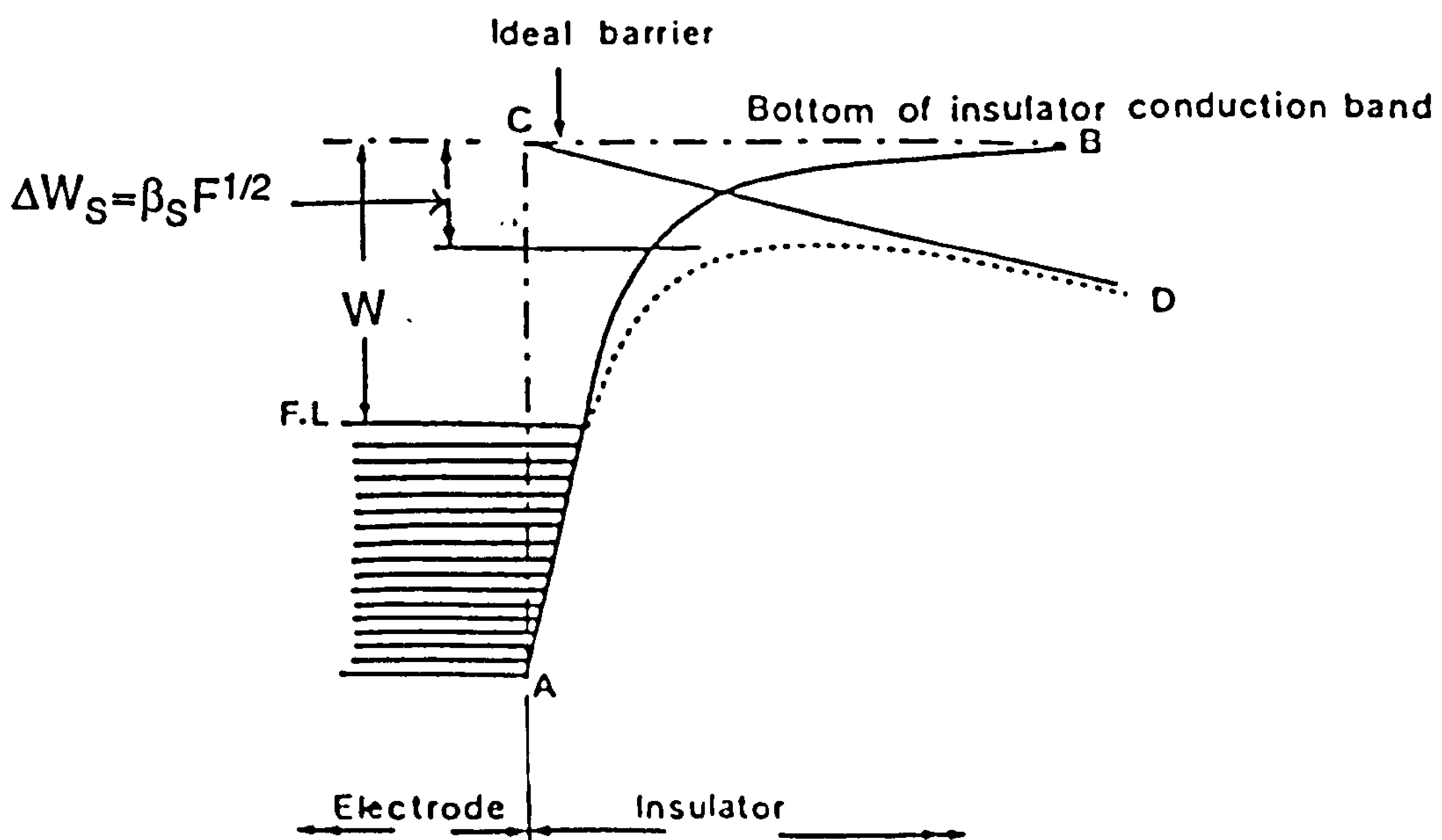

Fig. 2.8. Schottky effect.

electron is taken as x rather than 2x, and consequently the Poole-Frenkel barrier lowering coefficient is twice the Schottky coefficient.

$\beta_{P.F} = 2\beta_S$.

Fig (2.6) and (2.8) show the Poole-Frenkel and the Schottky effects respectively.

2-5-5. A.C CONDUCTION.

The increase of the conductivity with increase of the frequency as $\omega^{0.8}$ is due to a hopping mechanism as suggested by Pollak (1962). Later it was found in many oxide films, [Argall and Jonscher(1968) and Linsley *et al*(1970)], that the a.c conductivity exhibits in a given frequency range a dependence on frequency as

$$\sigma_{a.c}(\omega) \propto \omega^s$$

where s is in the range 0.5 to 1. It is temperature dependent varying between zero at high temperatures and unity at low temperatures around 100K. This region is found experimentally in a wide range of amorphous materials and it is a characteristic of hopping conduction. There is a higher frequency region where

$$\sigma_{a.c}(\omega) \propto \omega^2$$

This temperature independent quadratic term was first reported by Owen (1967). Mott (1969) suggested that the ω^2 region may be due to direct optical transitions between localized gap states. However, the magnitude of this direct absorption term was found by Pollak (1971) to be too small to be good agreement with his experimental results.

It is important to note that internal heterogeneities may cause a spread in the a.c conductivity for the same material leading to a square law dependence.

2-5-6. IONIC CONDUCTION.

Ionic conduction is due to the motion of charged defects. In the absence of a field the probability per unit time that a charge q makes a jump to a neighbouring equilibrium position is given by the expression

$$P(T) = v\exp(-W/kT)$$

where v is the vibration frequency of ions surrounding the defect. According to Mott and Gurney (1964), the barrier height W is reduced by an amount qFa/2 in the direction of the field F and is increased by the same amount in the reverse direction as illustrated in Fig (2.9) .

Under the applied field the activation energy of the defect will be W-qFa/2 in the direction of the field and it will be W+qFa/2 in the reverse direction of the field, so that the net probability per

second of advancing in the direction of the field is given [O'Dwyer(1973)] by

$$P(T) = \nu\exp[-(W-qFa/2)/kT]- \nu\exp[-(W+qFa/2)/kT].$$

$$= 2\nu\exp(-W/kT).\sinh(qFa/2kT) \ .$$

The current density for a defect density n is given by

$$J_{ion}= qnv$$

$$= 2aqn\nu\exp(-W/kT).\sinh(qFa/2kT).$$

The mobility is given by

$$\mu =(2a\nu/F).\exp(-W/kT).\sinh(qFa/2kT). \qquad (4\ )$$

For $qFa/kT<<1$; That is at low fields, then $\sinh(qFa/2kT)\simeq qFa/2kT$. Inserting this value in eq.(4) we obtain

$$\mu = (qa^2\,\nu/kT).\exp(-W/kT).$$

This relation shows that the mobility is independent of the field, hence, the conduction is ohmic.
The expression of $\sinh(qFa/kT)$ is given by

$$\sinh(qFa/kT) \ =(1/2)[\exp(qFa/2kT)-\exp(-qFa/kT)].$$

So at high fields ($F>10^5 V\ cm^{-1}$), that is when $qFa/kT >> 1$, the term $\exp(-qFa/2kT)$ will be negligible which means that the defects have only a negligible chance of jumping in the opposite direction to the field and the above expression for the $\sinh(qFa/kT)$ becomes

$$\sinh(qFa/kT) \simeq (1/2)\exp(-qFa/2kT) \quad .$$

Substituting this value in the current density equation given above we obtain

$$J_{ion} = qan\nu\exp[-(W-qFa/2)/kT] \quad .$$

Ionic conduction is usually characterised by a very low mobility of carriers less than $10^{-12} m^2 (Vs)^{-1}$ and high activation energy greater than 0.6 eV because of the height of the potential barrier.

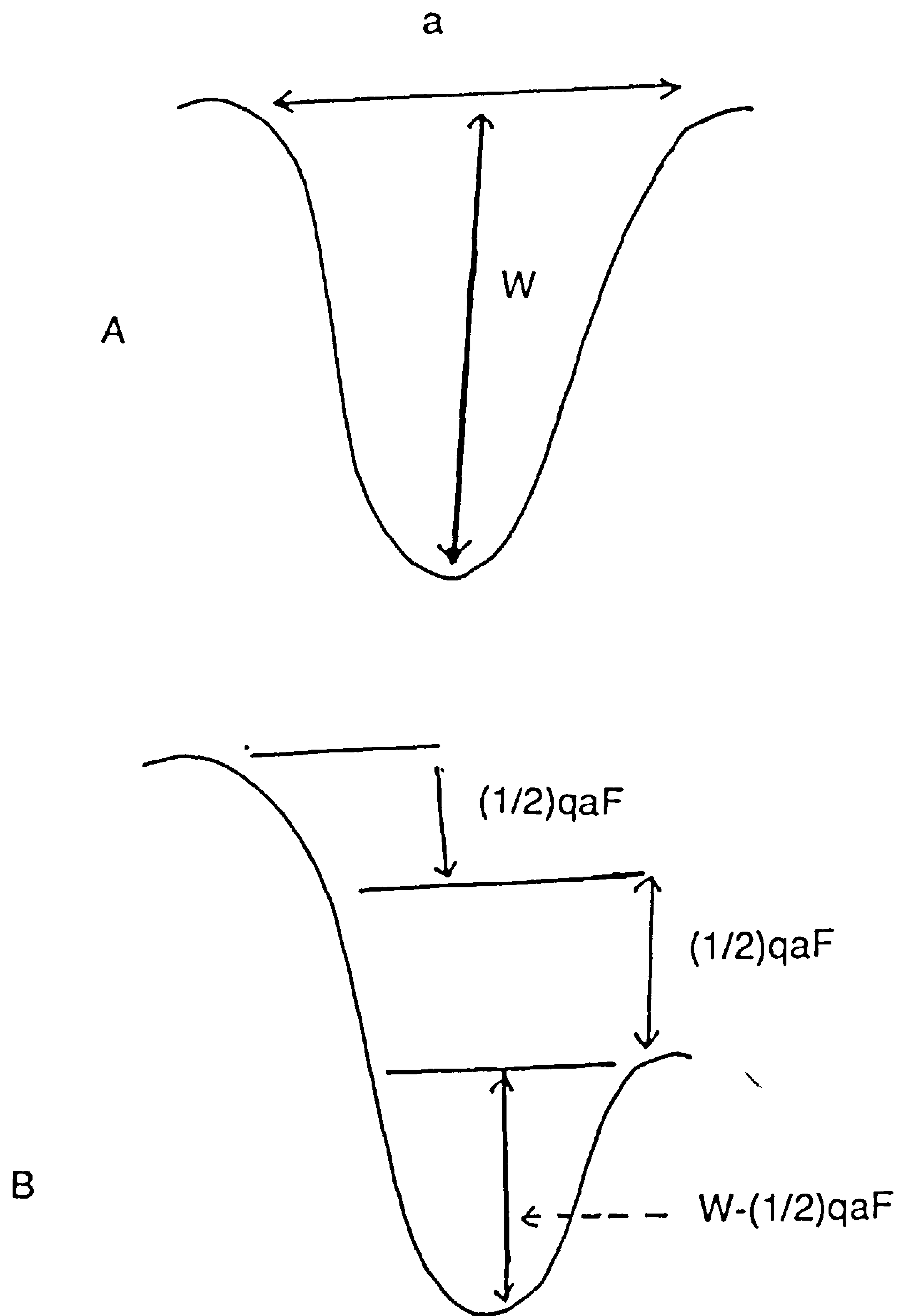

Fig. 2.9. Potential barrier around an ion. A) without application of field and B) with application of external field F.

CHAPTER 3. OPTICAL PROPERTIES OF AMORPHOUS SEMICONDUCTORS.

3-1. INTRODUCTION.

The sharp structure in the fundamental optical spectra of crystals is believed to be due to the existence of long-range order. In the absence of this long-range order, the sharp structure disappears. According to Mott (1969), in the amorphous state the co-ordination environment of each atom can always adjust itself to satisfy the valence requirement. Therefore, for instance the impurities do not influence the transport properties. However they contribute to the fluctuations of the internal potential. Thus no distinct absorption centres will be formed by such impurities. However they may increase the optical absorption near the absorption edge.

3-2. OPTICAL ABSORPTION EDGE.

Electronic transitions between the valence and the conduction bands are called direct if the maximum of the valence band and the minimum of the conduction band lie at the same point of k-space. If this is not the case then a phonon must be involved so that the transition can take place. The rule governing these transitions is the conservation of quasi-momentum during the transitions. In many amorphous semiconductors the absorption edge has the shape shown in Fig (3.1). The optical absorption

coefficient at the absorption edge of most amorphous semiconductors rises exponentially with the photon energy as shown in Fig (3.1) part (B). The other two regions are the weak absorption tail part (C) and the high absorption region part (A) which is due to interband electronic transitions.

The conductivity related to part (A) was calculated by Davis and Mott (1970) and it is given by

$$\sigma(\omega) = (1/3)\, \sigma_0(\hbar\omega - E_{opt})^3/\hbar\omega(\Delta E)^2 \qquad (3.1)\,.$$

where E_{opt} is equal to E_A-E_B.

This relation is obtained by assuming that fluctuations in the interatomic distance are small and both the initial and the final states are localized. However, this is not always the case. The most probable transitions are between localized and extended states. For this, Davis and Mott derived another formula for the conductivity;

$$\sigma(\omega) = \sigma_0(\hbar\omega - E_{opt})^2/\hbar\omega\, \Delta E. \qquad (3.2)$$

In this case E_{opt} is given by E_A-E_v or E_C-E_B. ΔE is the band width of the localized states just above the valence or below the conduction bands. E_{opt} is the optical gap and it is smaller than the mobility gap which is given by E_C-E_v. In many amorphous semiconductors, it appears that the quadratic relation fits the optical absorption data.

The optical absorption constant is given by the following relation

$\alpha = 4\pi/nc\sigma(\omega)$ (3.3)

Inserting (3.2) in (3.3) we obtain

$$\alpha\hbar\omega = B_0 (\hbar\omega - E_{opt})^2 . \quad (3.4)$$

Where $B_o=4\pi\sigma_0/nc\Delta E$. The optical gap can be obtained from the above relation (3.4).

It should be noted that the optical gap obtained by the above analysis is distinguished from the electrical gap determined from the temperature dependence of electrical conductivity.

3-3. LOW OPTICAL ABSORPTION.

The exponential tail at low photon energies is observed in many amorphous semiconductors and it could be due to transitions between localized states. If the density of these states varies exponentially with the energy then an exponential tail is expected [Tauc (1969), Lanyon (1963)]. The absorption constant is described by the following formula

$$\alpha(\omega) \propto \exp(\hbar\omega/E_t) \quad (3.5).$$

The energy E_t is almost temperature independent at low temperatures. In many semiconducting glasses, the value of E_t is

between 0.05eV and 0.08eV.

The exponential behaviour of the absorption constant defines the so-called Urbach (1953) edges which occur in many crystalline semiconductors. Trigonal and amorphous selenium both exhibit Urbach edges with similar slopes at room temperature. This is good evidence against the interpretation that the exponential tail is due to the transitions between localized states which are introduced by the disorder [Tauc (1969)].

Many suggestions have been made about the origin of the Urbach edge. Redfield (1965) proposed an electric field-broadening of the absorption edge. Davydov (1968) suggested excitation from vibrational sublevels of the lattice in order to account for the exponential edge and its change of slope with temperature.

Dexter (1967) showed that this exponential edge is produced by the quadratic Stark effect if the field distribution is Gaussian. His theory is based on the shift of the excitonic line by electric fields. However at high fields, greater than 2.10^6V/cm, the exciton Stark shift does not remain quadratic. Thus, Dow and Redfield (1970) proposed another model for the exponential edge based on the exciton broadening by electric fields with a Gaussian distribution.

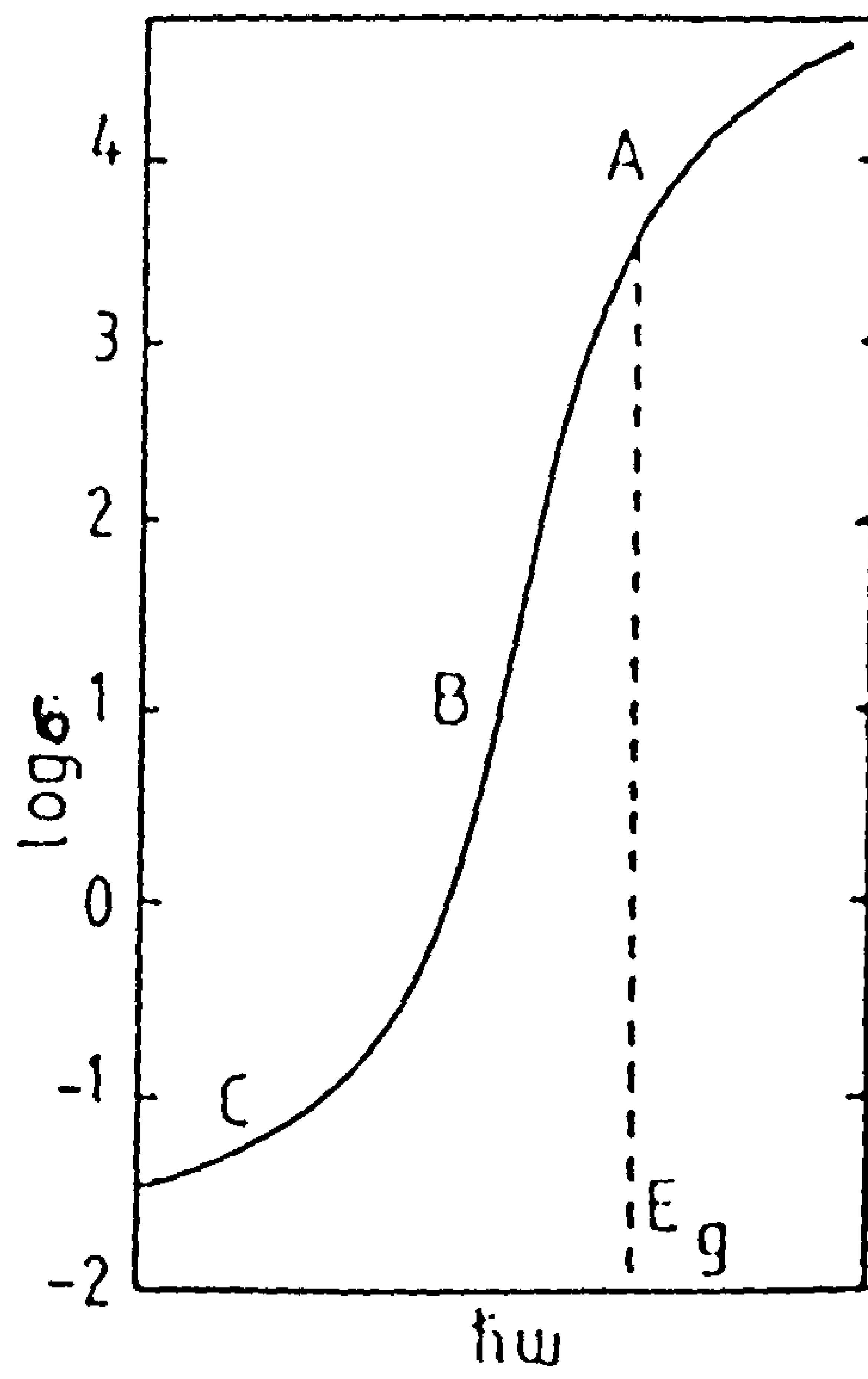

Fig. 3.1. Typical absorption edge of an amorphous material.

CHAPTER 4. EXPERIMENTAL WORK.

4-1. VACUUM EVAPORATION SYSTEM.

The devices for all experiments were prepared by thermal evaporation in vacuum under a pressure of about 10^{-6}torr. The geometry of a vacuum evaporation system, including the relative locations of sources, substrates, shutters, and thickness monitors, can vary over a wide range of possibilities. In the present work, the sources are below the substrates. Metal masks with openings of desired shape can be placed under the substrate by rotating a disc holder. The masks were used for the preparation of sandwich devices. A shutter is a shield which is placed between the source and the substrate to allow the processing of the source and cleaning of the substrate without contaminating the other. A shuttered substrate can be protected during the initial source heating to adjust the deposition rate, so that, when the shutter is opened the film can be grown at a preadjusted deposition rate. This is mainly important for the co-evaporation of two oxides from two different sources. In general the closer these two sources and the greater the distance between the substrate and the source, the more spatially uniform the film will be.

A metal shield is placed between the two sources to avoid contamination and to allow only one kind of material to be deposited on each quartz crystal monitor.

4-2 SOURCES OF EVAPORATION.

The sources that are used to supply thermal energy for the evaporation, should not react with the material to be evaporated and should have a low vapour pressure at the operating temperature. There are many different types of source heaters. Choice of particular heater is controlled by, the material to be evaporated, its quality and its uniformity.

The sources which were used for the evaporation of material in the present investigation were; a molybdenum boat, a tantalum boat, tungsten conical wire basket, and tungsten ten-turn wire helix.

The molybdenum boat was used for the evaporation of V_2O_5, a tantalum boat was used for the evaporation of TeO_2, SiO and WO_3, and conical and helical tungsten were used for the evaporation of aluminium as electrodes.

4-3 SUBSTRATE CLEANING.

Electron microscopy studies show that scratches, dust particles and surface imperfections on the substrate influence the properties of the film. Thus great care must be taken to use the substrates that are as smooth and clean as possible. Not only are the macroscopic features of the substrate important, but for many applications (e.g microelectronics) so are the microscopic

conditions. Therefore, the substrates were carefully cleaned before preparation of the film.
The substrates were first boiled in a solution of 2-3% detergent (Decon 90) and distilled water for about 20min and then rinsed in pure distilled water. The substrates were then boiled in distilled water for about 10min to remove any remaining detergent. The substrates were then placed in the steam of boiling isopropyl alcohol in a tower for about 10min, in order to remove the final traces of grease and detergent. They were left inside the tower to cool down to room temperature. Finally, the substrates were cleaned inside the vacuum chamber by a glow discharge at pressure of about 0.1torr for about 15min to remove any microparticles on the substrates.

4-4 EVAPORATION PROCEDURE.

The first step, before a film deposition procedure is to itemize the requirements of the film. These are determined by the applications and thus establish the deposition requirements. The material to be deposited determines the type of source heater that must be used. Once all deposition parameters have been established, the vacuum system is loaded with the source material, the substrates and the shutter covering the substrates. Once the system has been evacuated and suitable pressure is obtained (about 10^{-6}torr) a glow discharge is established. To outgas the evaporant, heating of the source should be slow. Once this is achieved, the shutter is removed and the thickness

monitor is switched on at the same time. All the films were deposited at room temperature. The procedures in the fabrication of a sandwich structure [figure(4.1)] are as follows.

Firstly, the masking system for the electrode is set under the substrates and the shutter is in place. The source heater is gradually heated by passing the current through it until a steady evaporation rate is achieved. Then the shutter is opened for a period corresponding to the required thickness and composition, and the electrodes are deposited. The shutter is then closed and the power is switched off. The composition of the film can be controlled by controlling the relative evaporation rates of the two oxides.

The evaporation rates, times, net frequency shifts on the crystal monitors, temperature and pressure are recorded. After switching off the source power, the samples are allowed to cool down gradually before air is admitted so as to avoid oxidation.

4-5. THICKNESS MEASUREMENTS.

The substrate for thickness measurement is masked by a thin wire in close contact to its surface as shown in figure(4.3). After evaporation the wire is removed and a thin film of aluminium is deposited on the substrate. The thickness of the oxide film is measured using a Sloan Instrument angstrometer (model M-100) which operates on the principle of multiple beam interferometry. The angstrometer is capable of measuring thickness from 10 to 2000nm with an accuracy of about $\pm$ 5%. Fig(4.2) shows the type

of fringes observed in the interferometer with parallel monochromatic beam at normal incidence of yellow sodium light of average wavelength λ= 589nm. The rings are viewed with a low power microscope.

The thickness t of the specimen is given by the relation

$$t= \lambda d/2D$$

where d is the fringe displacement and D is the fringe-to-fringe spacing, measured using a vernier micrometer eyepiece. The thickness is measured over different regions of the film and the mean value is taken.

The molar percentage of the constituent oxides is calculated as follows.

Suppose we have two oxides X and Y. The molar percentage of X is given by

$$n_x \% = 100.n_x/(n_x + n_y) \qquad (4.1)$$

The number of molecules n_x with mass M_x is equal to this mass divided by the mass m_x of each molecule

$$nx = M_x/m_x.$$

$$= t_x.S.\rho_x/m_x. \qquad (4.2)$$

And

$$n_y = t_y.S.\rho_y/m_y. \qquad (4.3)$$

where t_x, m_x, ρ_x are the thickness, the mass and the density of molecules of the oxide X, and t_y, m_y, ρ_y are the thickness, the mass and the density of molecules of the oxide Y.
The thickness of the film is proportional to its frequency shift;

$$t_x = C_x.\, \Delta f_x. \qquad (4.4)$$

Using (4.2), (4.3) and (4.4), the relation (4.1) becomes

$$n_x\% = 100/(1 + C\ \Delta f_y/\Delta f_x)$$

Where C is a constant equal to

$$C = (m_x.C_y.\rho_y)/(m_y.C_x.\rho_x)$$

And the molar percentage of the oxide Y is

$$n_y\% = 100\% - n_x\%.$$

4-6 ELECTRICAL MEASUREMENTS.

The d.c and a.c electrical measurements are carried out inside the vacuum system at about 10^{-5} torr to avoid any gaseous contamination. The vacuum chamber (bell-jar) is 14 inch high and

12 inch diameter and is evacuated by a water-cooled Edwards Speedivac oil diffusion pump (model 2038) backed by a Speedivac rotary pump (model ISC30).
The pressure inside the system can be controlled by an Edwards needle valve.
The backing and chamber pressure are monitored by a Pirani and a Penning ion gauge respectively. The sample temperature is lowered by pouring liquid nitrogen into a tank attached to the top plate of the chamber by a stainless steel pipe.The bottom of the tank is made of copper and the top and the walls are made of stainless steel to reduce any heat losses by conduction. The heating power is provided by a Variac (output 0- 275V, 8A) auto-transformer. The device temperature is measured by Cu/constantan Comark electronic thermometers.
For good thermal contact, the thermocouple is attached to a substrate by silver paste. The electrical connections to the electrodes are made by using pressure contacts of copper strips and silver paste.

4-6-1 D.C MEASUREMENTS

Fig(4.4) shows the circuit used for studying the d.c I-V characteristic. The bias voltage is provided by a power supply type LB 200.2 (50V, 2A). The current through the sample is measured by an electronic Avometer (A) type EA113. A Farnell digital multimeter (F.D.M) model DNM3 is used to monitor the voltage across the sample. Both the d.c and a.c electrical

measurements were made in the temperature range -120 to 120^0c for most samples.

4-6-2 A.C MEASUREMENTS

The a.c measurements were determined by applying an alternating voltage across the sample inside the vacuum system described above. This voltage is supplied by a Hewlett Packard impedance analyzer working in the range 5Hz to 13MHz, model 4192ALF. It is a fully automatic, high performance test instrument designed to measure a wide range of impedance parameters. Its frequency accuracy is $\pm$ 50 ppm ($23^0c \pm 5^0C$). Its maximum resolution is 1MHz. The output level is variable from 5mV to $1.1V_{rms}$ with 1mV resolution.

The parameters which were measured in the present work are the conductance, the capacitance and the quality factor Q.

The accuracy of these measurements is 0.1%. An a.c signal of $0.5V_{rms}$ is supplied across the sample. The errors in the measurements can be minimized by using a four-terminal high frequency test fixture (model 16047C) which is supplied with the impedance analyzer.

Adjustments can be made to minimise the errors due to parasitic elements in the circuit zero offset. In this experimental work the a.c measurements were made in the frequency range 100Hz to 4MHz.

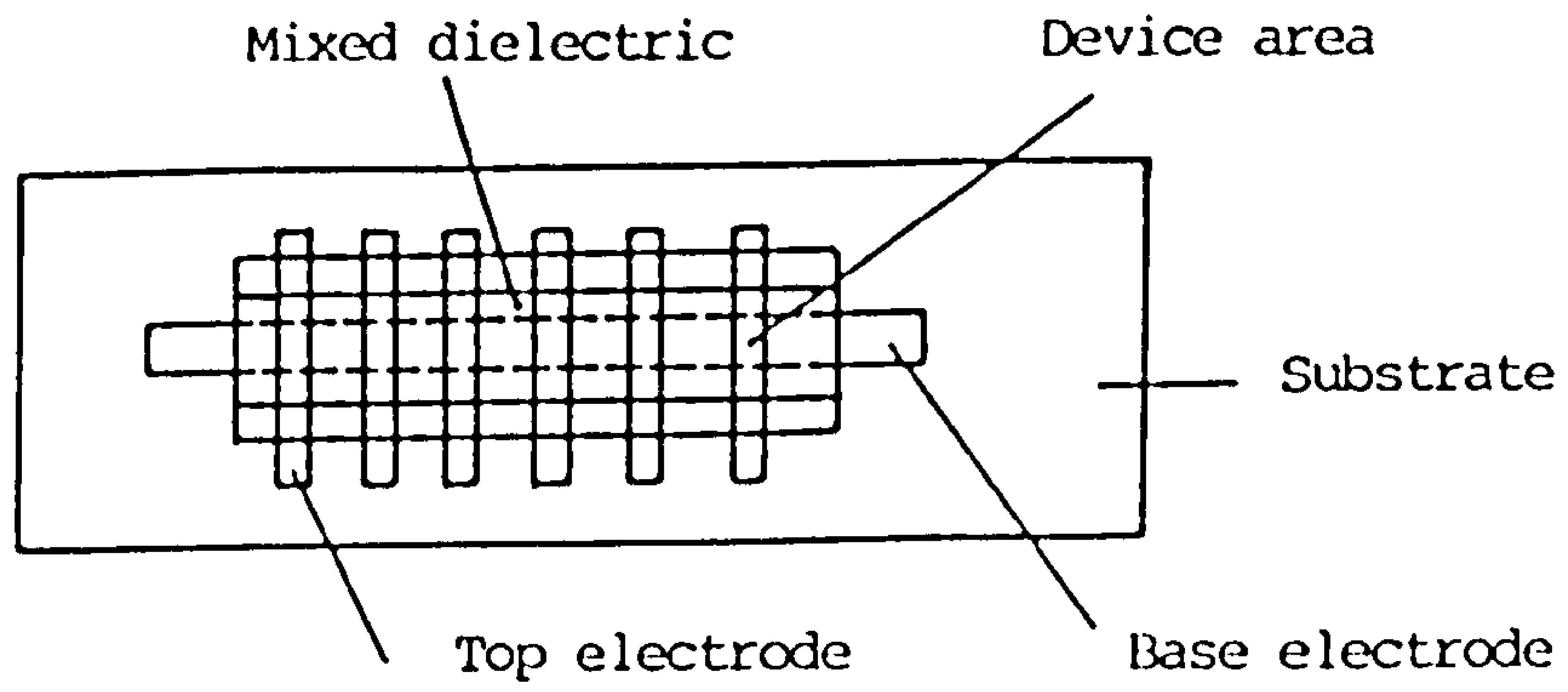

Fig. 4.1 Sandwich structure.

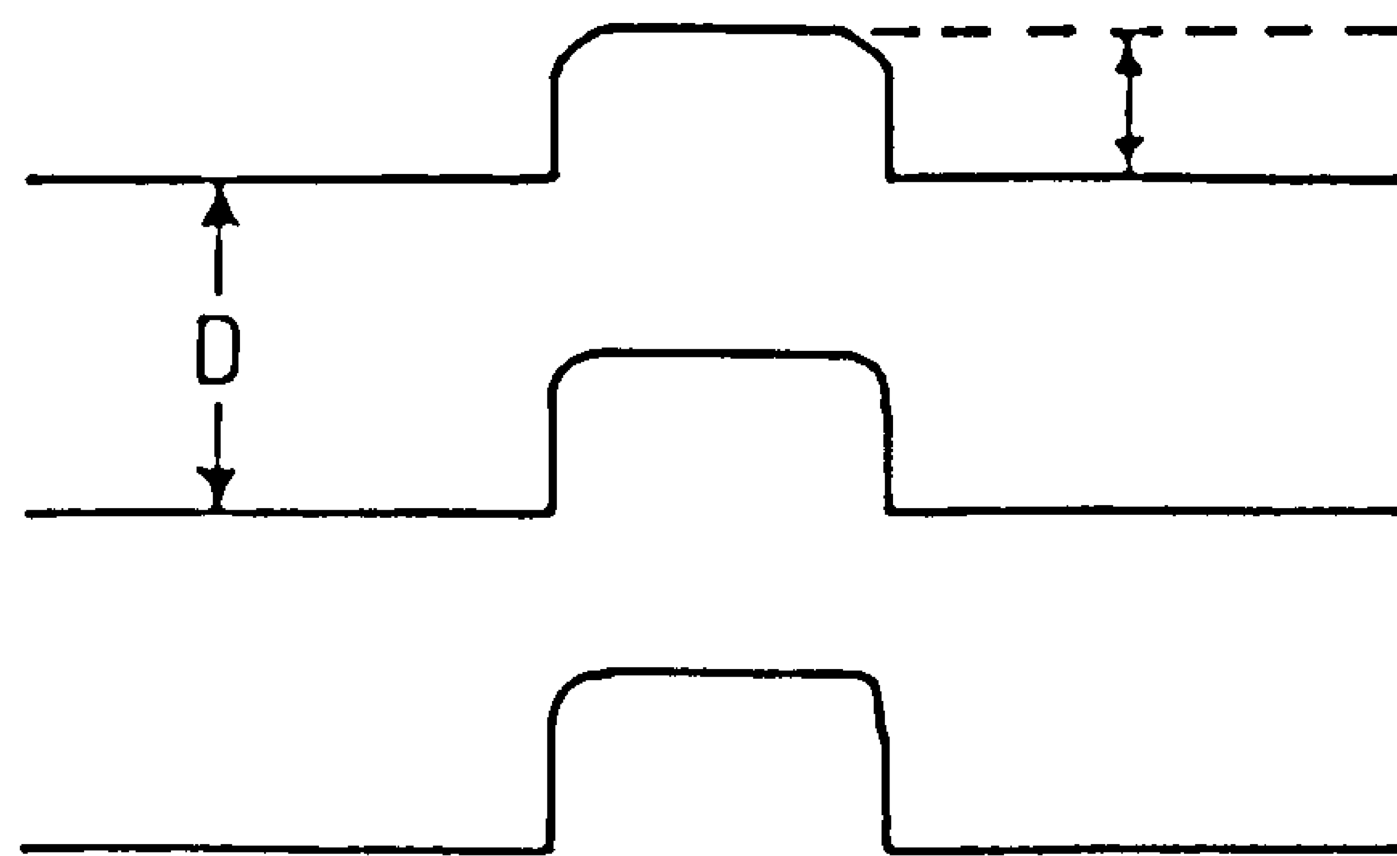

Fig. 4.2. Typical fringe pattern.

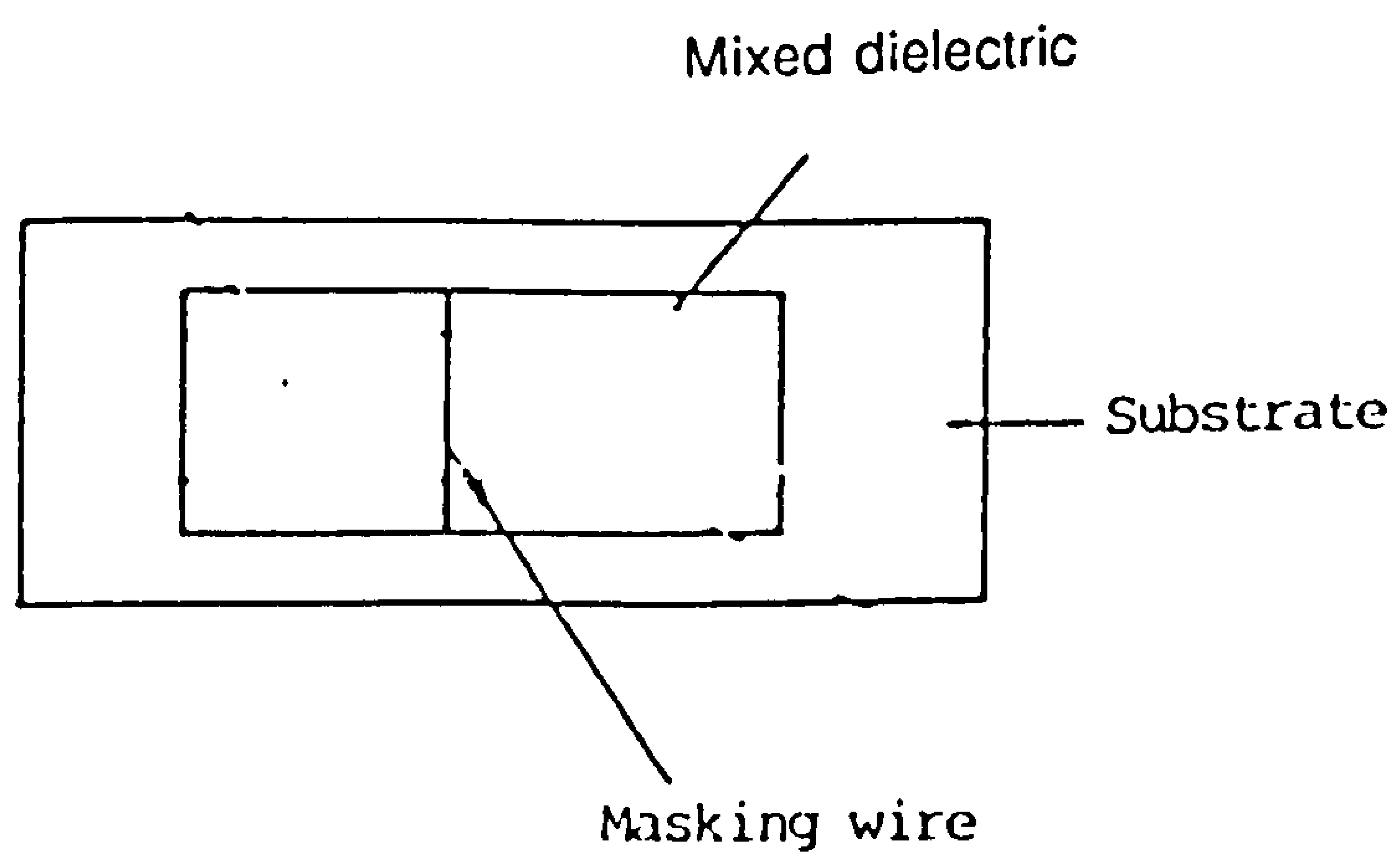

Fig. 4.3 Sample for thickness measurement.

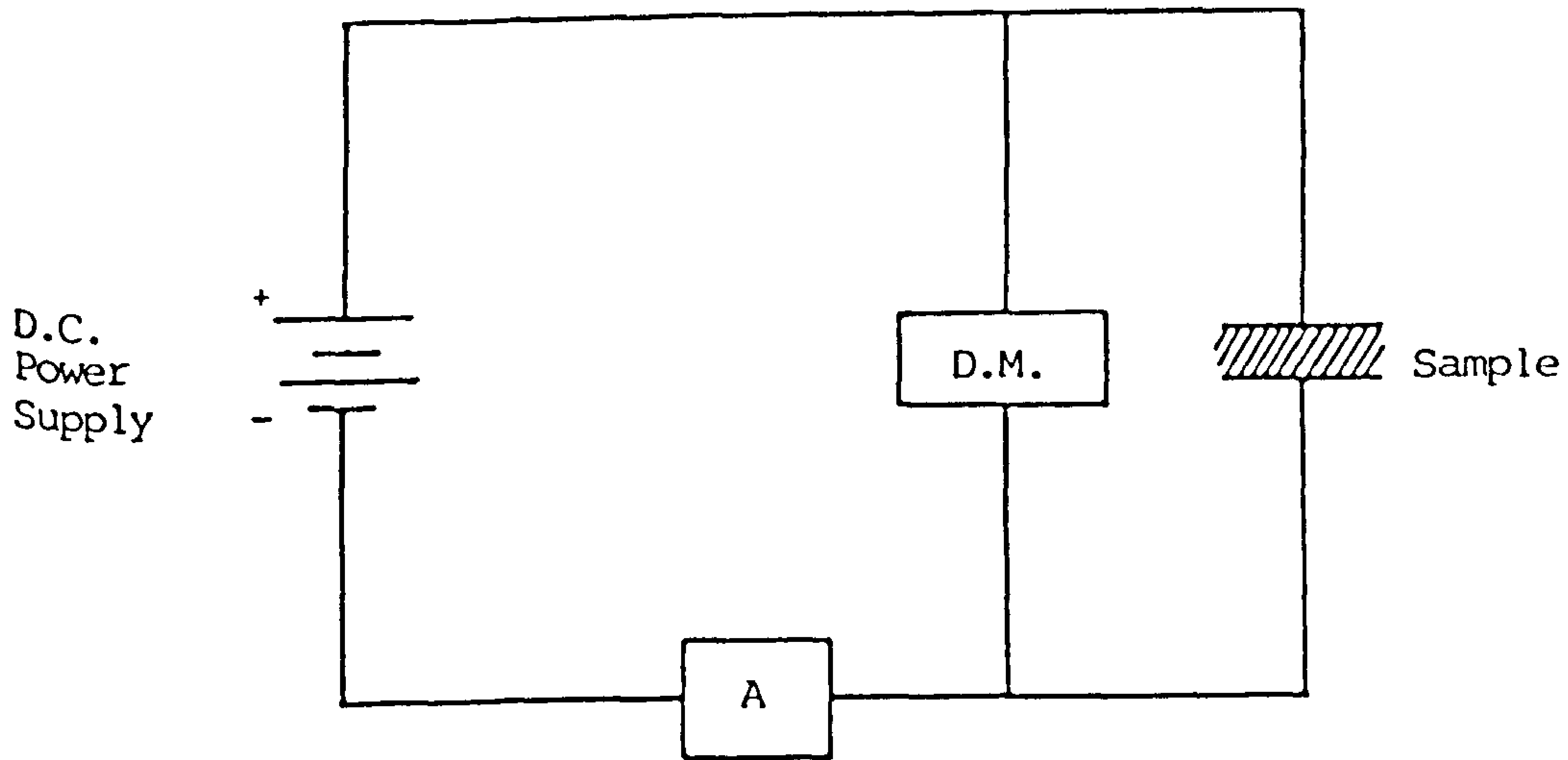

Fig. 4.4. Schematic circuit diagram for studying preformed characteristics.

4-7 OPTICAL MEASUREMENTS.

The optical measurements were made in two spectral regions; the ultra-violet and the infra-red region (2.5 to 50μm). Corning glass substrates were used for the U.V., and monocrystalline silicon wafers were used as substrates for the IR measurements because they are transparent for wavelengths greater than 1.1μm.
The optical measurements in the ultra-violet and visible regions were made using a Perkin-Elmer (Model Lambda3) double beam spectrophotometer and the infra-red measurements were made using a Perkin-Elmer (Model 683) double beam spectrophotometer.
The effects of the substrate on the U.V and I.R characteristics were minimized by placing another cleaned uncoated substrate in the path of the reference beam.
The intensity of the transmitted light is given by the following relation .

$$I=I_0\exp(-\alpha t).$$

where I is the intensity of the transmitted light, I_0 the intensity of the incident light, t the thickness of the sample and α is the optical absorption coefficient.
The absorption coefficient can be calculated from the above relation.

$$\alpha=(1/t).\ln(I_0/I).$$

4-8 ELECTRON DIFFRACTION STUDY.

Electrons are scattered by the electrostatic potential due to the atomic nuclei and their clouds. The maximum of the electrostatic potential distribution given by Fourier analysis corresponds to that of its electron density. The latter is at the atoms, hence the position of the atoms is determined by the electrostatic potential distribution maxima.

In order to obtain the intensity of the scattering the thickness of the specimen must be about $10^{-2}\mu m$ to $10^{-1}\mu m$ for electron diffraction and the experiments must be carried out in high vacuum because electron beams are absorbed in air.

The electron diffraction method has a difficulty in distinguishing between atoms with the same atomic number Z. In this case, one has to use the neutron diffraction method because it does not depend on the atomic number. However, in our work we are mainly interested in whether there is a lack of long-range order or not, that is, whether the potential is random or not. Thus the electron diffraction method is suitable in the present work. For this purpose, films of thicknesses in the range $10^{-2}\mu m$ to $10^{-1}\mu m$ were deposited by vacuum co-evaporation on carbon-coated mica substrates held at room temperature and were investigated in an electron microscope (JEOL model JEM7) by electron diffraction and micrographs.

CHAPTER 5. RESULTS AND DISCUSSION OF V_2O_5/TeO_2 THIN FILMS.

5-1. INTRODUCTION.

Amorphous thin films in in the system Al-V_2O_5/TeO_2-Al are readily prepared with up to 68 mole%V_2O_5. It has been established [Mackenzie (1964)] that electrical conductivity depends upon the vanadium being present in different valency states and it is accepted that the electrical transport mechanism in these materials involves the electron transfer from V^{4+} to V^{5+} centres. Thus, if the spacing between these ions increases we expect the conductivity to decrease and as a result the polaron effect will be neglected. This can be done by varying the TeO_2 content [or by incorporating any glass former (Schmid(1968))]. The films studied in this Chapter with different compositions and thicknesses are listed in table (5.1)

5-2. D.C CONDUCTION.

The variation of current with voltage up to 2V at various temperatures, for different compositions of V_2O_5/TeO_2 thin films is shown in figures (5.1), (5.2), (5.3). It is seen that the current is ohmic at low voltages and increases non-linearly at high voltages. It is also observed that as the TeO_2 content is increased, the current increases more quickly and the I-V curve

tends to have an exponential shape rather than linear.

It is well known that at high electric fields, the conduction may be due to either space-charge-limited current (S.C.L.C), tunnelling, Schottky or Poole-Frenkel(1938) effects. Electrons can tunnel through the insulator from one electrode to the other provided its thickness is less than 5nm. However, in the present work all the samples are thicker, in the range 153-332nm. Therefore tunnelling conduction is rejected. In the case of the S.C.L.C, there must be a region where the current is generally proportional to V^2 [(Mott and Gurney (1940)], which is again not observed in our case because log(I) versus log(V) plots do not show any distinct regions with slopes equal to 2. Thus the possibilty of S.C.L.C can also be ruled out. We are left with the choice of Schottky or Poole-Frenkel effects or may be a combination of the two. It is difficult to decide whether the conduction mechanism is due to Schottky or Poole-Frenkel effects because both effects are described by a similar relation of the form

$$I \propto \exp(\beta E^{1/2}/kT).$$

were I is the current, E is the applied electric field across the sample, k is the Boltzmann constant, T is the absolute temperature and β is the field lowering coefficient.

Figures (5.5), (5.6) and (5.7), show the log(I) versus $V^{1/2}$ plots for various compositions of V_2O_5/TeO_2 amorphous thin films and they are straight lines at higher fields. This would suggest a function

of the form

$$I = I_0 \exp(\beta V^{1/2}). \qquad (5.1).$$

which is consistent with the presence of field-assisted electrode emission of carriers, (Schottky effect) or internal field emission, (Poole-Frenkel effect). On the other hand, it is likely that in the amorphous dielectric, which is in our case obtained in thin films, there can be impurity centres embedded in the dielectric specimen. If the impurity centre can be ionised, then the free electron made available by this process is free for conduction until it is captured by another trapping centre (ionised site)[Hill (1967)]. This process of conduction is governed by the following relation.

$$I \propto \sinh(\theta V^{1/2}). \qquad (5.2)$$

where θ is a constant depending on temperature.

The relation (5.2) gives very similar curves to (5.1) in the range of applied voltage 0.2-2V. Therefore we think that this mechanism of conduction in this voltage range is also possible to occur.

The experimental values of β for different compositions and at different temperatures are given in table (5.1).

The log current versus 1/T plots at different voltages shown in figure (5.4), are clearly linear and there is a clear distinction between the low and the high temperature regions with widely different values of the activation energy.

Table (5.1). Experimental values of the field lowering coefficient $\beta(10^{-4}eV\ V^{-1/2}cm^{1/2})$ for various compositions of V_2O_5/TeO_2 thin films and at different temperatures.

68%V_2O_5		27%V_2O_5		22%V_2O_5	
153nm thick		331nm thick		301nm thick	
T(K)	β	T(K)	β	T(K)	β
288	2.16	294	3.48	295	4.20
300	2.25	306	4.39	305	4.34
318	2.51	320	5.02	315	4.48
328	2.42	333	6.33	333	7.32

Table (5.2). Activation energy W and d.c conductivity σ_{dc} at T=300K and voltage V=1.4V for the same samples as in table(5.1).

%mol.V_2O_5	$\sigma_{dc}(\Omega^{-1}cm^{-1})$	W(eV)
68	$3.90X10^{-7}$	0.43
27	$5.69X10^{-8}$	0.49
22	$1.15X10^{-9}$	0.50.

The linear dependence of log(I) versus 1/T at low temperatures indicates that localized states are present in the gap and conduction is by hopping between them. On the other hand, it is known that polaron conduction is very important in transition metal oxide glasses such as V_2O_5/TeO_2 [Mott(1968)]. However, we think that in this composition (27%V_2O_5-73%TeO_2) the spacing between metal ions (V^{4+}, V^{5+}) is too large to expect the hopping of polarons. Therefore, we think that these localized states are electronic states formed by the atomic disorder and emission or absorption of phonons is involved in this mechanism of conduction at low temperatures [Davis and Mott(1970)].

With increasing V_2O_5 content, it is possible that a polaronic band will be formed if the overlap integral between the polaronic states is sufficiently large. This phenomenon is similar to that of the impurity states in a highly-doped semiconductor.

With the increase of temperature a transition from hopping to free band conduction takes place. This transition occurs at around 280K [figure (5.4)].

As the content of V_2O_5 is increased the conductivity increases. This can be seen by comparing the I-V characteristics of 27%V_2O_5/73%TeO_2 and 68%V_2O_5/32%TeO_2 shown in figures (5.2) and (5.3) respectively. By looking at figure (5.3) we can say that ohmic conduction is dominant up to 2V particularly at low temperatures indicating that the rate of the carrier generated density inside the specimen is still equal to that injected from the electrode. We think that this balance is maintained up to 2V

because of the presence of a high concentration of transition metal ions (V^{4+},V^{5+}) in the sample whose I-V characteristic is shown in figure(5.3) and thus, polaron effects can not be entirely neglected. In fact the mechanism of conduction in samples where the content of V_2O_5 is high, should be discussed in terms of polaronic conduction because in transition metal oxides, such as V_2O_5, the activation energy W_{po} due to the distortion of the molecule when an extra electron is added to it, is an important term in the expression of the total activation energy [Mott(1968)] which can be expressed as

$$W=(1/2)W_D+W_{po}. \qquad (5.3).$$

where W_{po} is the hopping activation energy due to the polarisation and W_D is the activation energy due to the disorder [Miller and Abrahams(1960)].

Figure (5.14) shows the plot of log(I) versus 1/T for the same sample as in figure(5.3). It is seen that the log(I) variation with 1/T is not linear. These results are clearly different from those obtained on $27\%V_2O_5/73\%TeO_2$ amorphous thin film [fig(5.4)]. In the latter, the mechanism of conduction is similar to that of impurity conduction, while the results obtained on the former are in a good agreement with those obtained on vanadium-tellurite glasses by Dhawan *et al* (1982) [fig(5.11)]. The non-linearity of the log(I) versus 1/T plots is expected in polar solids such as amorphous vanadium-tellurite because the polaron activation

energy W_{po} and the activation energy W_D due to the disorder, are both expected to decrease as the temperature is lowered [Mott(1968)] and the conductivity of this type of conduction is usually given by

$$\sigma(T)=(1/T)n(1-n)\ c\ \exp(-W/kT). \qquad (5.4)$$

where c is a constant, W is the total activation energy given by the relation (5.3) and n and (1-n) are the mole fractions of the two types of ion [$n=V^{4+}/Vtotal$ and $1-n=V^{5+}/Vtotal$].

Because of the curvature, the calculation of the activation energy cannot be precise. However, for a fixed temperature there is a general tendency for the activation energy to increase as the amount of vanadium is decreased. Some values of the activation energies for different compositions at fixed temperatures are given in table (5.2).

5-3. A.C CONDUCTION.

The a.c measurements have been taken in the frequency range 100Hz-1MHz and temperature range 208K-333K for V_2O_5/TeO_2 thin films of different compositions and different thicknesses (153nm-331nm). The frequency dependence of a.c conductivity can be aproximated as

$$\sigma_{a.c} \propto \omega^s. \qquad (5.5)$$

where ω is the angular frequency and the index s is temperature dependent and varies between 0.5 at temperatures around 300K and 1 at low temperatures around 100K or less. This result (0.5<s<1), has been found experimentally in a wide range of materials which all have one common characteristic, that conduction is due to hopping between localized states [Pollak and Geballe (1961)], [Mott and Twose (1961)]. Many amorphous or glassy materials have been found to exhibit the same type of behaviour; for example, Linsley *et al* (1970) found a similar behaviour in the V_2O_5/P_2O_5 glass system.

The variation of a.c conductance with frequency at different temperatures for different compositions and thicknesses of V_2O_5/TeO_2 thin films is shown in figures (5.8), (5.9), (5.10).

Figure (5.9) shows a clear distinction between three regions at high temperatures (e.g 333K). The first region is at low frequencies where the conductivity is almost constant up to 1kHz due to the increasing d.c conductivity, the second region is at intermediate frequencies around 8kHz where the conductivity obeys the relation (5.5) with s in the range 0.4 at 333K and 0.58 at 294K, and the third region is at high frequencies where the conductivity variation with frequency tends towards a frequency-squared dependence; at the same time the a.c conductivity in this high frequency region tends to become temperature independent. This is typical of behaviour which has also been observed in chalcogenide glasses [Owen and Robertson (1970)] as well as in vanadium phosphate glasses [Linsley *et al* (1970)]. Figure (5.9) shows that at low temperatures the

conductivity consists of two regions; (a) the low frequency region with the index s ranging from 0.5 to 0.8 indicating that hopping conduction is dominating at low temperatures in a wide range of frequencies from 0.1kHz to around 20kHz, and (b) the high frequency region with s tending towards the value 2. The fact that the a.c conductivity tends towards the d.c conductivity at low frequencies clearly indicates that in this composition (27%V_2O_5-73%TeO_2), the mechanism of conduction is connected with the same localized states for both d.c and a.c electrical conduction.

Figure (5.12) shows the plot of the capacitance versus log(ω) for the same sample as in figure (5.9). It is seen that at high temperatures the capacitance decreases as the frequency is increased. This may be due to a formation of space-charge at the interface of the metal-semiconductor contact, and it becomes constant at high frequencies. At low temperatures the capacitance is almost constant in the whole frequency range from 0.1kHz to 400kHz indicating that no appreciable space charge is created in the structure, hence the conduction is bulk limited in this frequency range and at low temperatures.

Figure (5.13) shows the plot of the capacitance versus log frequency for 68%V_2O_5/32%TeO_2. The large increase of the capacitance as the frequency is decreased is thought to be caused by ionic build up at the electrode. By comparing the capacitance of this sample to that of 27%V_2O_5/73%TeO_2 we can say that this space charge is caused by the high concentration of vanaduim ions.

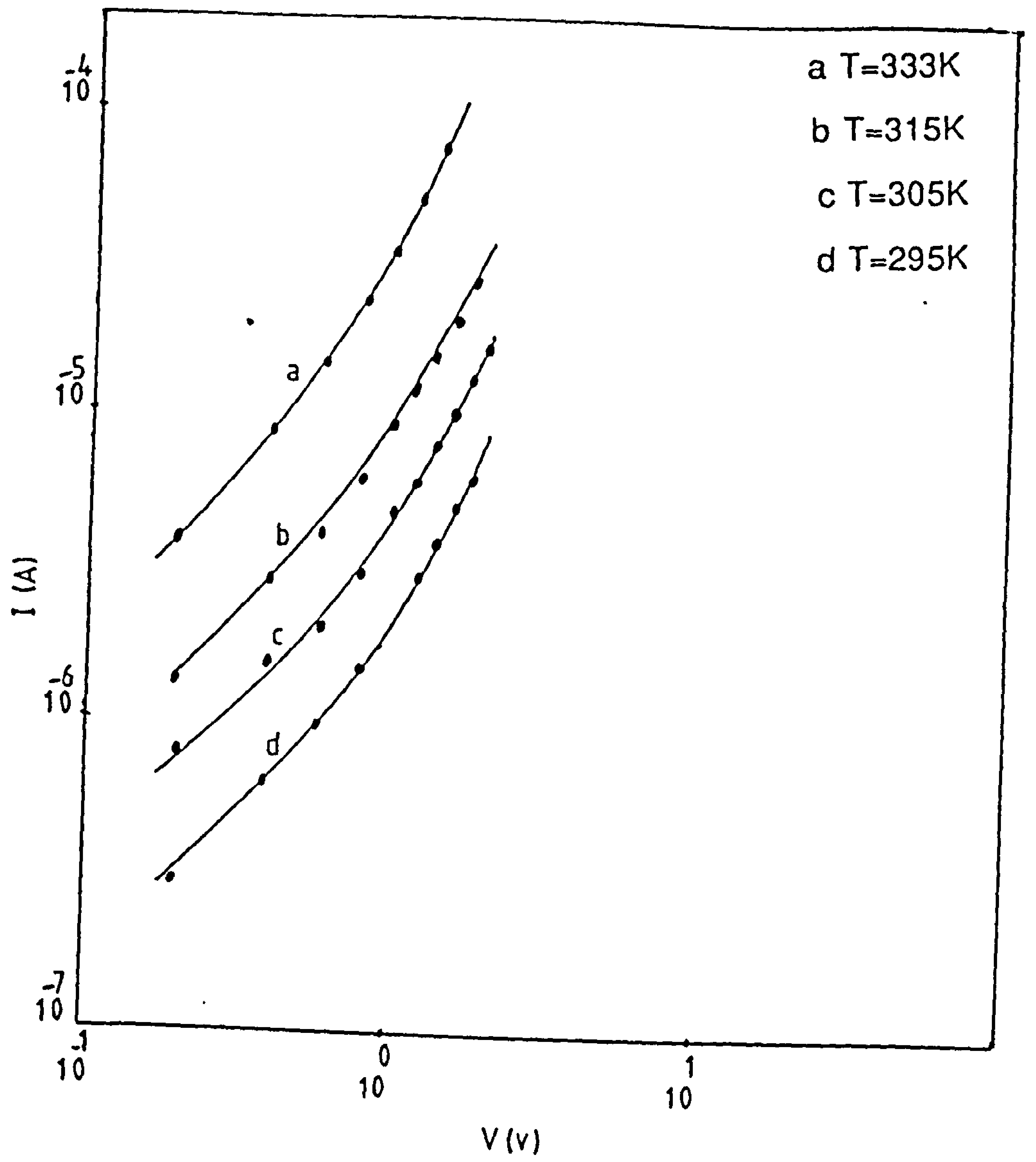

Fig. 5.1. I-V characteristics of $22\%V_2O_5/78\%TeO_2$ thin film.

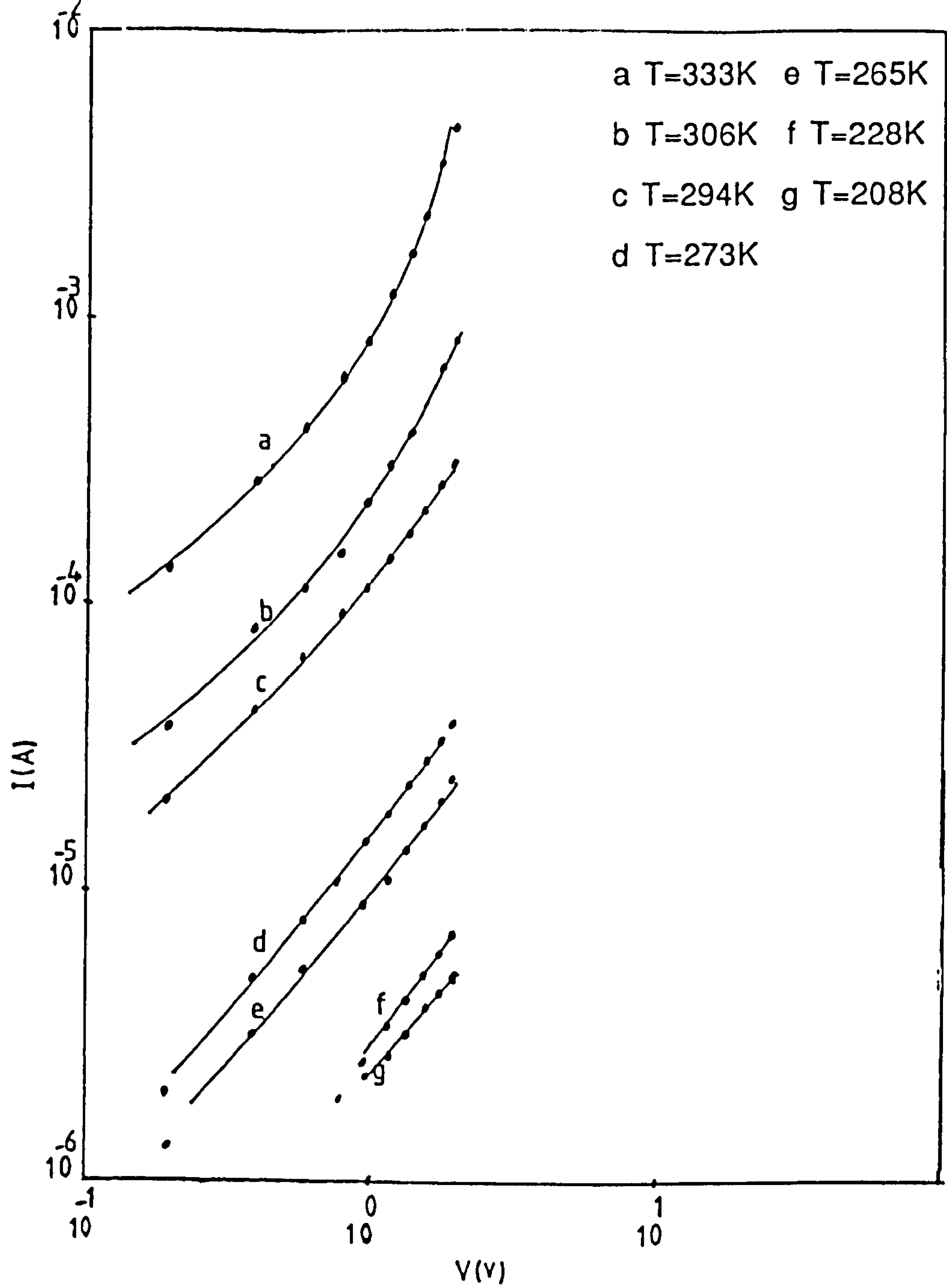

Fig. 5.2. I-V characteristics of $27\%V_2O_5/73\%TeO_2$ thin film.

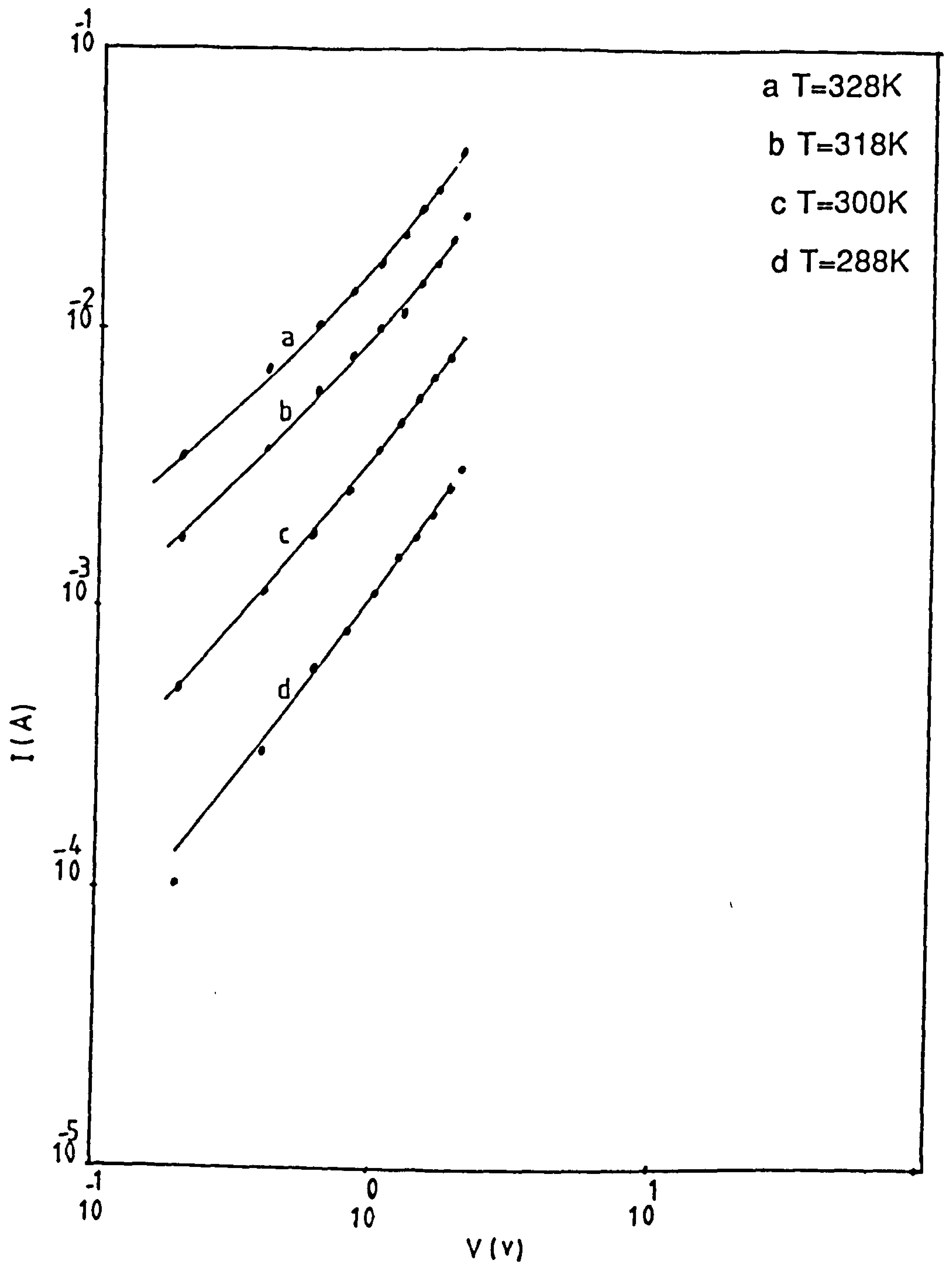

Fig. 5.3. I-V characteristics of $68\%V_2O_5/32\%TeO_2$ thin film.

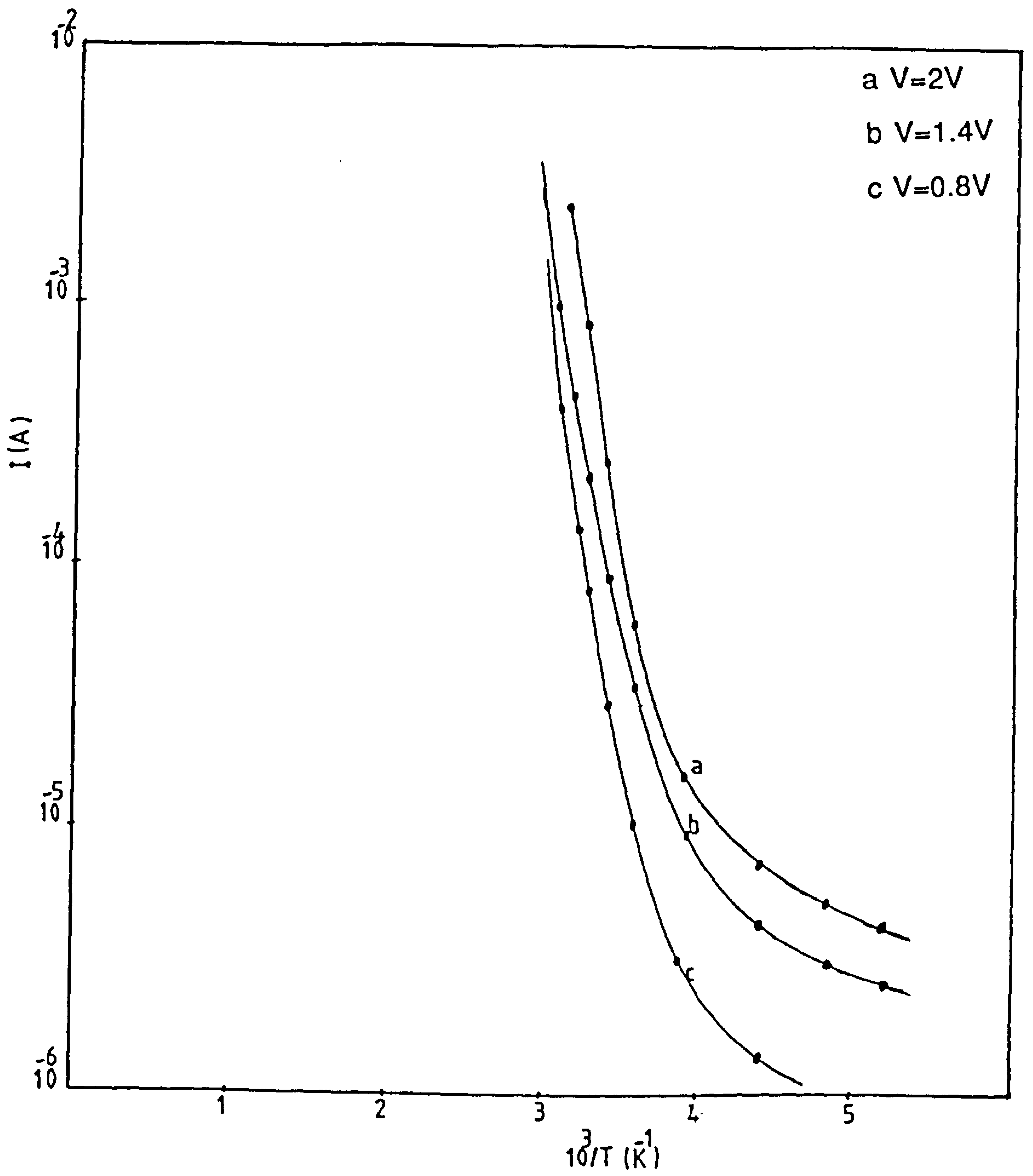

Fig. 5.4. log(I) versus1/T for $27\%V_2O_5/73\%TeO_2$ thin film.

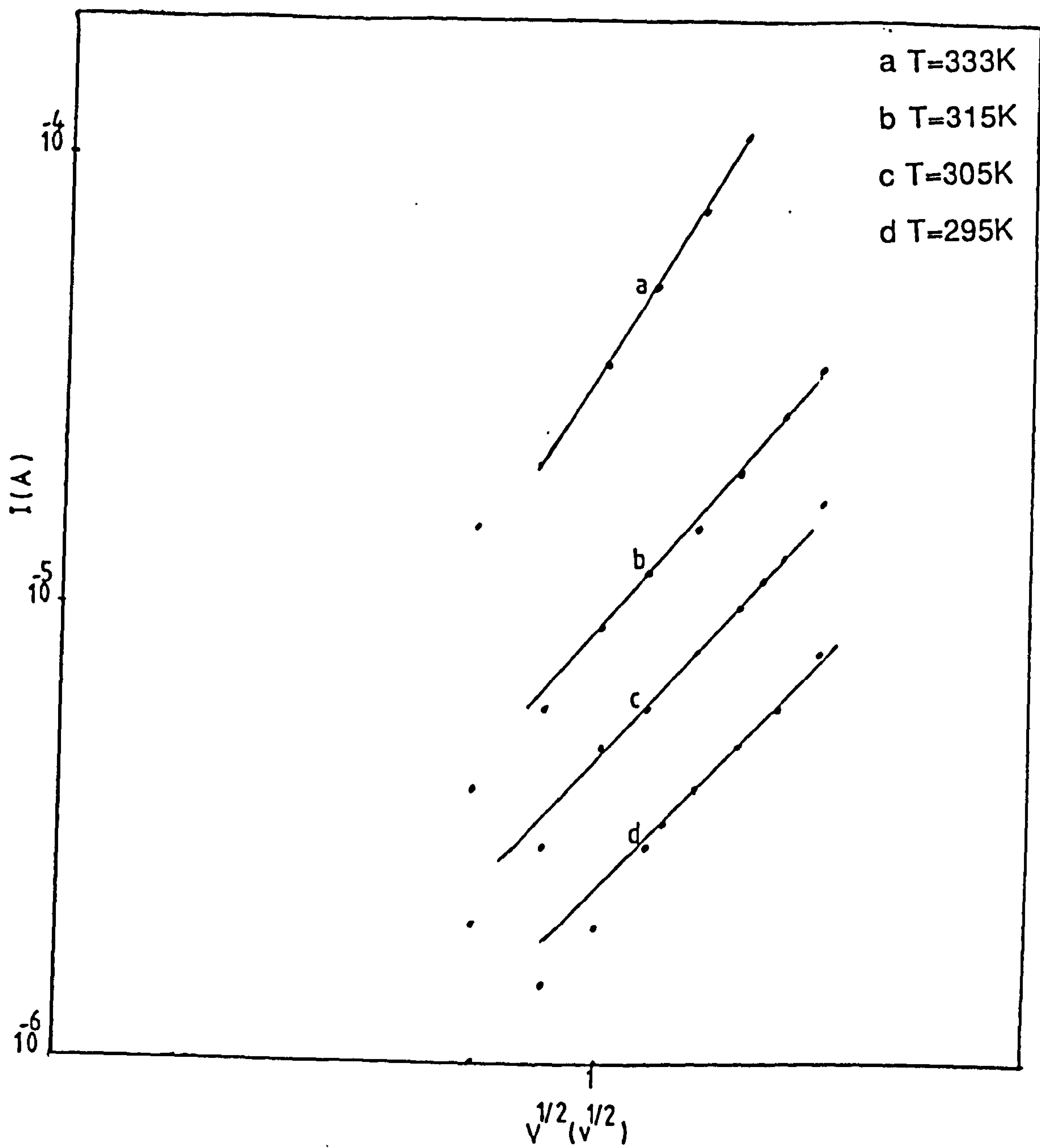

Fig. 5.5. log(I) versus $V^{1/2}$ for $22\%V_2O_5/78\%TeO_2$ thin film.

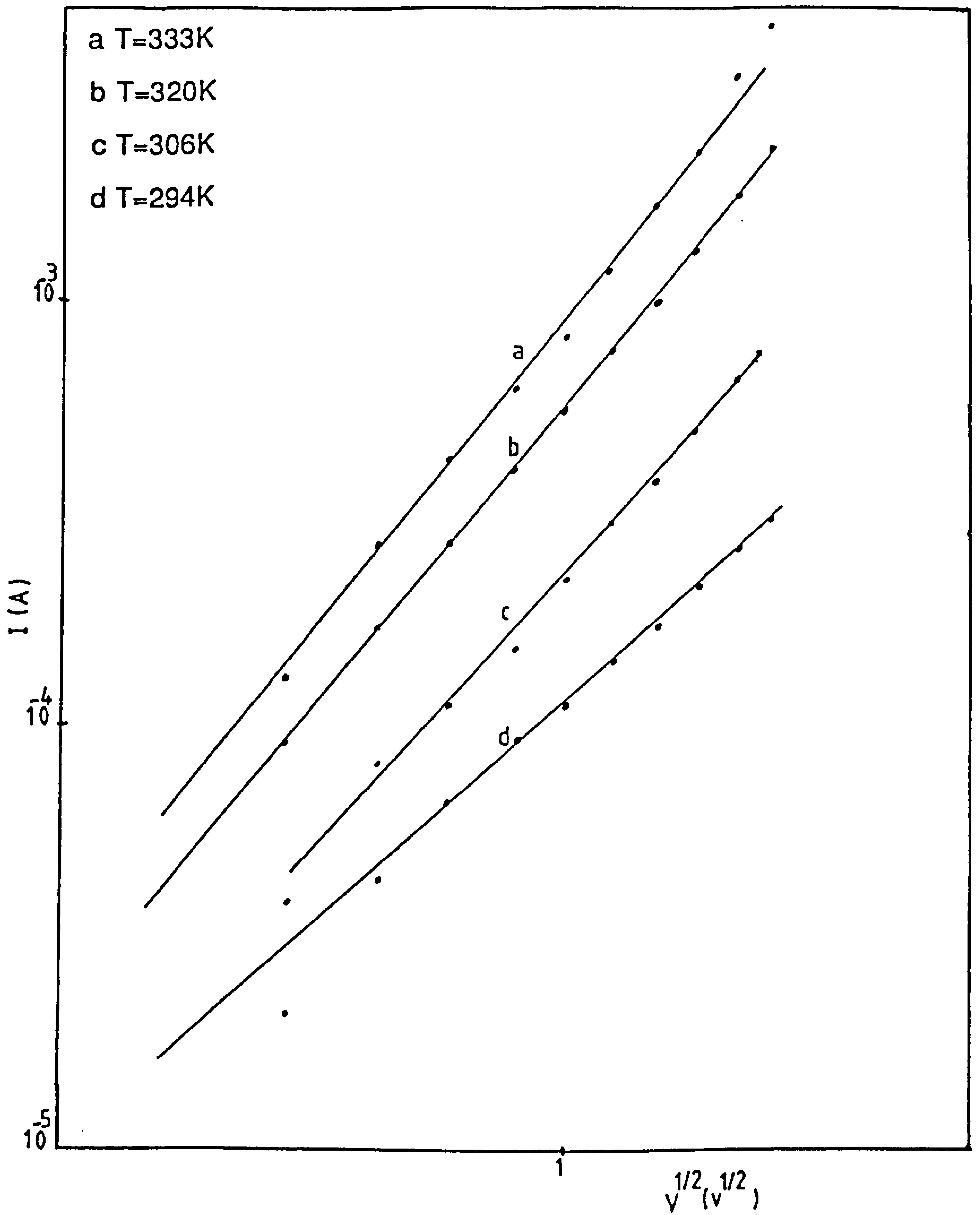

Fig. 5.6. log(I) versus $V^{1/2}$ for $27\%V_2O_5/73\%TeO_2$ thin film.

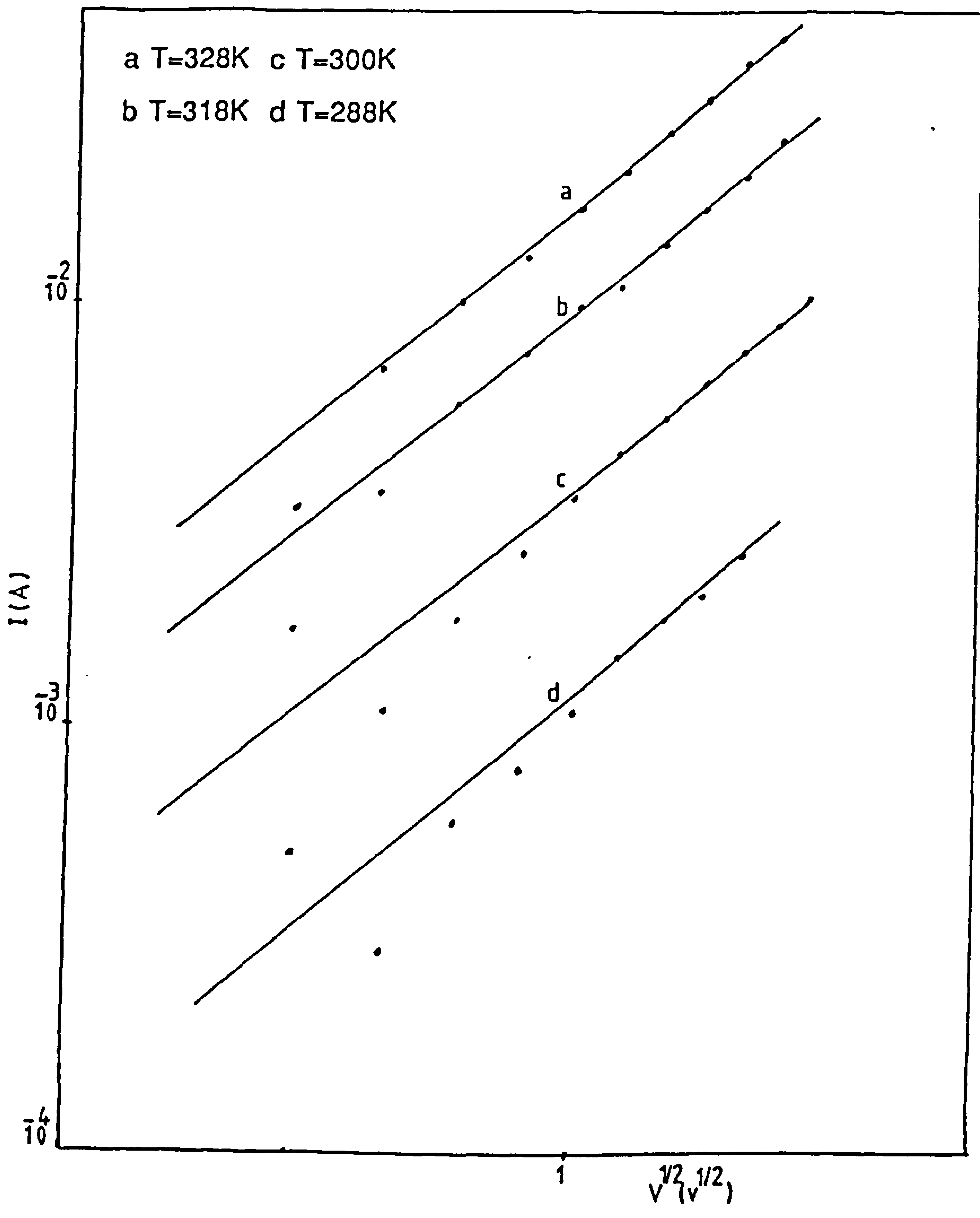

Fig. 5.7. log(I) versus $V^{1/2}$ for $68\%V_2O_5/32\%TeO_2$ thin film.

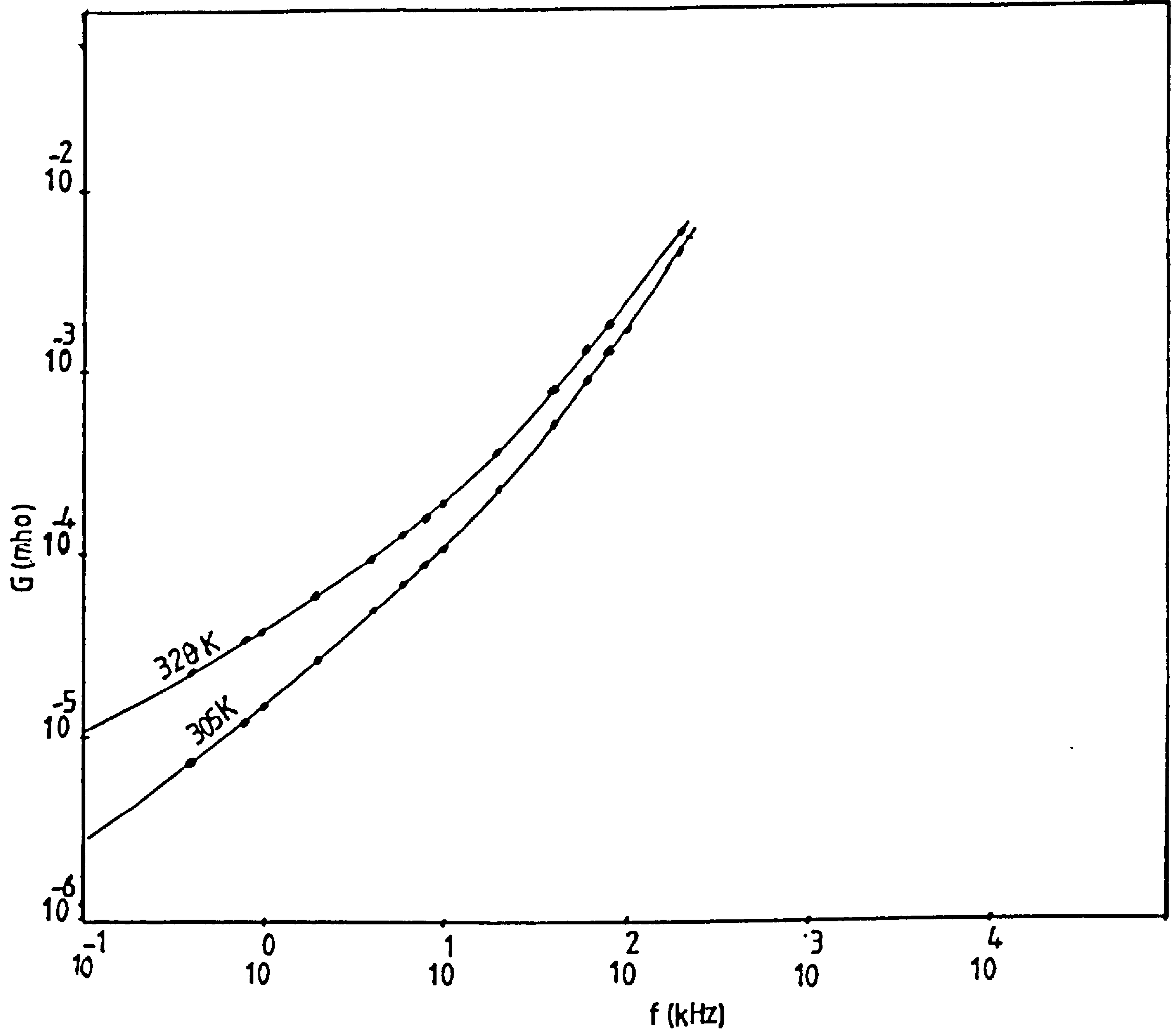

Fig. 5.8. A.C conductance versus frequency for $22\%V_2O_5/78\%TeO_2$ thin film.

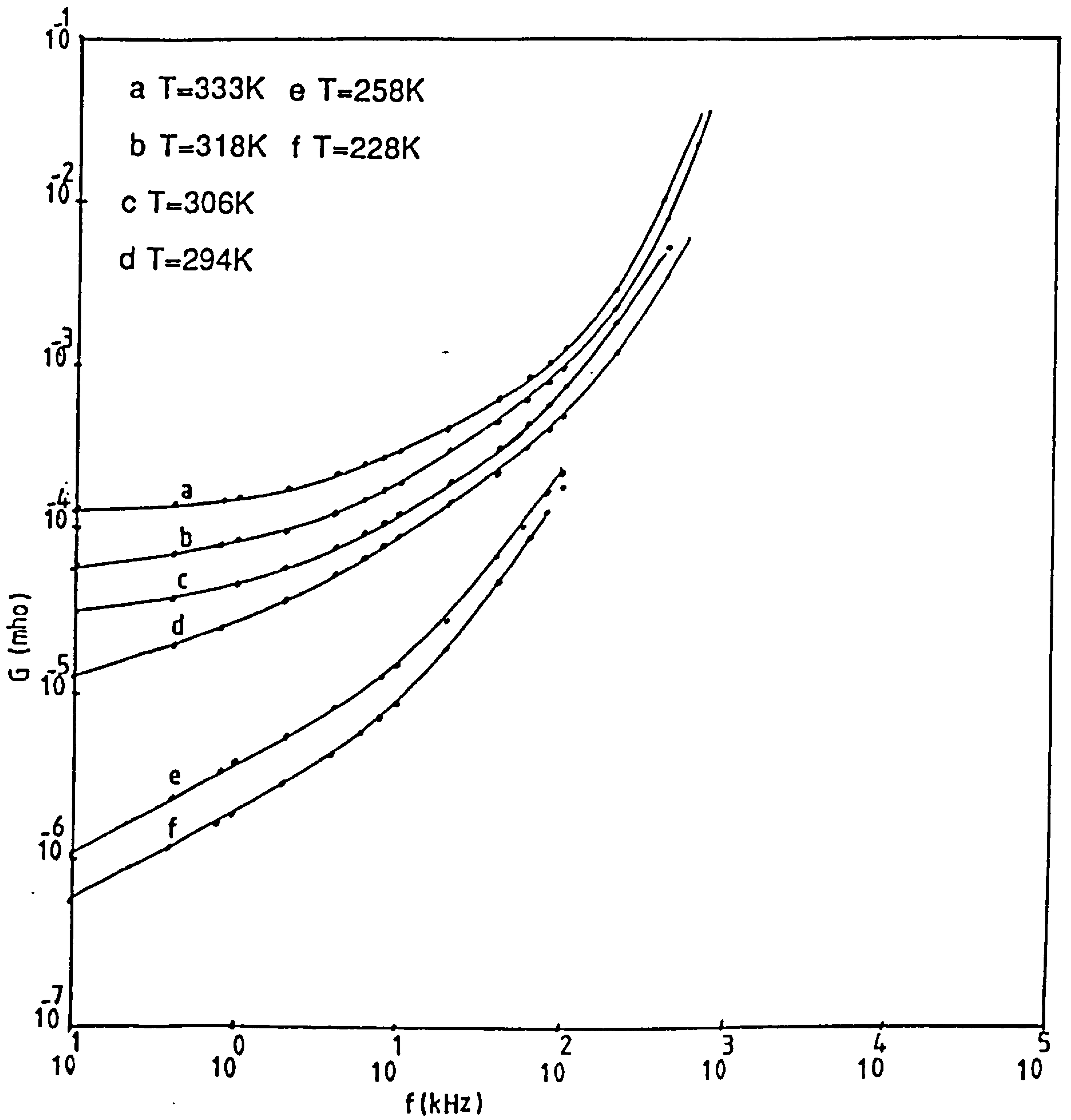

Fig. 5.9. A.C conductance versus frequency for $27\%V_2O_5/73\%TeO_2$ thin film.

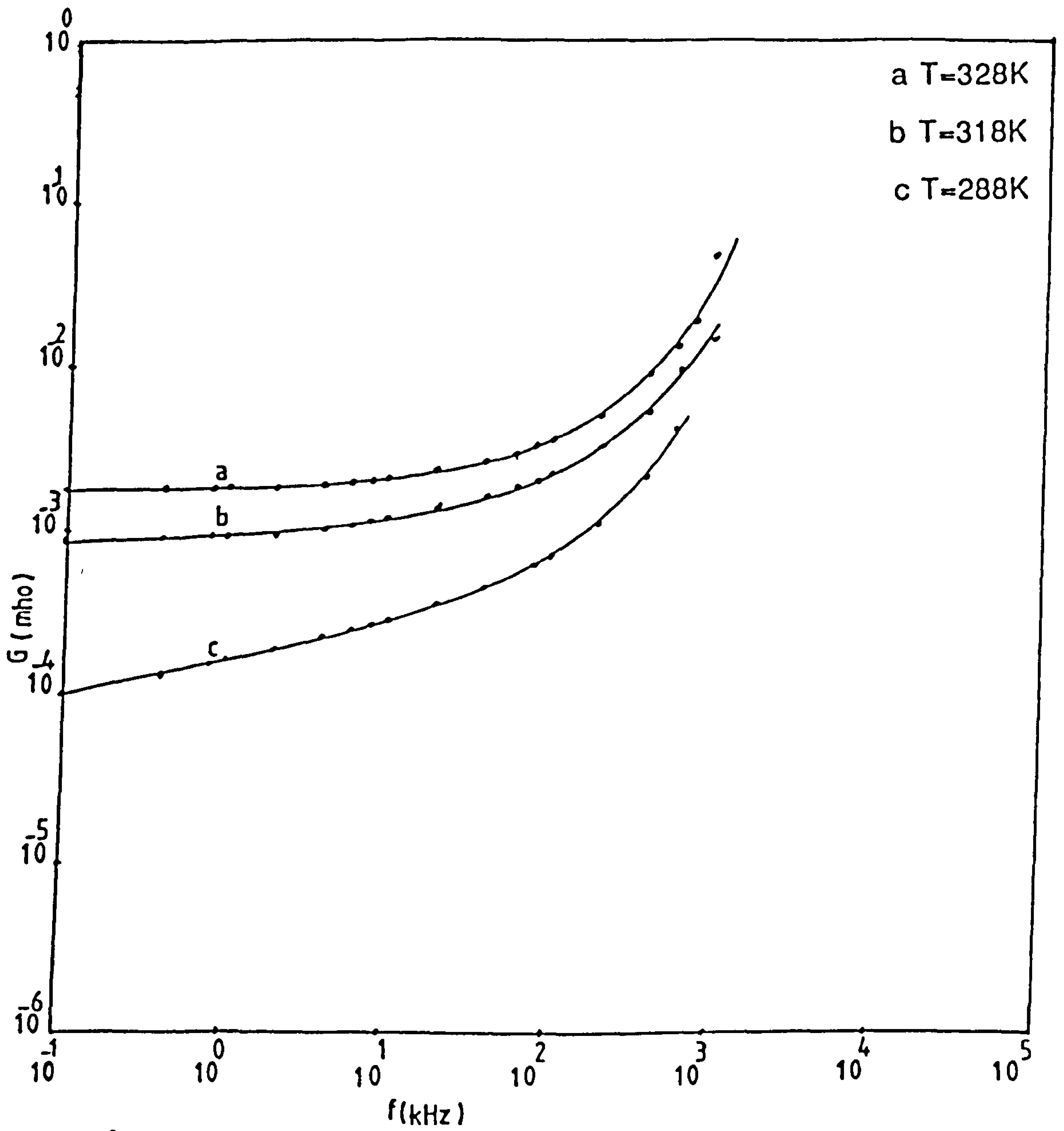

Fig.5.10. A.C conductance versus frequency for $68\%V_2O_5/32\%TeO_2$ thin film.

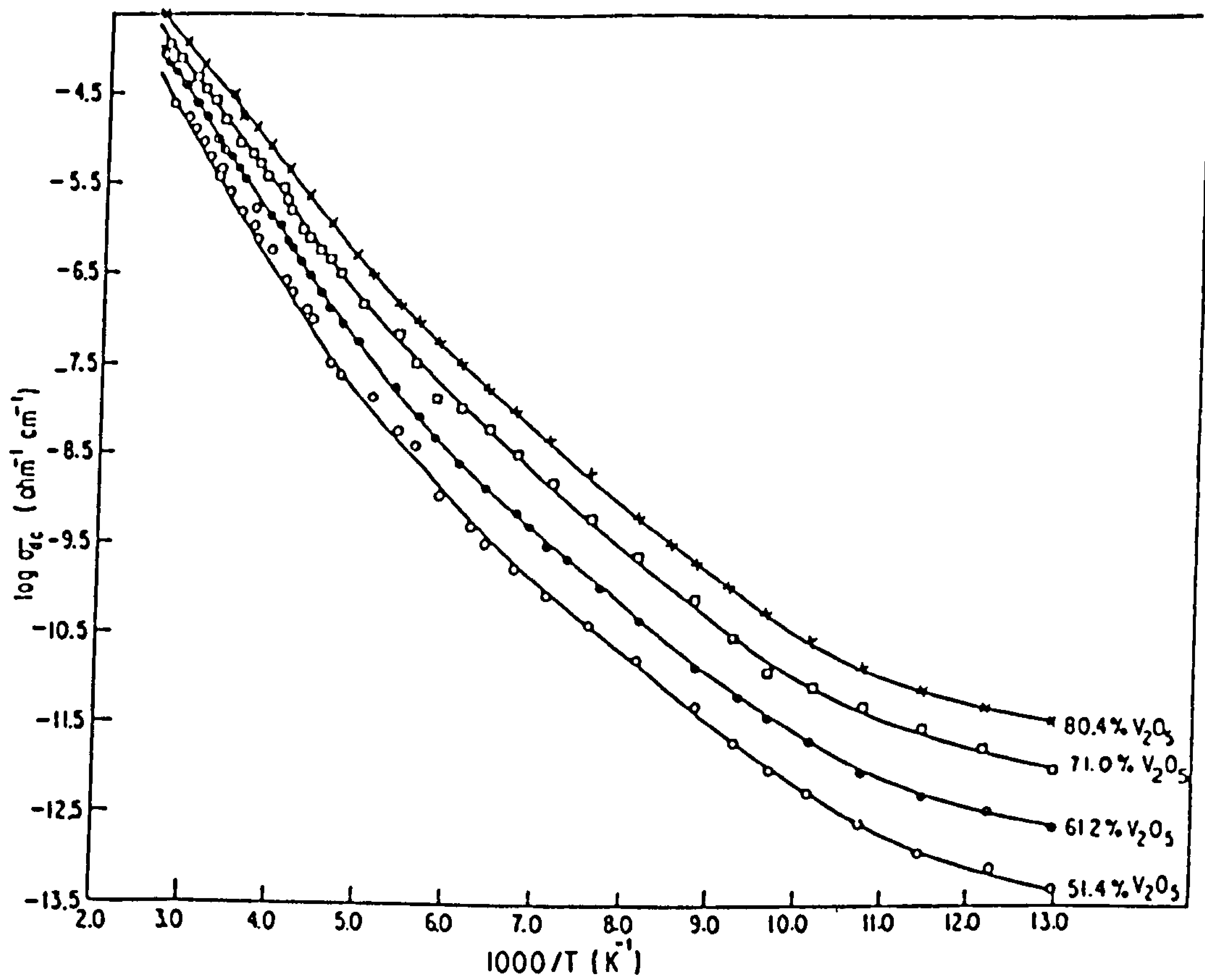

Fig. 5.11 Plot of log σ_{dc} versus $1000/T$ for four vanadium-tellurite glasses. (Dhawan *et al* (1982))

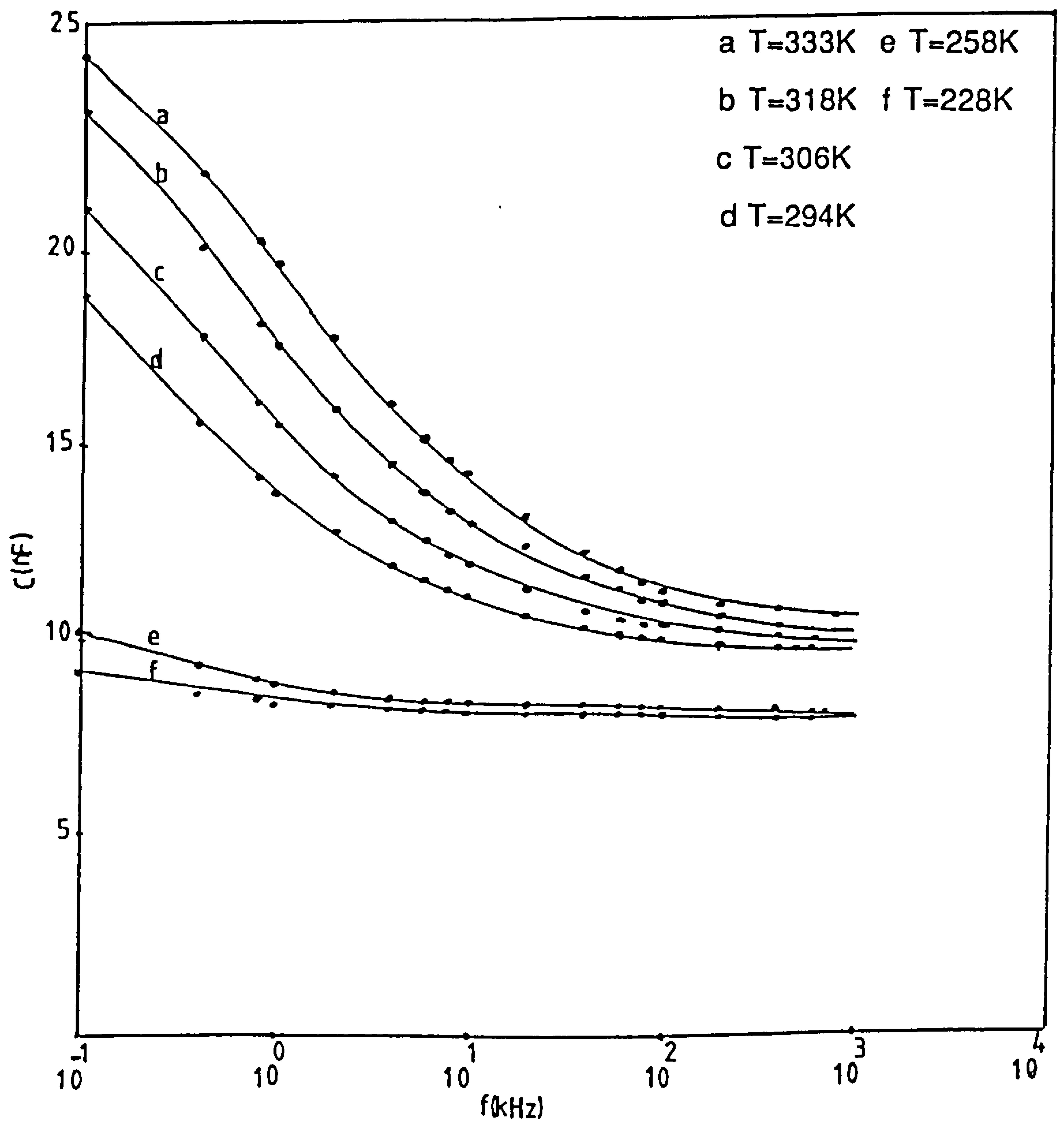

Fig. 5.12. Capacitance versus frequency for $27\%V_2O_5/73\%TeO_2$ thin film.

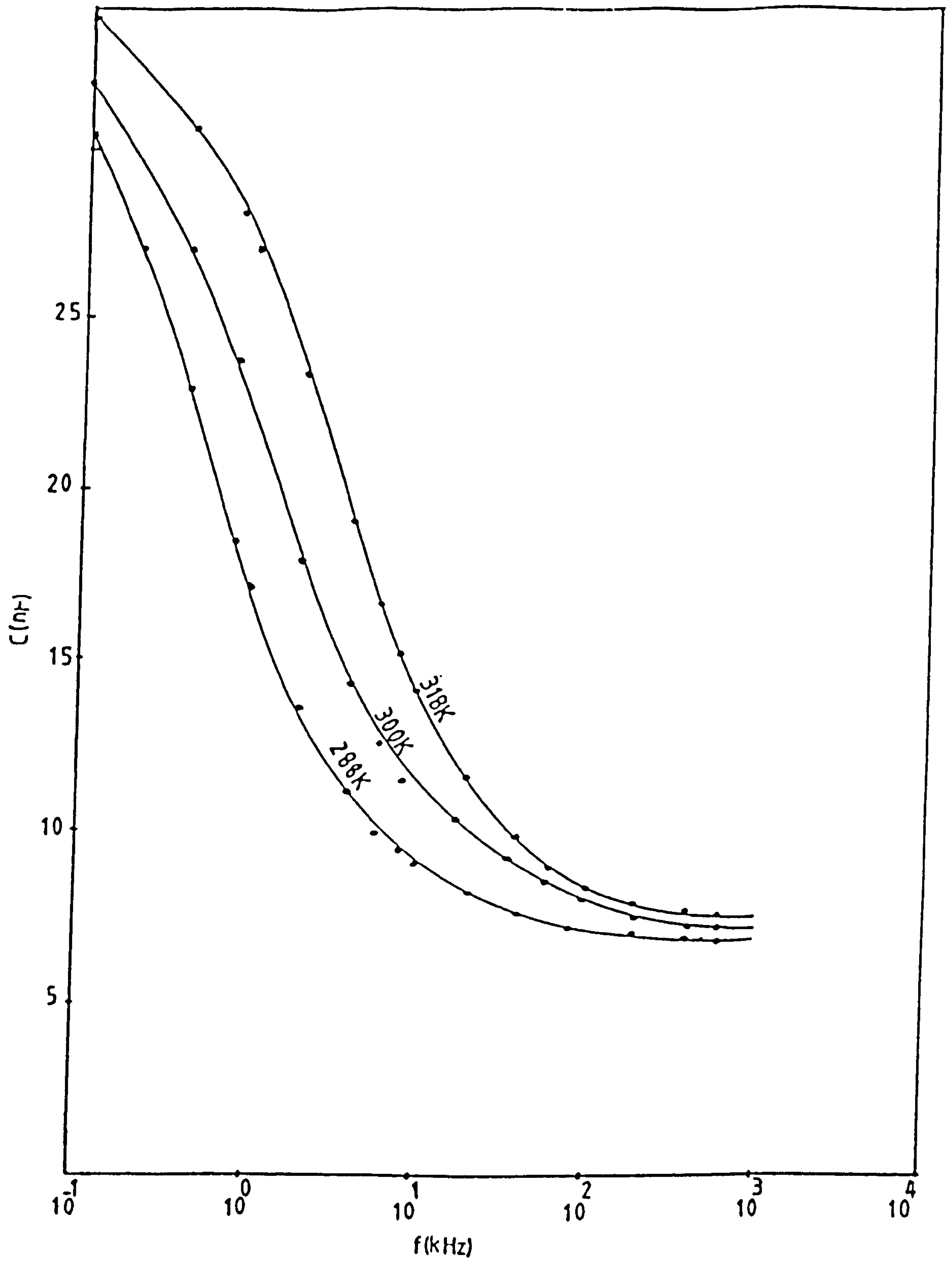

Fig. 5.13. Capacitance versus frequency for 68%V_2O_5/32%TeO_2 thin film.

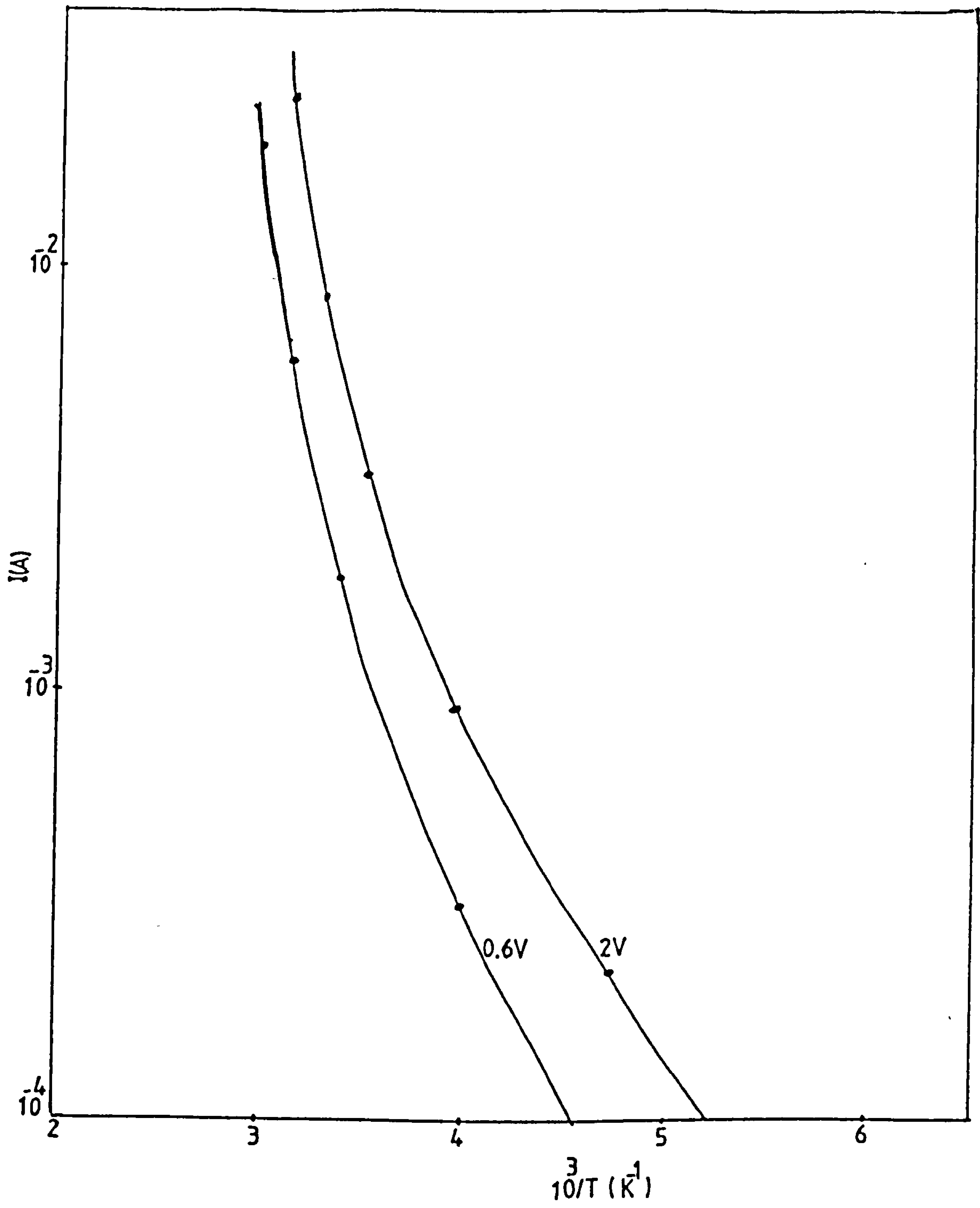

Fig. 5.14. log(I) versus 1/T for $68\%V_2O_5/32\%TeO_2$ thin film.

5-4. OPTICAL ABSORPTION EDGE OF V_2O_5/TeO_2 THIN FILMS.

5-4-1. INTRODUCTION.

The properties of semiconducting glass, such as those based on V_2O_5, have been of increasing interest over the years, with much of the work being done on glasses based on the V_2O_5/P_2O_5 system. Their optical properties have received considerably less attention than their electrical properties, though some work has been done in the infrared and visible regions [Anderson and Compton (1970)], [Denton *et al* (1954)] and [Janakirama-Rao (1965), (1966)].

5-4-2. RESULTS AND DISCUSSION OF V_2O_5/TeO_2 OPTICAL ABSORPTION EDGE.

Curves of the optical transmittance as a function of wavelength for different compositions of V_2O_5/TeO_2 co-evaporated layers are presented in figure (5.15). It is seen that the transmittance is very low indicating that the optical absorption coefficient is very high (higher than $10^3 cm^{-1}$).

The absorption coefficient $\alpha(\omega)$ was calculated by using the following relation.

$$\alpha(\omega)=(1/t).\ln(I_0/I). \quad (5.6).$$

where I_0 and I are the incident and the transmitted intensities of

light respectively and t is the thickness of the specimen.
The logarithm of the absorption coefficient is plotted in figure(5.16) as function of photon energy $h\omega$. It is seen that $\log(\alpha)$ versus $h\omega$ is linear in the range 10^4-$10^5 cm^{-1}$. These results lead to the conclusion that the absorption coefficient in the long-wavelength tail of the fundamental absorption edge shows an exponential dependence on photon energy.

$$\alpha \propto \exp(h\omega/E_t). \qquad (5.7).$$

where E_t is a constant depending on temperature.
Equation(5.7) which is known as Urbach's relation [Urbach(1953)] is usually obtained for α less than $10^4 cm^{-1}$ in most amorphous semiconductors. The values of E_t were calculated from the slopes in figure (5.16) and are 0.73eV and 0.50eV for 68%V_2O_5/32%TeO_2 and 51%V_2O_5/49%TeO_2 (216nm thick) respectively. These values are higher than those found in amorphous semiconductors, thus it is possible that equation(5.7) may in this case, govern part A which is shown in figure(3.1). On the other hand the plots shown in figure(5.16) may not have exponential form. Thus more values of α less than $10^4 cm^{-1}$ are needed to see the actual form of these plots. However, as is shown in figure(5.15) it is difficult to obtain small values of α.

In all band models (see chapter 2), the localized states due to the

atomic disorder, are close to the band edges rather than deep in the bands. Most of the workers (Cohen *et al*, Mott *etc.*) agreed that the states are localized below E_C and above E_B which are sharply defined energies called the mobility edges [Cohen *et al* (1969)]. These localized states play an important role in the optical absorption edge and their contribution to the optical transitions may be seen through the following arguments. Davis and Mott(1970) derived an equation for the optical absorption coefficient $\alpha(\omega)$ as a function of photon energy $\hbar\omega$.

$$\alpha(\omega)\hbar\omega=B(\hbar\omega-E_{opt})^n \quad (5.8).$$

where n is an exponent, ω is the angular frequency of the incident radiation, B is a constant and E_{opt} is defined as the optical energy gap of the material, and it corresponds to the smallest energy separating the localized states that are close to one of the two bands and the extended states of the other one [see the Davis-Mott model(1970) section (2.3)].A similar equation with n=2 was derived by Tauc *et al*(1966). However, the definition given to E_{opt} by these authors is different from that given by Davis and Mott. Tauc *et al* defined it as the energy separating the localized states above E_B and those below E_C.

Equation(5.8) with n=2 offers the best fit to the optical absorption data in most amorphous semiconductors. However, in the case of amorphous V_2O_5/TeO_2 thin films, we have chosen n=3/2 instead of n=2 because of the following arguments. Nuclear

magnetic resonance studies show that the coordination number of the vanadium ions in the glass is the same as for the vanadium ions in crystalline V_2O_5 [France and Hooper(1968)], [Landsberger and Bray(1969)] and that their site symmetry is similar to that in the crystal. As a consequence, one would expect the same electronic transitions in both non-crystalline and crystalline V_2O_5. In fact, it was found in the latter (V_2O_5 single crystal) that the absorption coefficient fits the condition for direct forbidden transitions,

$$\alpha\hbar\omega=B(\hbar\omega-E_{opt})^{3/2}. \quad (5.9).$$

much better than it fits the condition for direct allowed transitions [Bardeen *et al* (1956)] and [Bodo' and Hevesi(1967)], given by

$$\alpha=B_1(\hbar\omega-E_{opt})^{1/2}. \quad (5.10).$$

Al-Ani and Hogarth(1985) have also used equation(5.9) to determine the optical gap of V_2O_5/SiO amorphous thin films and they found that it gives a better fit to their optical absorption data. In addition the optical absorption properties of V_2O_5/P_2O_5 glasses show that the fundamental absorption arises from direct forbidden transitions (eq.(5.9)) and occurs at about 2.4eV at room temperature [Anderson and Compton(1970)]. Therefore, in the present work on V_2O_5/TeO_2 thin films, we have plotted in

Fig. 5.15. Optical transmittance as function of wavelength for V_2O_5/TeO_2 thin films. a) 68% V_2O_5 and b) 51% V_2O_5.

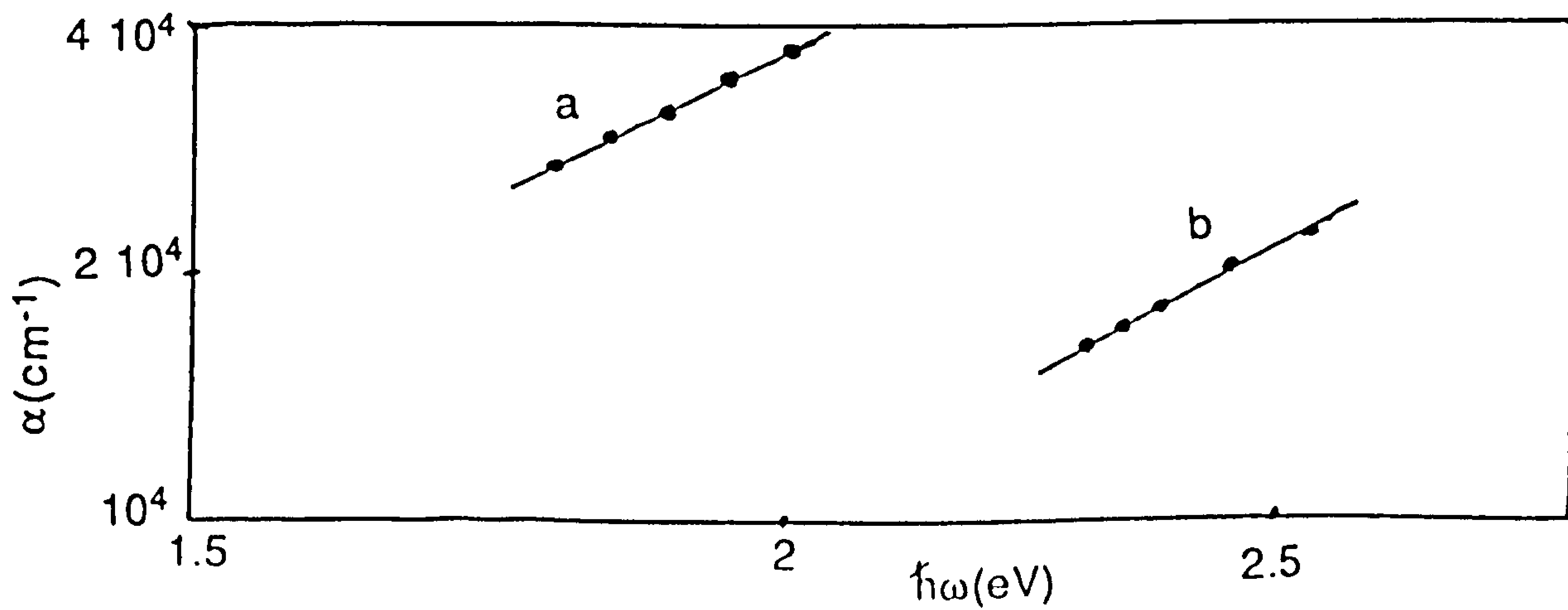

Fig. 5.16. log(α) versus ħω for V_2O_5/TeO_2 thin films. a) 68% V_2O_5 b) 51% V_2O_5.

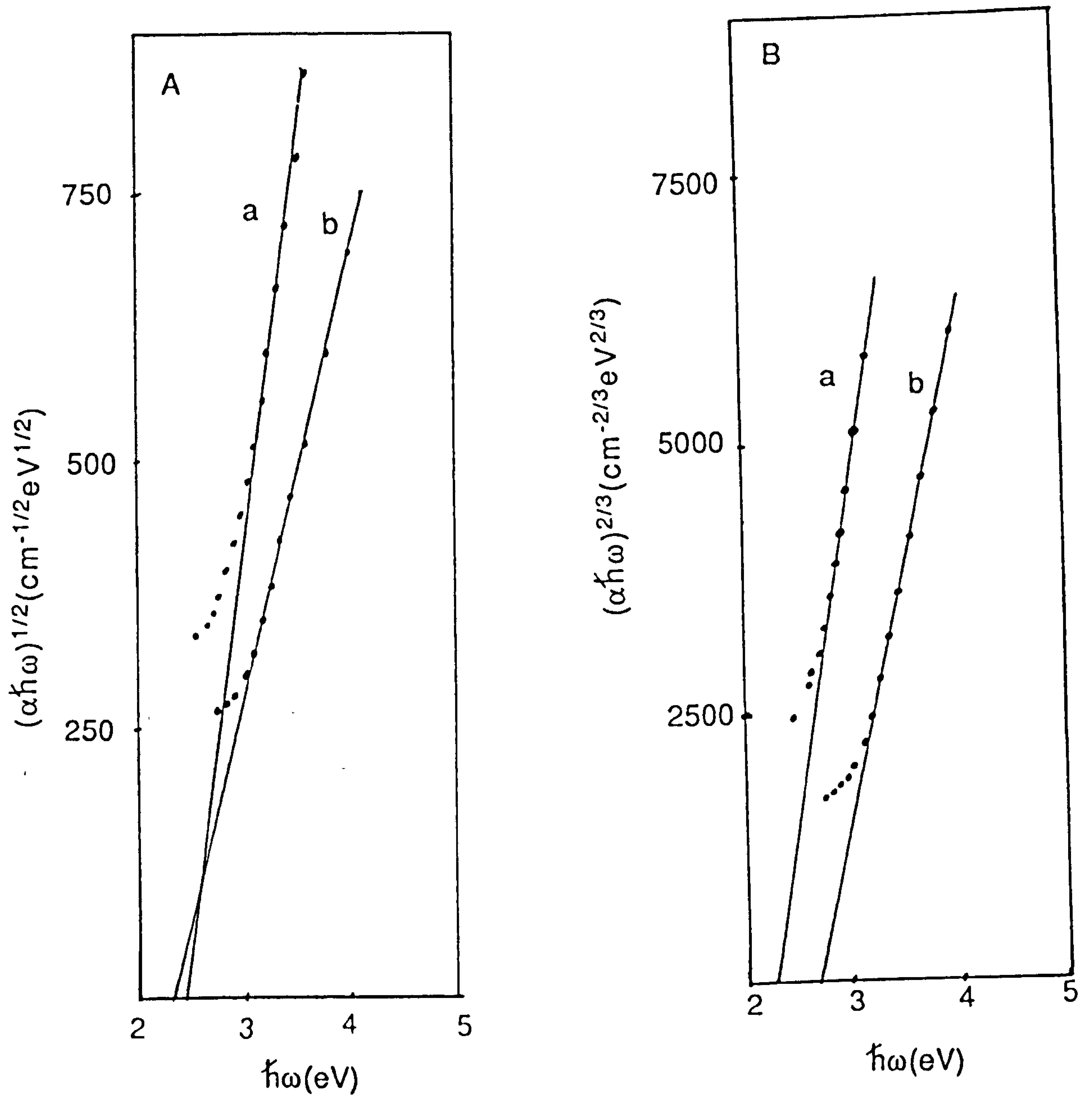

Fig. 5.17. A) $(\alpha\hbar\omega)^{1/2}$ and B) $(\alpha\hbar\omega)^{2/3}$ versus $\hbar\omega$ for V_2O_5/TeO_2 thin films. a) 68%V_2O_5 and b) 51%V_2O_5.

figure(5.17) $(\alpha\hbar\omega)^{2/3}$ as well as $(\alpha\hbar\omega)^{1/2}$ as a function of photon energy $\hbar\omega$. Both plots give straight lines, hence, it is difficult to see which equation is the best to fit our data. However, equation(5.9) gives reasonable values of E_{opt} better than those given by equation(5.8) with the exponent n equal to 2. These values of E_{opt} given by equation(5.9), are 2.27eV and 2.70eV for 68%V_2O_5/32%TeO_2 and 51%V_2O_5/49%TeO_2 respectively. Those given by $(\alpha\hbar\omega)^{1/2}$ are 2.40eV and 2.30eV

5-5 ELECTRON MICROSCOPE STUDY OF V_2O_5/TeO_2 THIN FILM.

The structure of layers of about 40nm thickness was investigated in an electron microscope (JEO model JEM7) by electron diffraction and micrographs. For this purpose the thin film of V_2O_5/TeO_2 was deposited on a carbon-coated mica substrate held at room temperature. Figure (5.18) shows the electron micrograph and diffraction pattern at temperature higher than 523K for a V_2O_5/TeO_2 thin film. It is seen that a polycrystalline sample has a diffraction pattern which is typical for the crystalline material, i.e sharp rings, whereas for amorphous layers at room temperature, this structure is smeared out [figure (5.19)]. These state changes from amorphous to the crystalline state are due to an increase in temperature which causes a softening of the material, and as a result the atoms seek a more stable state by rearranging themselves inside the specimen [figure (5.18)] with a

resulting successive saturation of the free valencies. Another important consequence due to an increase in temperature, is the decrease of the spin density observed for example by Arshak and Hogarth (1986) in annealed SiO/BaO. They attributed this to a rearrangement of the atoms and to the removal of voids which causes a decrease in the number of unsaturated bonds.

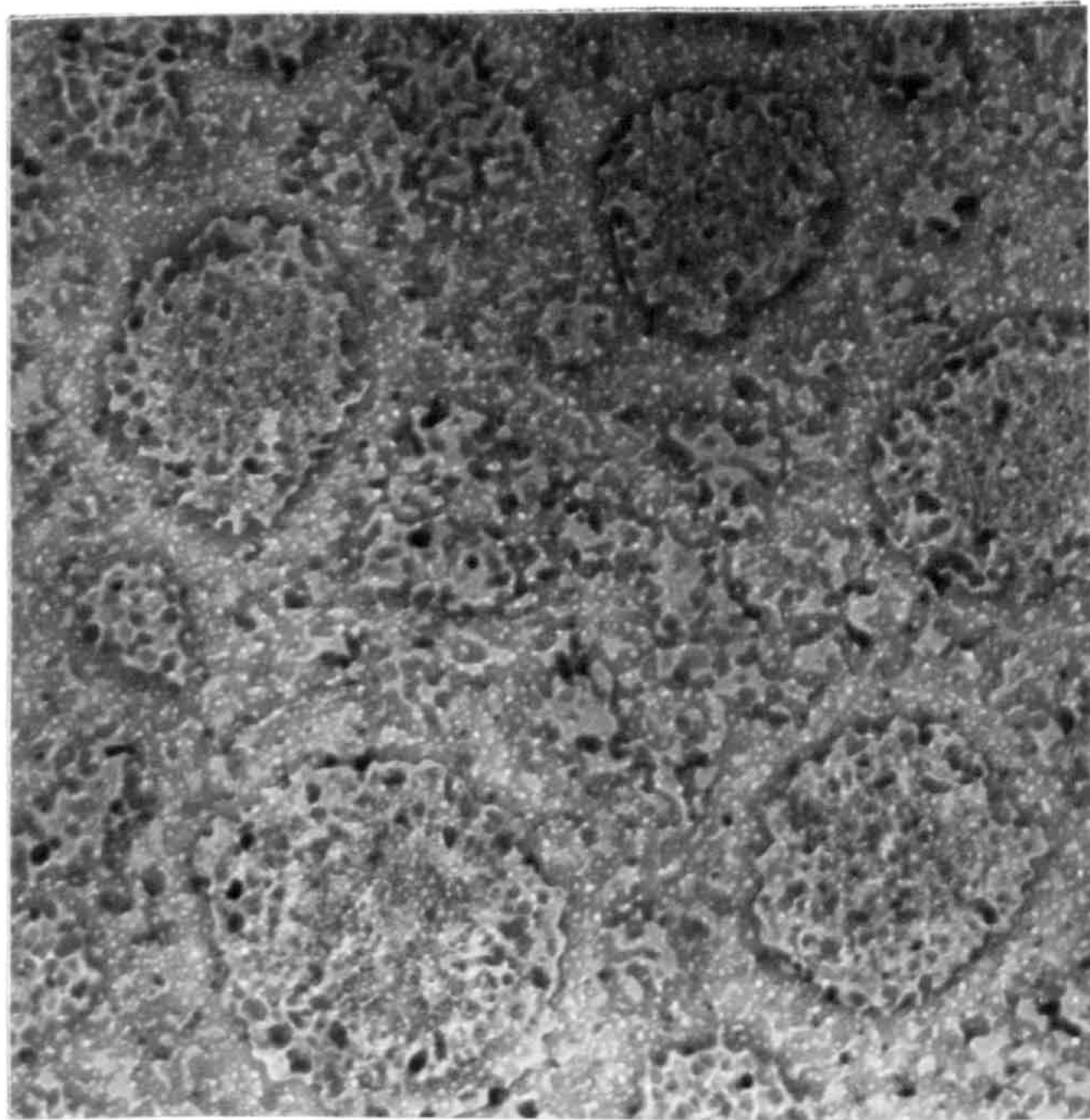

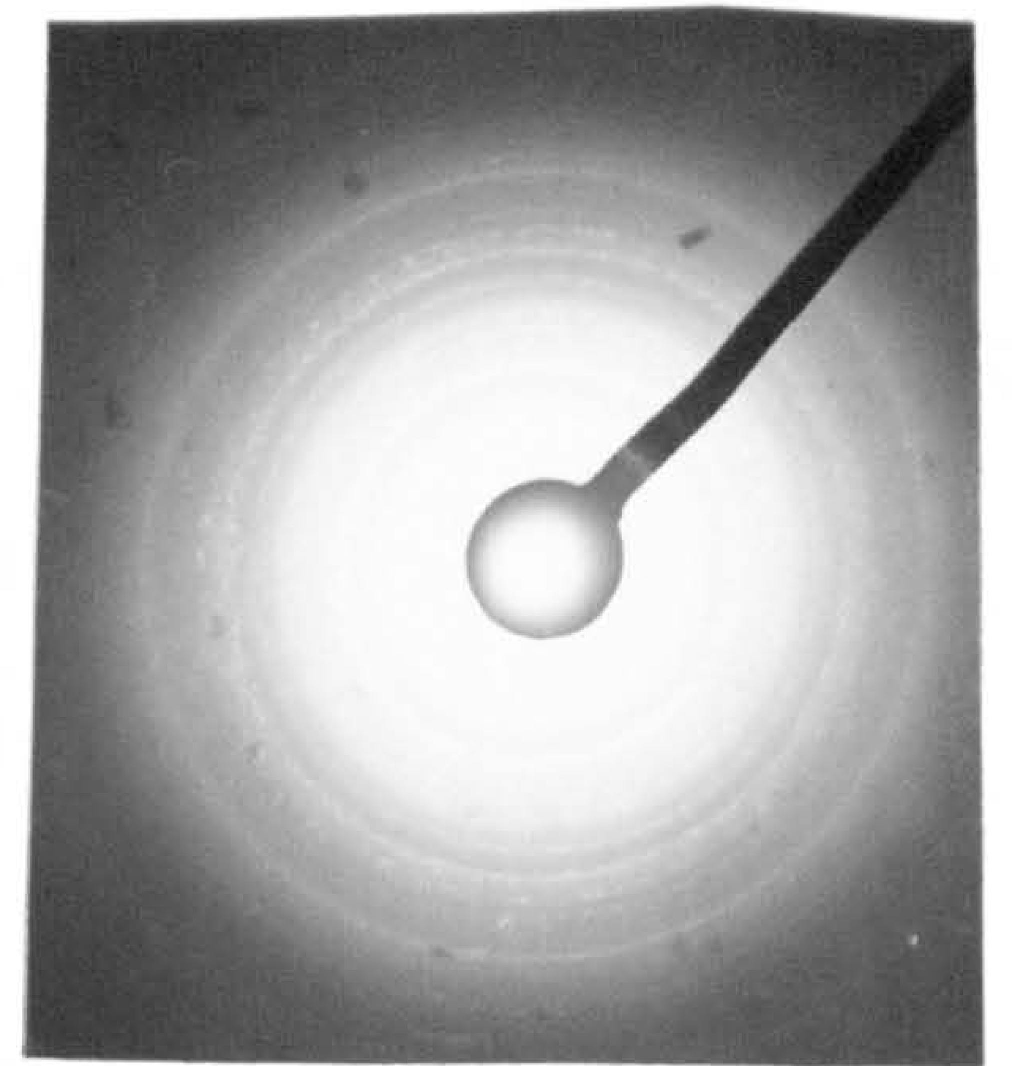

Micrograph

Diffraction pattern

Fig. 5.18 Electron micrograph and diffraction patterns of V_2O_5/TeO_2 thin film after annealing

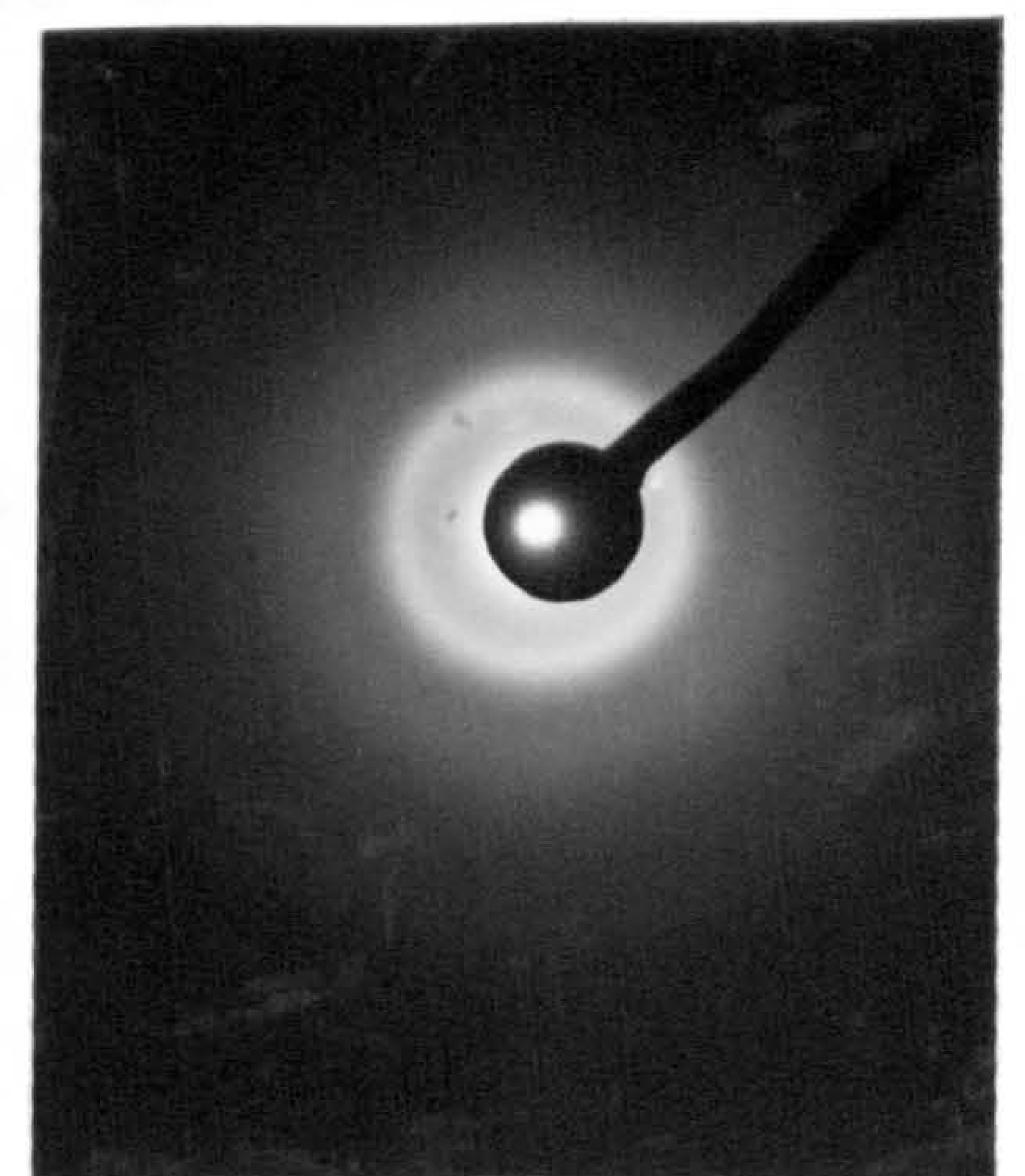

Micrograph

Diffraction pattern

Fig. 5.19 Electron micrograph and diffraction patterns of V_2O_5/TeO_2 thin film at room temperature.

CHAPTER 6. RESULTS AND DISCUSSION OF WO_3/CeO_2 THIN FILMS.

6-1. INTRODUCTION

Razzaq and Hogarth (1988) have studied the electrical and optical properties of V_2O_5/CeO_2 amorphous thin films for different compositions in the range 53%-90% of CeO_2. Their experimental results show that at low temperatures, conduction is by hopping of electrons from one site to the other within the energy range of localized states. With the increase of temperature a transition from hopping to free band conduction takes place. Their results which were not explained in terms of polaron conduction, may arise because the mechanism of the conduction is dominated by the presence of the high content of CeO_2 in the structure. WO_3 is also a transition metal oxide and its properties were studied by Crowder and Sienko (1963), and Sawada and Danielson (1959). It was therefore of interest to compare the mechanism of conduction in V_2O_5/CeO_2 to that in WO_3/CeO_2 amorphous thin films in order to see whether the polaronic conduction is dominant or not. The films with different compositions and thicknesses are listed in table(6.1).

6-2. A.C AND D.C ELECTRICAL CONDUCTION IN WO_3/CeO_2 THIN FILMS.

The phenomenon of anomalous absorption current upon the application of a constant potential diffence, has been observed in most thin films where the content of WO_3 is higher than 60%. Initially the current rises very quickly to well above the steady state d.c value and then decays over a period of time. This excess of current above the steady state is caused by polarization in the sample. These polarization effects were also observed by Mansingh *et al* (1978) in WO_3 amorphous thin films. Due to contact barrier effects the d.c conductivity of a sample such as 81%WO_3/19%CeO_2 could not be measured in the sandwich form. However, the I-V characteristic of 58%WO_3/42%CeO_2(175nm thick) shown in figure (6.1) is more steady than that of 81%WO_3/19%CeO_2(176nm thick) indicating that the effects of polarisation are reduced as the content of CeO_2 increases. Therefore, we have studied only a.c properties of the samples in which the effects of polarisation are observed. Figures (6.5), (6.6) and (6.7) show respectively the plots of log(G), capacitance and log(tanδ) versus frequency of an Al-81%WO_3/19%CeO_2-Al thin sandwich structure.

In the frequency range 0.1kHz-10kHz and at low temperatures, the a.c conductivity can be expressed as

$$\sigma(\omega) \propto \omega. \qquad (6.1).$$

The capacitance shown in figure (6.6) is constant at reduced temperatures (T=163K) indicating that the a.c conduction is bulk limited in the frequency range 0.1kHz-10kHz.

Equation (6.1) is expected for the mechanism of conduction which involves a thermally-activated rotation of a dipole [Mott and Davis (1979)]. However, we think that in the case of WO_3/CeO_2 thin amorphous films, the rotation of this dipole corresponds to the jump of the charge carrier over an energy barrier from one localized point to another. A wide distribution of such energy barriers would give a number of loss peaks at different frequencies giving a resultant loss that may be nearly constant with frequency as it is shown in figure (6.7) at T=163K, and in the frequency range 0.1kHz-10kHz. As the temperature is increased up to 363K, the index s given by the formula $\sigma(\omega)=A\omega^{S}$ decreases to a value 0.5 (fig(6.5)) suggesting that conduction is by hopping of electrons between localized states [Pollak and Geballe (1961)]. Figure (6.6) shows that at T=163K the capacitance is constant in the frequency range 0.1kHz-100kHz and figure (6.7) shows that $\tan\delta$ is proportional to ω in the frequency range 10kHz-100kHz, hence, the dielectric loss ε'' is proportional to ω;

$$\varepsilon''=A.\omega \qquad (6.2)$$

where A is a constant.

The a.c conductivity is given by

$\sigma(\omega)=\varepsilon''.\omega.$ (6.3).

Inserting the relation (6.2) into (6.3) we obtain the following relation of the a.c conductivity.

$\sigma(\omega)=A.\omega^2.$ (6.4).

The fact that the capacitance is constant in the frequency range where the quadratic relation (eq;(6.4)) of the a.c conductivity is obeyed, means that the ω^2 dependence may be caused by a spurious resistance which is associated with the evaporated electrodes. To explain this effect, Street *et al* (1971) considered an equivalent circuit (sample and leads) consisting of a resistance R_l in series with a parallel R_s-C_s (resistance and capacitance of the sample) combination. Below a certain frequency ω_c the measured conductance and capacitance are those of the sample. However, above this critical frequency given by

$\omega_c=(C_s^2R_sR_l)^{-1/2},$ (6.5)

the conductance $G=\omega^2C_s^2R_l$, if C_s is constant, will be proportional to ω^2. According to Street *et al* (1971), at high frequencies the measured capacitance C_p and resistance R_p should tend to a lead capacitance C_l and a lead resistance R_l respectively. However, the capacitance in figure (6.6) shows a large dispersion at high frequencies and the conductivity in figure (6.5) shows no

saturation region. Therefore, we suggest that the square-law dependence on frequency of the the Al-81%WO_3/19%CeO_2-Al thin amorphous film in the region shown in figure (6.5) is not due to lead resistance or inductance and hence the measured capacitance and conductance are those of the sample.

Plots of log conductance, capacitance and log tanδ as functions of log frequency of an Al-58%WO_3/42%CeO_2-Al thin sandwich structure at different temperatures are shown in figures (6.2), (6.3) and (6.4) respectively. The a.c conductivity $\sigma(\omega)$ can be expressed as;

$$\sigma(\omega)= A\omega^{S} \qquad (6.6)$$

were A and s are parameters. From figure (6.2) it can be seen that in the frequency range 0.1kHz-2kHz, the exponent s decreases from 1 to 0.5 with increasing temperature. This mechanism of conduction involves the hopping of electrons between localized states as described by Pollak and Geballe (1961). In the frequency range 2kHz-10kHz, the value of s is slightly greater than 1 and the a.c conductivity is still temperature dependent. Thus, this a.c conduction behaviour must be due to an electronic hopping mechanism [Argall and Jonscher(1968)].
The high frequency a.c conductance (10kHz-10^2kHz) shown in figure (6.2) for the sample Al-58%WO3/42%CeO2-Al is temperature independent and is proportional to ω^2. At the same time the capacitance shown in figure (6.3) for the same sample is

constant and the loss $\tan\delta$ is proportional to ω. At higher frequencies it is clearly shown in figure (6.2) that the a.c conductance is independent of frequency (saturation) and the capacitance decreases quickly with increasing frequency. Therefore, following Street *et al* (1971) one may invoke the effect of the lead resistance above the critical frequency ω_c given by equation (6.5). In fact the behaviour of the a.c conductivity as the frequency is varied may be divided into three main regions according to the experimental results on the Al-58%WO_3/42%CeO_2-Al thin amorphous film;

A). LOW FREQUENCY REGION (0.1kHz-10kHz).

In this region the measured a.c conductance and capacitance are those of the sample.

B). MID FREQUENCY REGION (10kHz-10^2kHz).

In this region the capacitance is constant, the loss $\tan\delta$ is proportional to ω and the conductivity is proportional to ω^2 .

C). HIGH FREQUENCY REGION (above 10^2kHz).

In this region the a.c conductance is independent of frequency and the capacitance decreases with increasing frequency. This behaviour of the conductance and capacitance in the mid and high frequency regions could be due to the lead resistance and capacitance [Street *et al* (1971)]. Therefore, the measured conductance and capacitance of Al-58%WO_3/42%CeO_2-Al in the

mid-and high-frequency regions could not be those of the sample. The capacitance variation with frequency of this sample is very similar to that reported by Roberts *et al* (1980) for anthracene. Figure(6.8) shows the variation of log conductance with inverse of temperature. It can be seen that at low temperatures the a.c conductivity is frequency dependent; the conductivity first increases slowly and then rapidly with temperature, and at higher temperatures it is seen that the conductivities at different frequencies merge with each other suggesting that the slope at high frequencies is independent of frequency. This behaviour of the conductivity of a 81%WO_3/19%CeO_2 thin film is very similar to that reported by Mansingh *et al* (1977) for amorphous WO_3 films. However, in WO_3 films the transition from hopping to band conductions occurs at about 125K, while in 81%WO_3/19%CeO_2 thin films it occurs at about 267K and the conductivity of WO_3/CeO_2 is higher than that of WO_3 thin film. The value of the activation energy is found to be equal to 0.7eV at high temperatures and 0.03eV at low temperatures. This small value would suggest that the mechanism of conduction at low temperatures is by hopping of carriers between localized states in the gap. On the other hand polaron formation in WO_3/P_2O_5 glasses has been reported by Sayer and Lynch(1973) and it is thought that it may affect the electrical properties of WO_3. However, figure(6.8) shows that at low temperatures the mechanism of conduction is very similar to that of hopping conduction between impurity states in a doped semiconductor and thus, apart from an increase in the activation

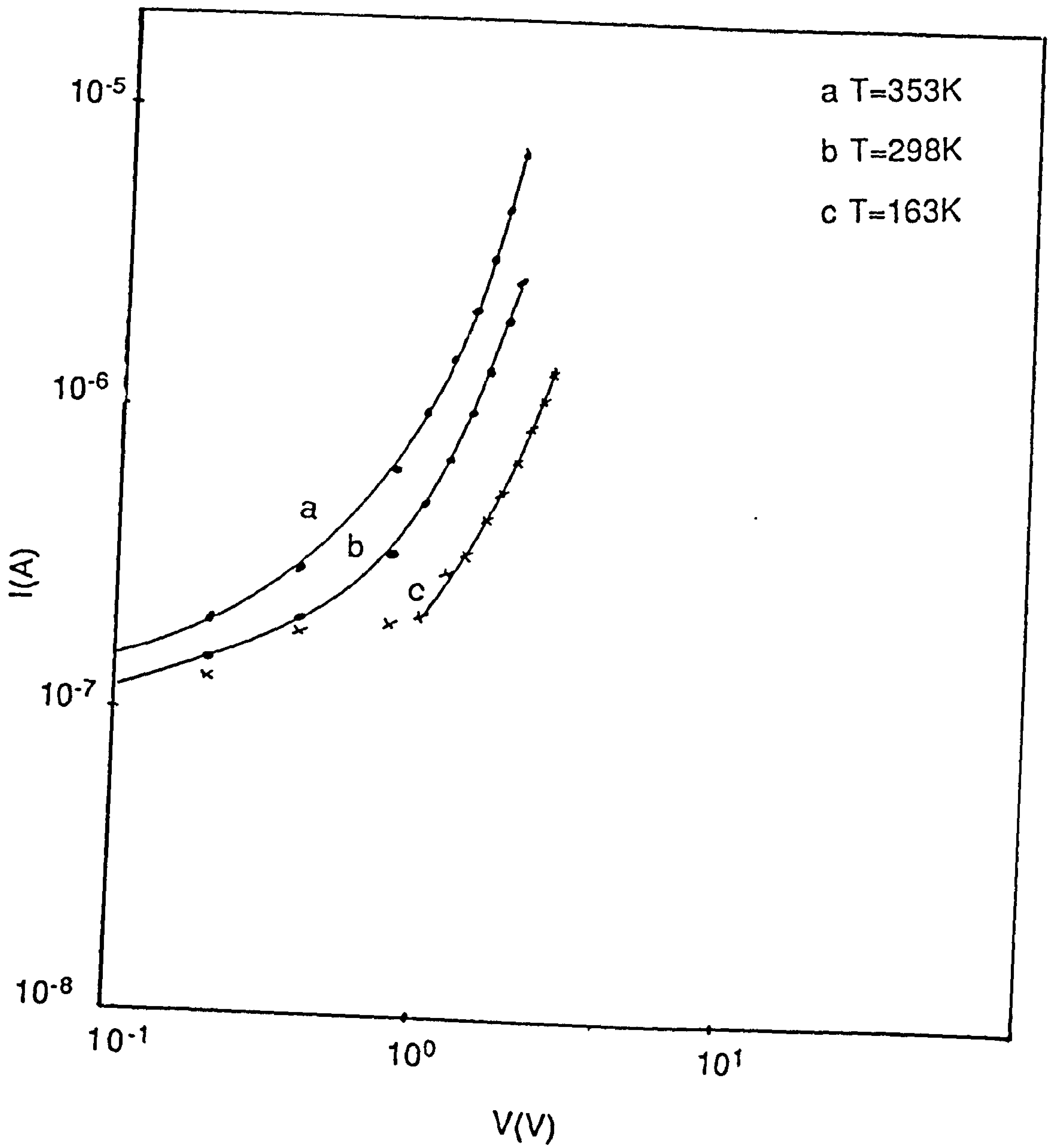

Fig. 6.1. I-V characteristic of $58\%WO_3/42\%CeO_2$ thin film.

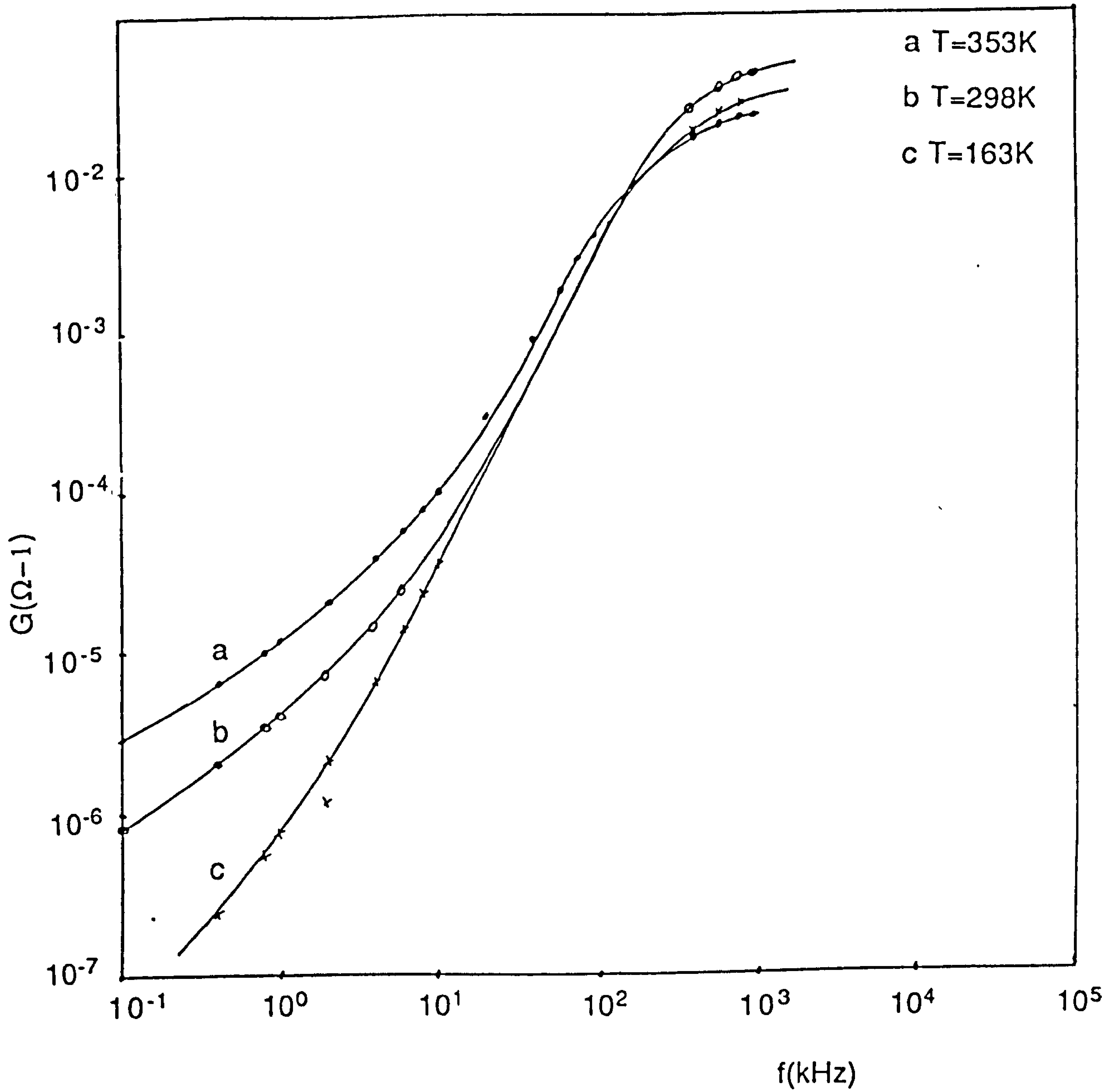

Fig. 6.2. A.C conductance versus frequency for 58%WO_3/42%CeO_2 thin film.

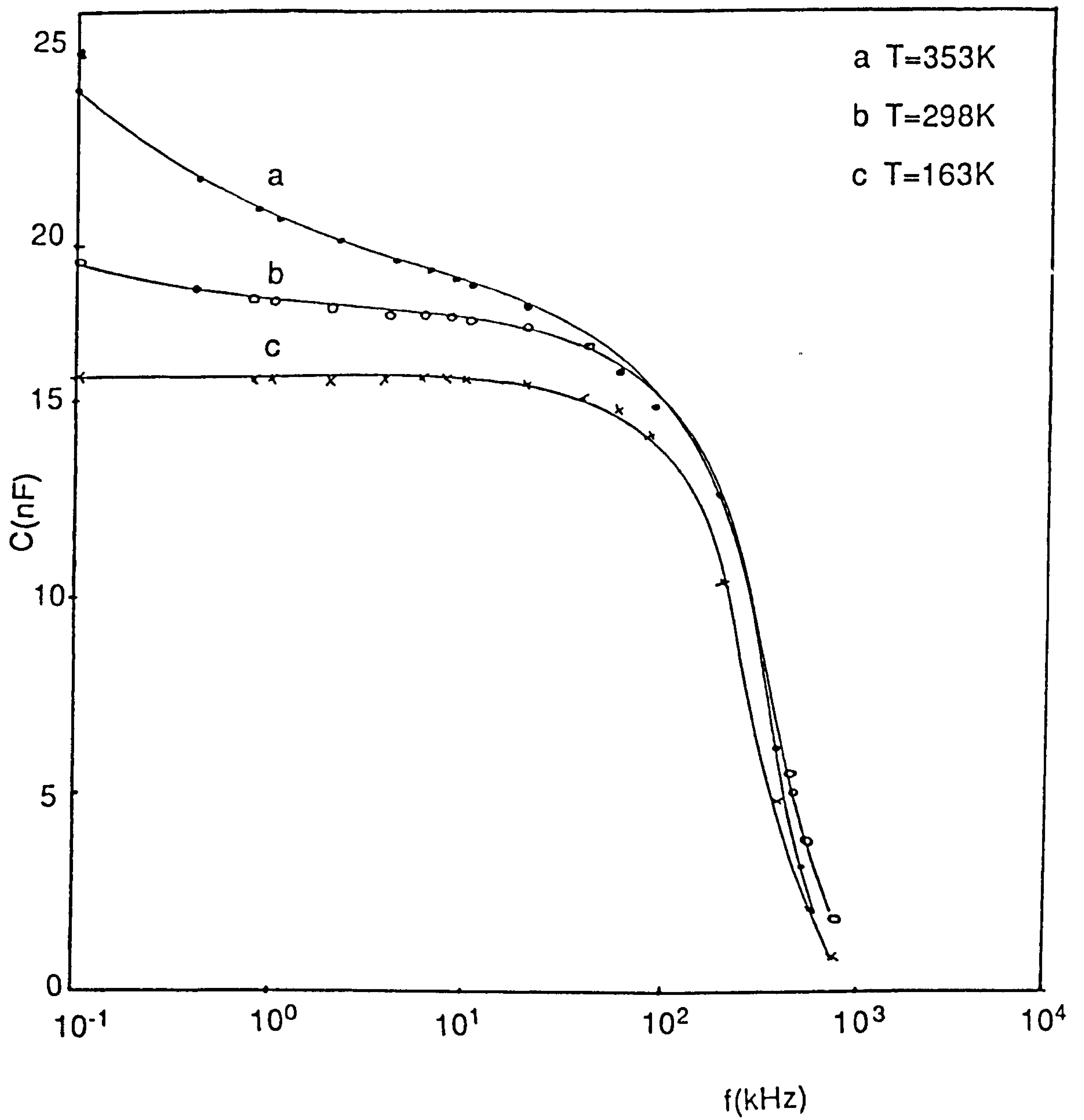

Fig. 6.3. Capacitance versus frequency for 58%WO_3/42%CeO_2 thin film.

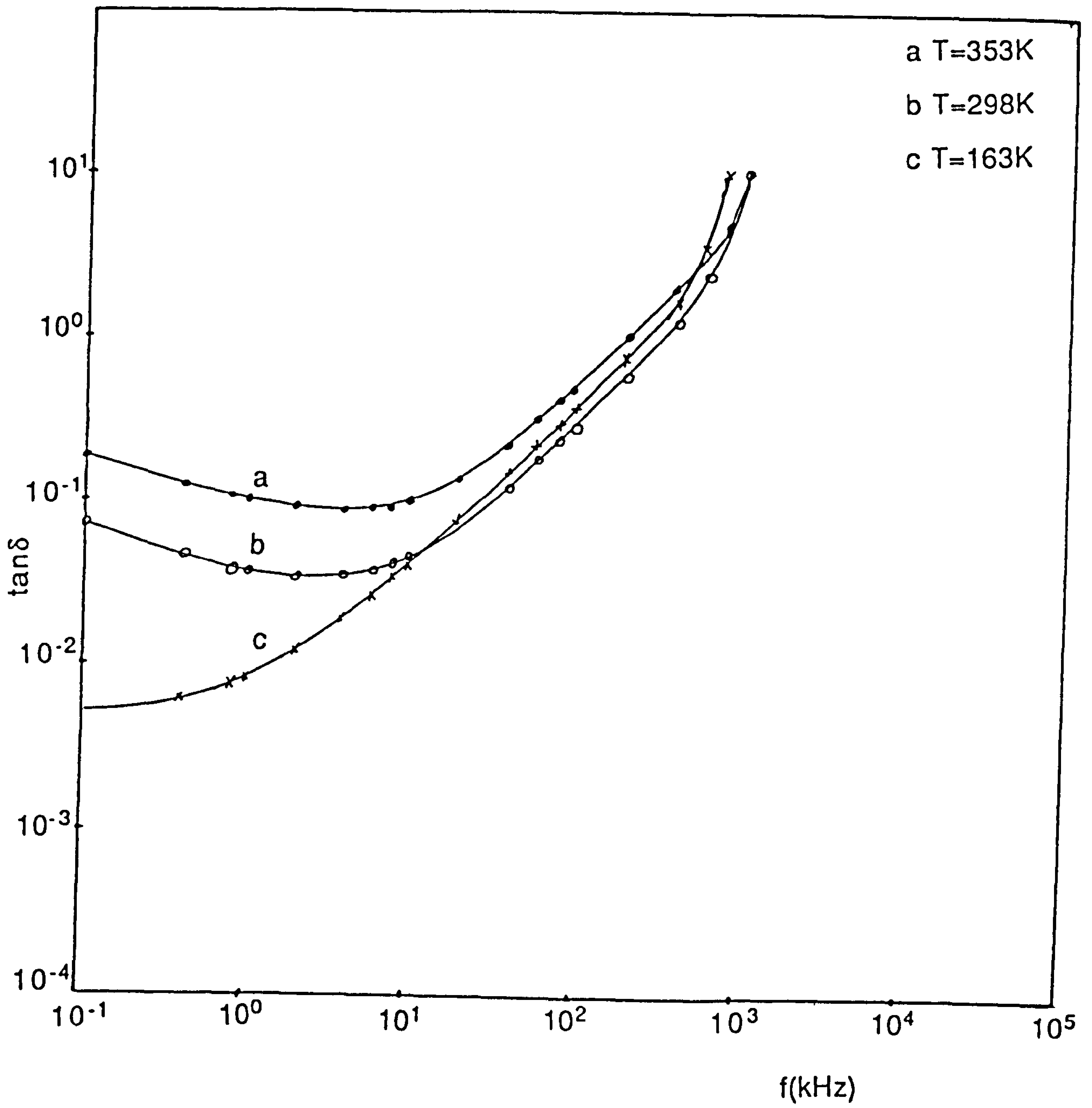

Fig. 6.4. Tanδ versus frequency for 58%WO_3/42%CeO_2 thin film.

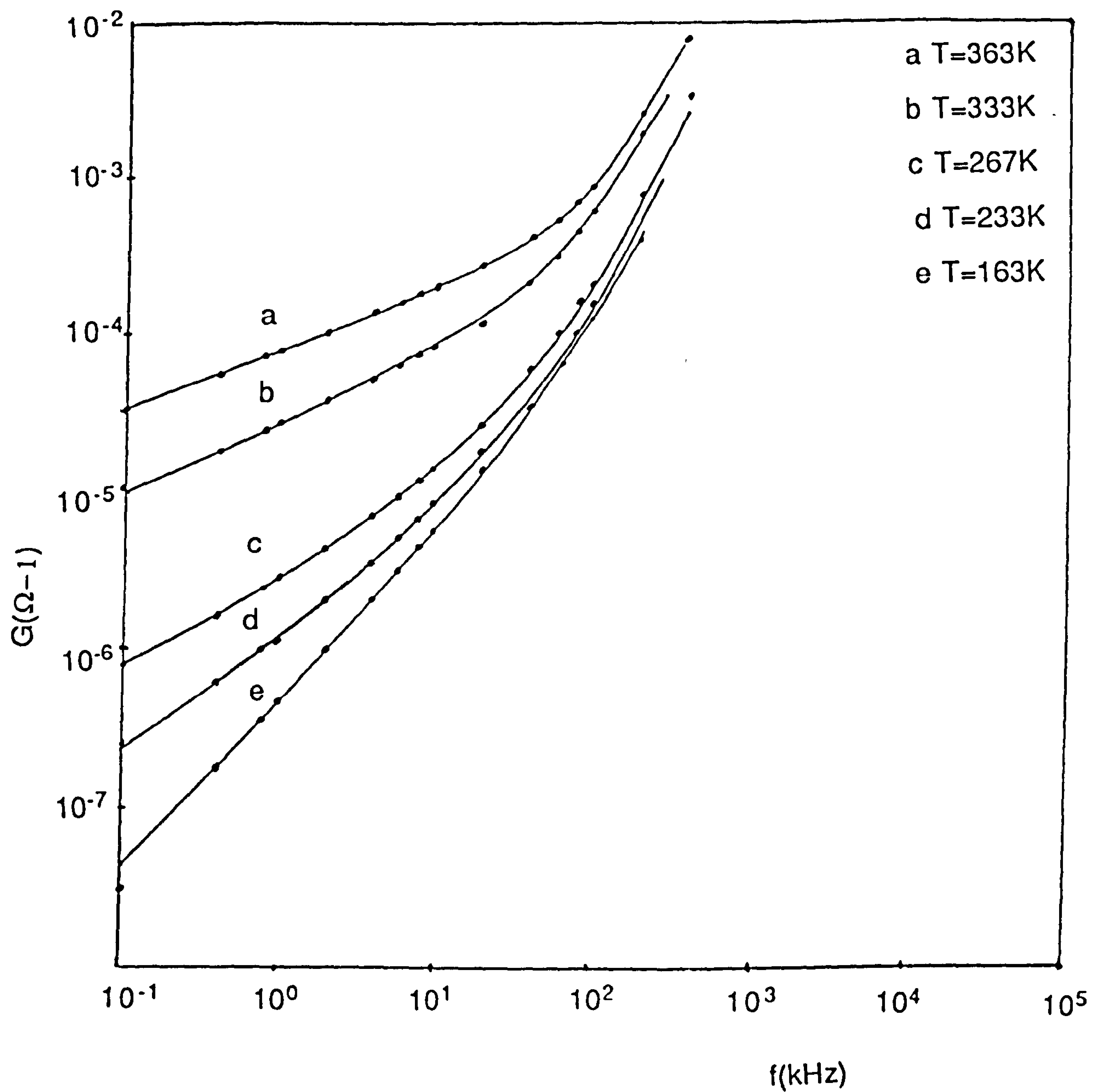

Fig. 6.5. A.C conductance versus frequency for 81%WO_3/19%CeO_2 thin film.

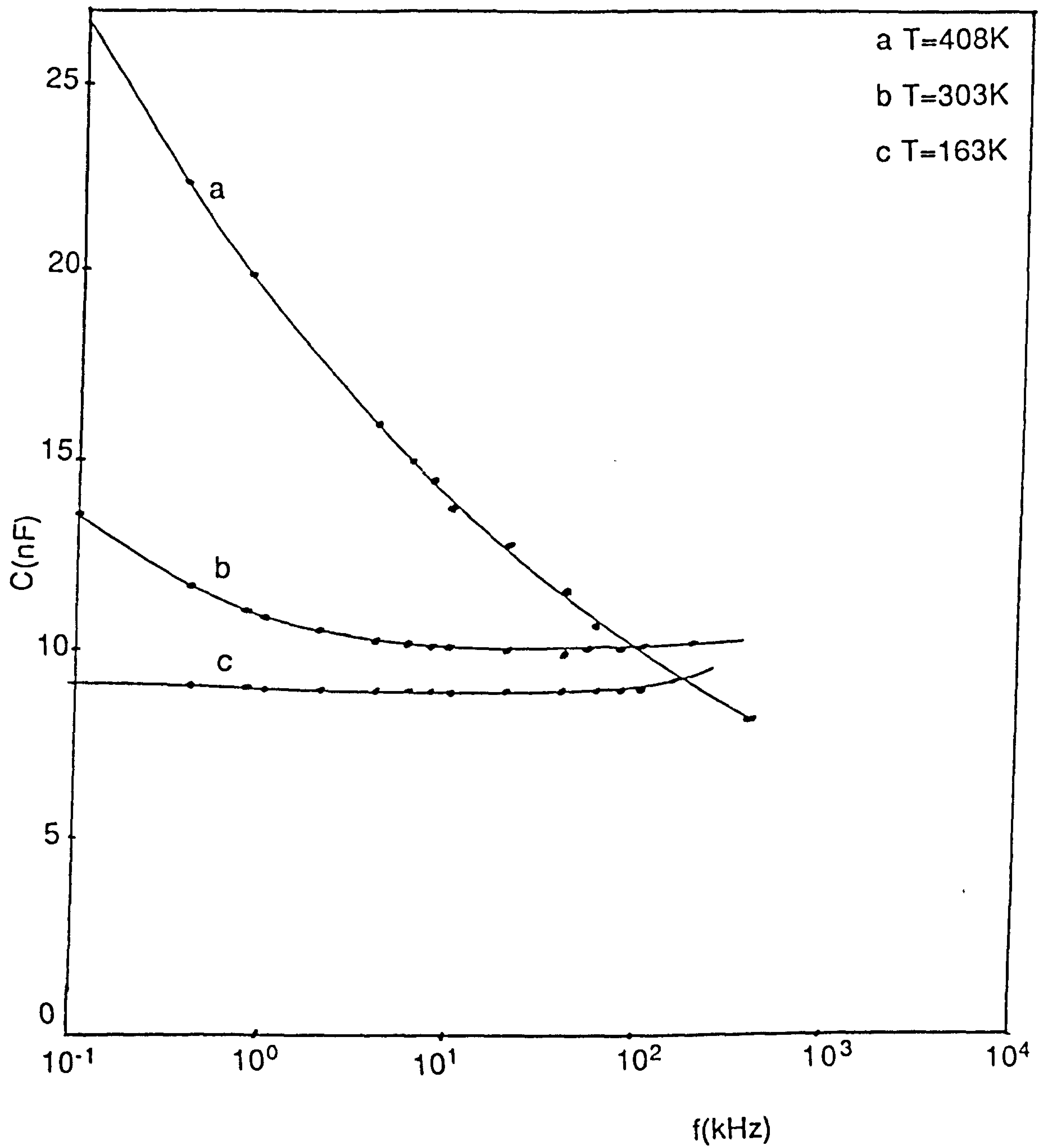

Fig. 6.6. Capacitance versus frequency for 81%WO_3/19%CeO_2 thin film.

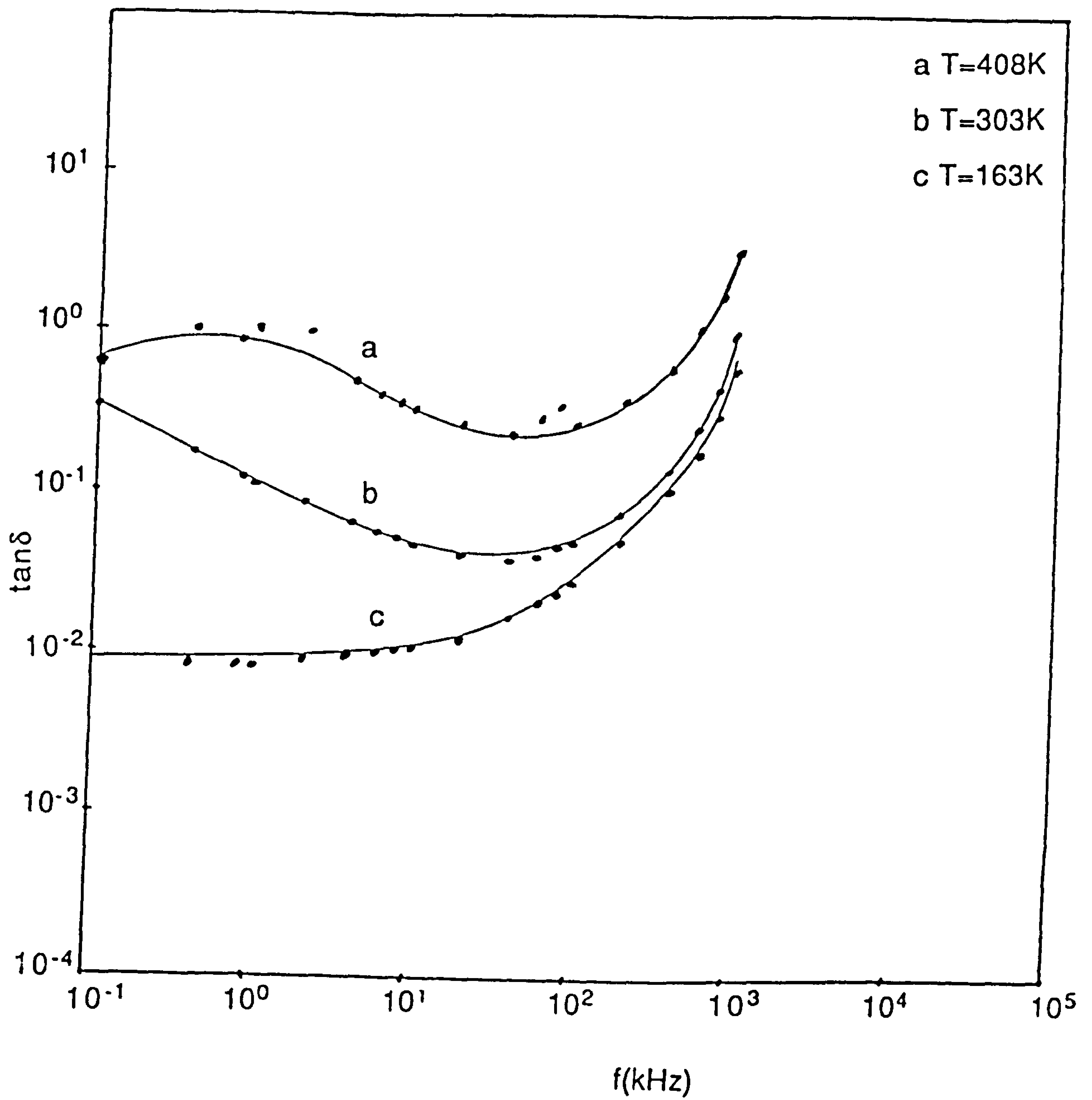

Fig. 6.7. Tanδ versus frequency for 81%WO_3/19%CeO_2 thin film.

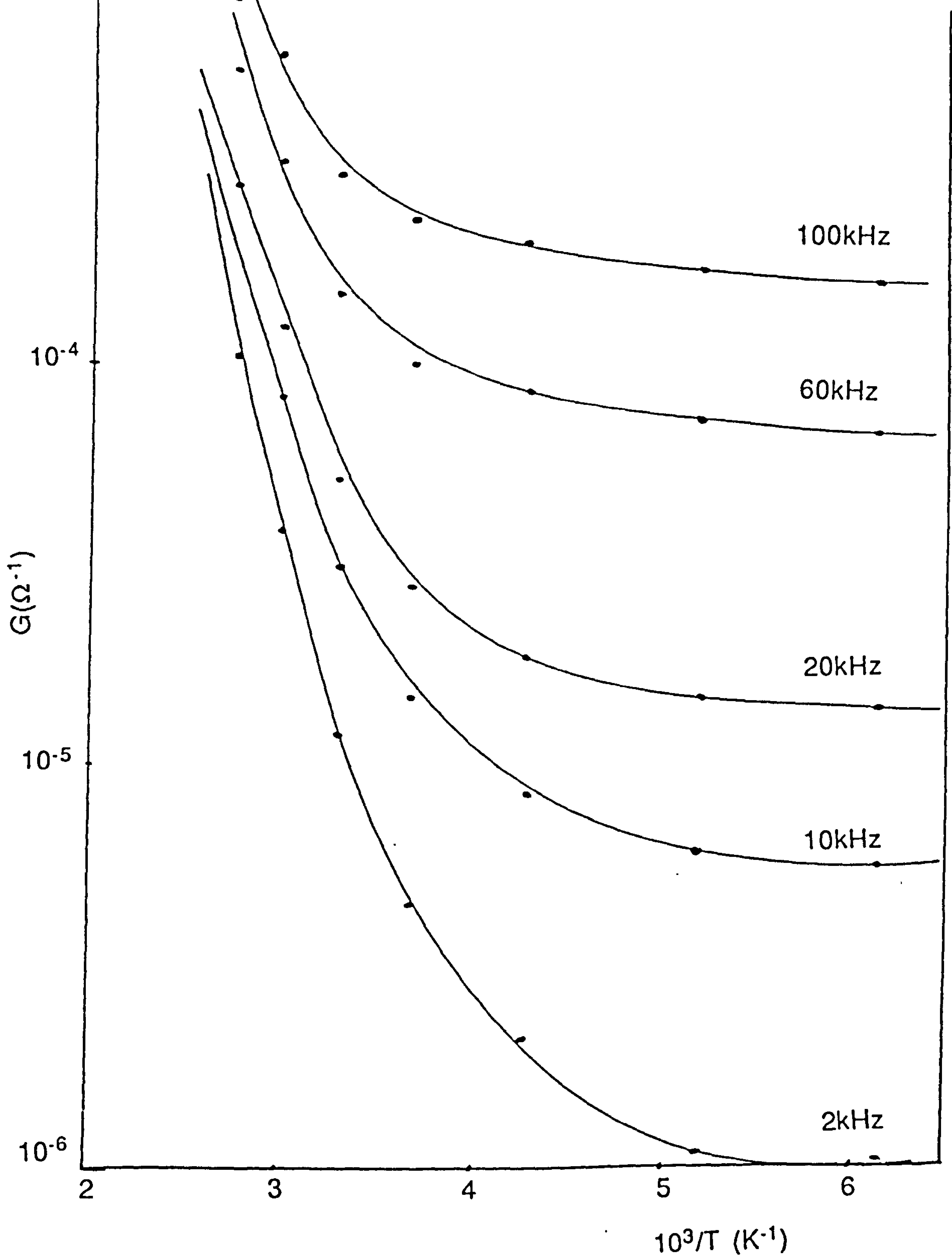

Fig. 6.8. log conductance versus1/T for 81%WO_3/19%CeO_2 (176nm thick) at given frequency.

energy by an amount of W_{po} [the hopping energy of polaron given by equation(5.3)], the polaronic effects do not substantially alter the above analysis.

6-3. OPTICAL ABSORPTION EDGE OF WO_3/CeO_2THIN FILMS

The optical transmission of amorphous WO_3/CeO_2 thin films of various compositions and for different thicknesses is illustrated in figure (6.9). It is observed that the fundamental absorption edge is sharp, very much more like that of crystalline materials. It is also observed that the positions of the absorption edges move towards longer wavelengths with the increase of CeO_2 content. As the content of cerium oxide is further increased the positions of the absorption edge return towards shorter wavelengths.

The absorption coefficient $\alpha(\omega)$ was calculated as follows;

$$\alpha(\omega) = (1/t).\ln(I_o/I). \qquad (6.7)$$

where I is the intensity of the transmitted light through the film, I_o is the intensity of the incident light and t is the thickness of the film.

If we assume that transitions of electrons occur between localized and extended states as described by Davis and Mott(1970), then the spectral dependence of the absorption coefficient will follow the square law dependence given by these

authors.

$$\alpha\hbar\omega = B(\hbar\omega - E_{opt})^2 \qquad (6.8)$$

where E_{opt} is the optical energy gap, $\hbar\omega$ is the incident photon energy and B is constant.

Figure (6.10) shows the plots of $(\alpha\hbar\omega)^{1/2}$ as a function of photon energy. It is seen that the plots are linear for higher energies which is in a good agreement with the relation (6.8) indicating that the transitions involved are non-direct.

The values of E_{opt} and B for different compositions and thicknesses are recorded in table (6.1).

Figure (6.11) shows the plot of $\log(\alpha)$ versus $\hbar\omega$. A linear region is observed in the range $2.10^3 cm^{-1}$-$4.10^4 cm^{-1}$, which means that this region is governed by a similar relation to that of Urbach(1953);

$$\alpha(\omega) \propto \exp(\hbar\omega/E_t). \qquad (6.9)$$

where α is the absorption coefficient, $\hbar\omega$ is the incident photon energy and E_t is a constant calculated from figure (6.11) as follows

$$E_t = 1/(a.\ln(10)). \qquad (6.10)$$

where a is the slope of the curve shown in figure (6.11).

The values of E_t for different compositions and thicknesses at room temperature are tabulated in table (6.1) from which it is observed that the optical energy gap is independent of the thickness for the same compositions, but there is a systematic shift of E_{opt} towards lower energies and of E_t towards higher energies as the content of CeO_2 is increased from 0% to 50%. This is in a good agreement with the C.F.O (1969), and Mott and Davis (1970) theories which suggest that the extent of the localized states near the mobility edge increases with the increase of disorder in the amorphous structure. As the content of CeO_2 is further increased, E_{opt} and E_t tend to shift back to higher and lower energies respectively. It seems that this effect is the one most probable to occur in an amorphous material made of two materials of comparable optical energy gaps and is similar to a phenomenon associated with an impurity band in a crystalline semiconductor. The localized impurity states will overlap as the concentration of the impurity is increased. However according to Mott(1968) the effect of the impurities may be neglected in the amorphous state, but they contribute only to the disorder. Therefore by analogy, it may be assumed that CeO_2 contributes to the disorder and thereby creates localized states in the gap. As the content of CeO_2 is increased some of the localized states overlap and hence their effective density is reduced just as in the case of the impurity states. Thus the value of E_t decreases and E_{opt} returns back to higher energies. This effect has been also observed in other mixed oxide thin films [Al-Ani and

Hogarth(1984), Islam and Hogarth (1987), Ilyas and Hogarth (1983), and Arshak and Hogarth (1986)].

The values of the constant B given by equation (6.8) are of the order of $10^5 cm^{-1} eV^{-1}$ which is in good agreement with the theoretical value [Davis and Mott (1970)].

In the above arguments we have assumed that E_t depends on the lack of the long-range order. However this may be not the case in certain materials as is discussed in Chapter 7-3.

Table (6.1). Values of E_{opt} and E_t at room temperature for various compositions and thicknesses of WO_3/CeO_2 thin films.

%mol.WO_3	E_{opt}(eV)	E_t(eV)	t(nm)
100	3.25	0.20	294
97	2.91	0.20	193
81	2.81	0.26	294
81	2.81	0.26	176
72	2.78	0.24	182
48	2.81	0.10	104

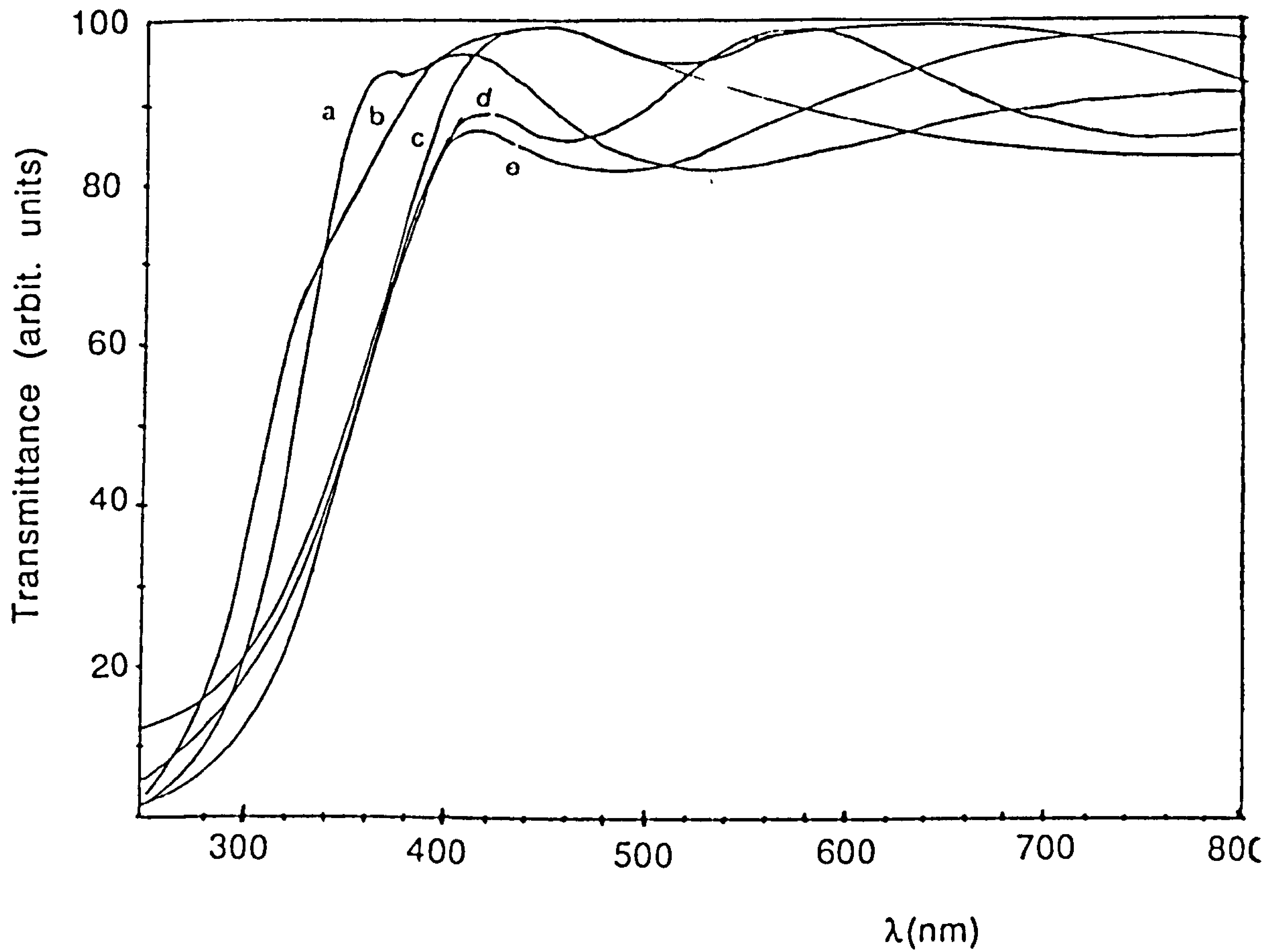

Fig. 6.9 Optical transmittance as function of wavelength for different compositions of WO_3/CeO_2 thin films.

a) 100%WO_3 (294nm thick)

b) 97%-- (193nm thick)

c) 48%-- (104nm thick)

d) 81%-- (294nm thick)

e) 81%-- (176nm thick)

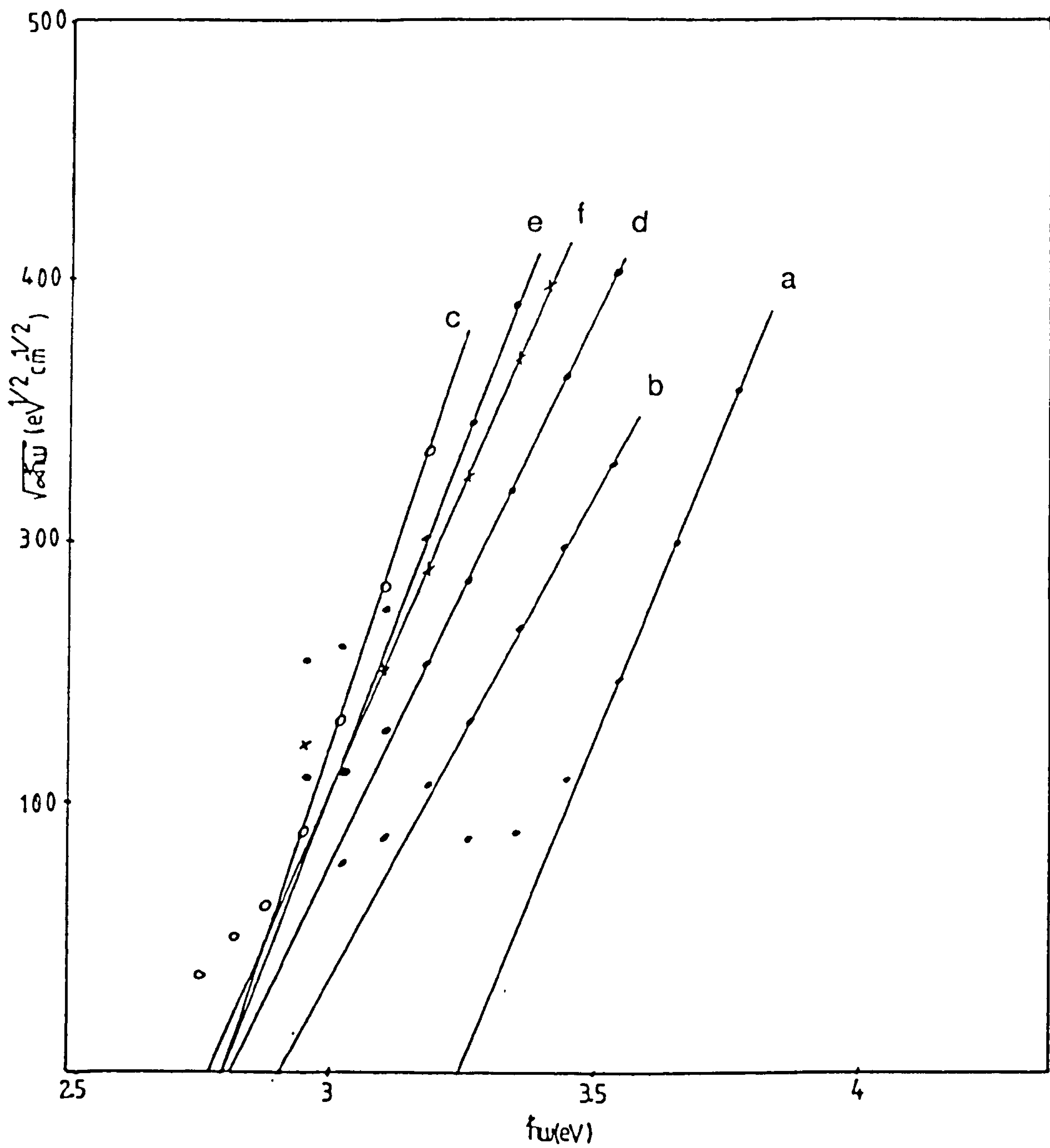

Fig. 6.10. $(\alpha\hbar\omega)^{1/2}$ versus photon energy for different compositions of WO_3/CeO_2 thin films.

a) 100% WO_3 (294nm thick).

b) 97%-- (193nm thick).

c) 48%-- (104nm thick).

d) 81%-- (294nm thick).

e) 81%-- (176nm thick).

f) 72%-- (182nm thick).

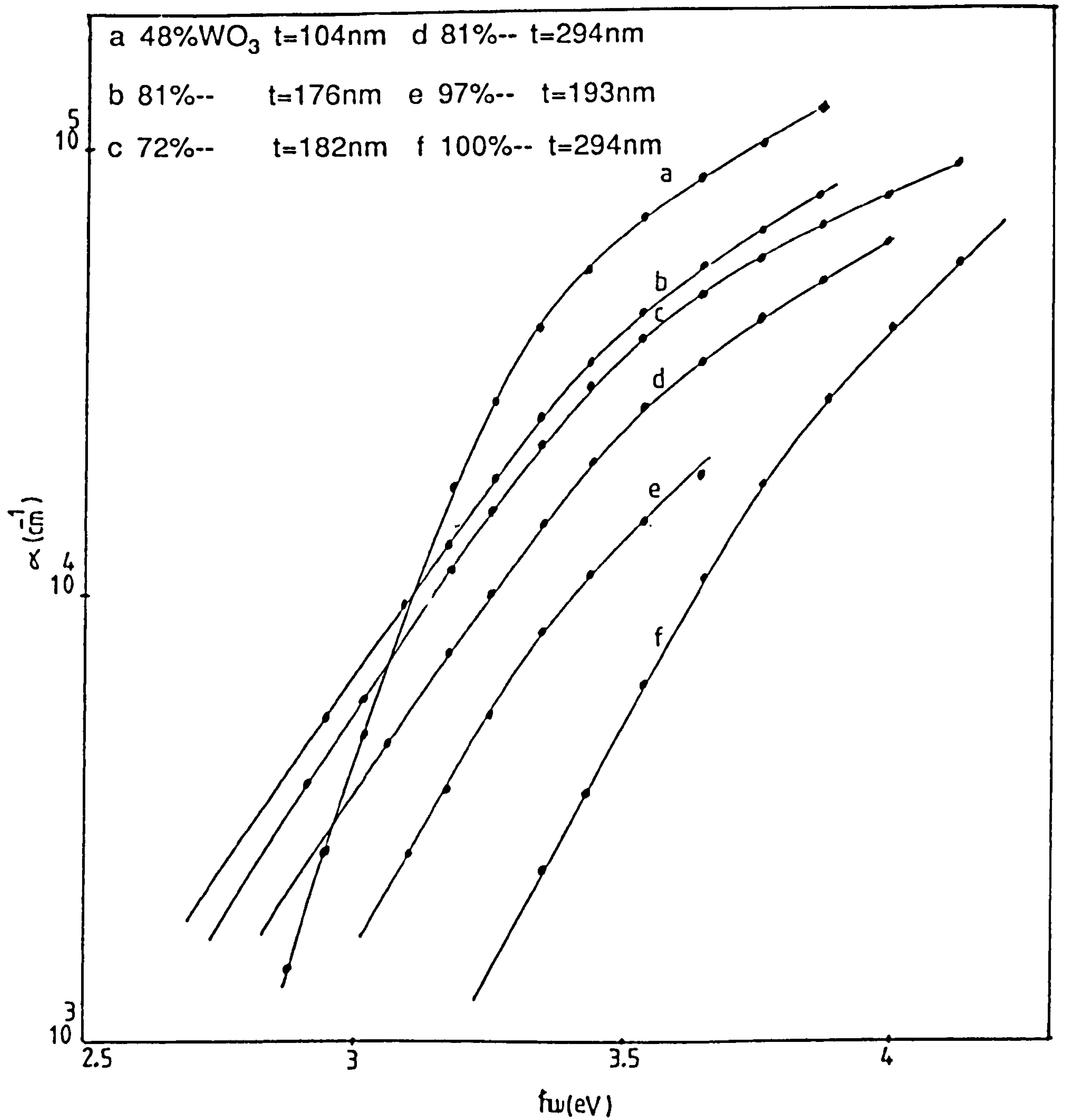

Fig. 6.11. log(α) versus photon energy for different compositions of WO_3/CeO_2 thin films.

6-4 ELECTRON MICROSCOPE STUDY OF WO_3/CeO_2

The film of WO_3/CeO_2 was prepared on a carbon-coated mica substrate held at room temperature and was studied in the transmission electron microscope. The electron micrographs and the diffraction patterns were obtained at room and high temperatures. The diffraction pattern and the electron micrograph at room temperature are shown in figure (6.12) and those at high temperature are shown in figures (6.13) for a WO_3/CeO_2 thin film. Figures (6.12) and (6.13) show that the WO_3/CeO_2 thin film has an amorphous structure at both room and high temperatures and no structural phase changes have been observed as the temperature was increased. However, the electron micrograph shown in figure (6.13) for the same sample shows a random distribution of small metallic islands about the same shape. The growth of these islands could be the main reason of the observed decrease of the d.c conductivity as the temperature is raised. This phenomenon is expected to occur in amorphous materials containing substantial amounts of other transition metal ions. In comparing these results to those of V_2O_5/TeO_2 (Chapter 5) one can say that the amorphous structure of WO_3/CeO_2 is thermally more stable than that of V_2O_5/TeO_2 thin films.

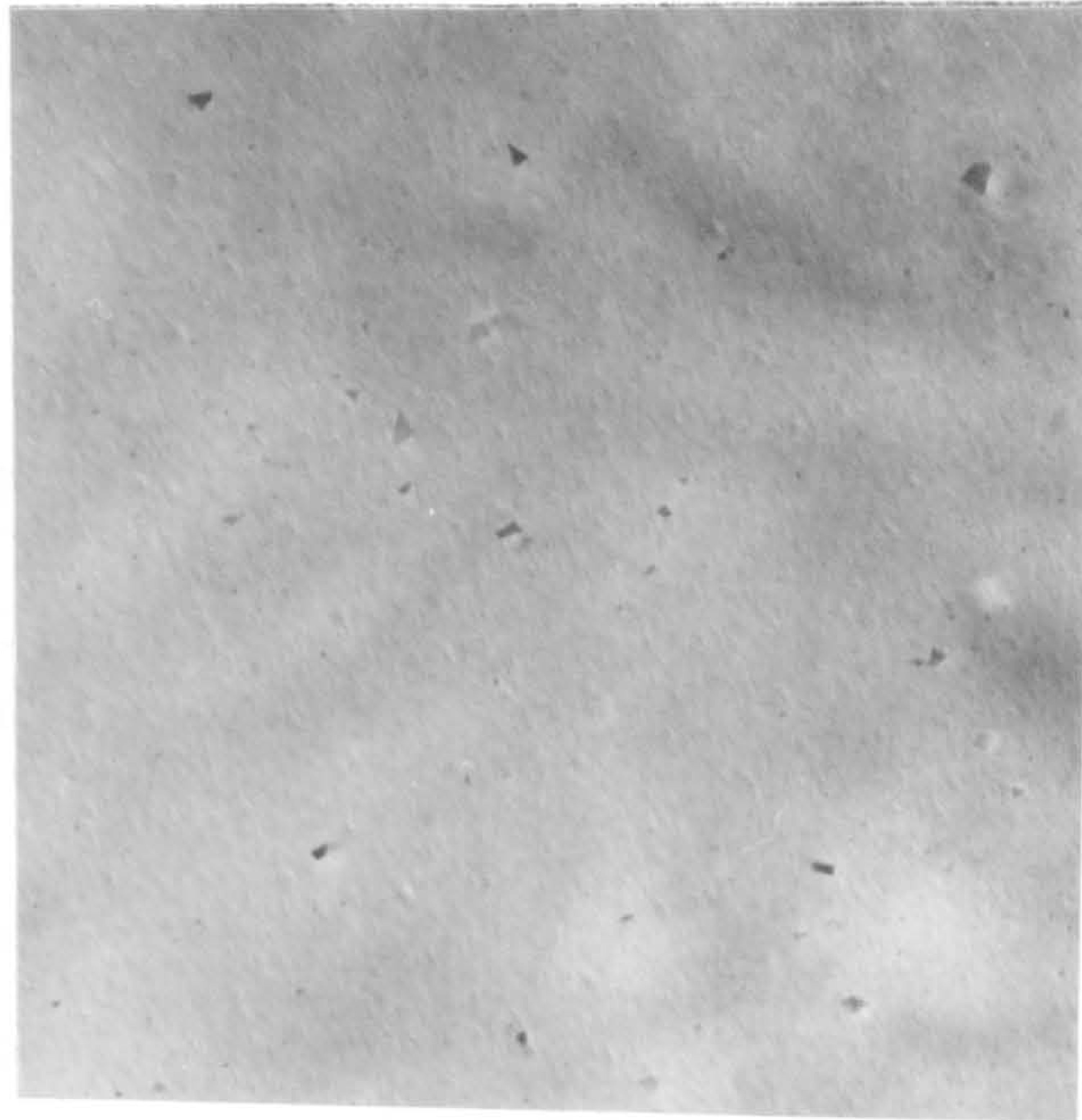

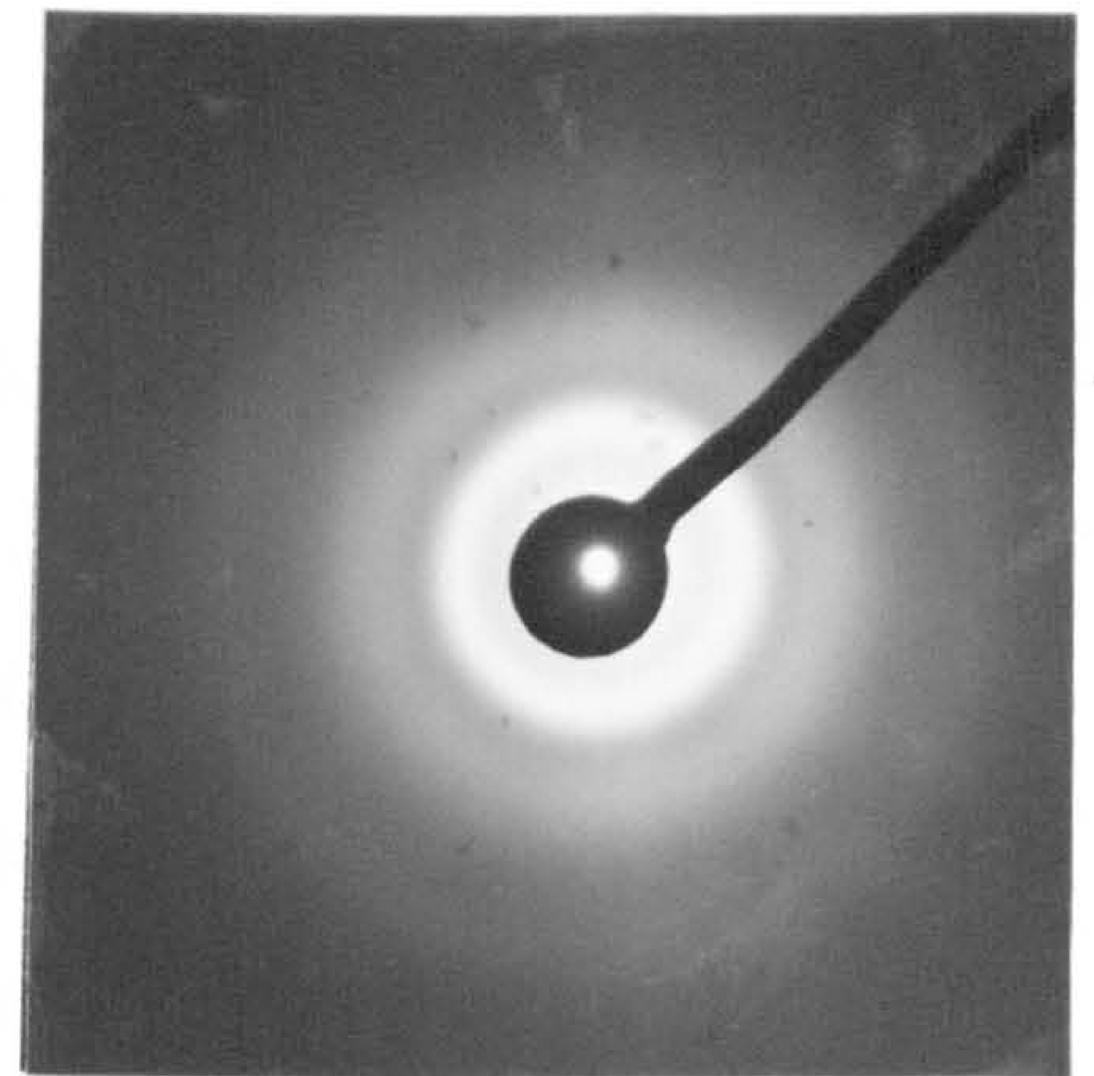

Micrograph Diffraction pattern

Fig. 6.12. Electron micrograph and diffraction patterns of WO_3/CeO_2 thin film at room temperature.

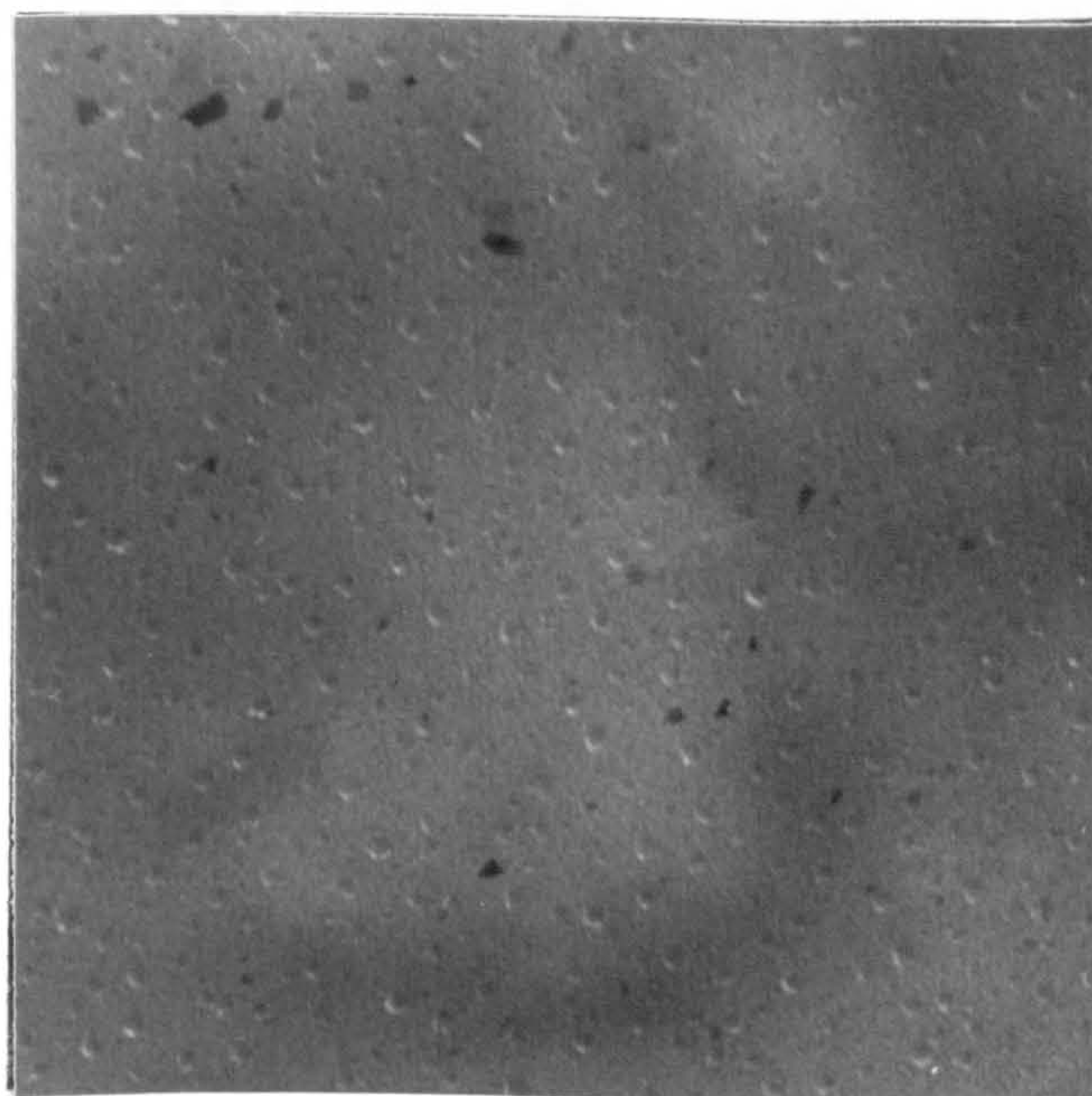

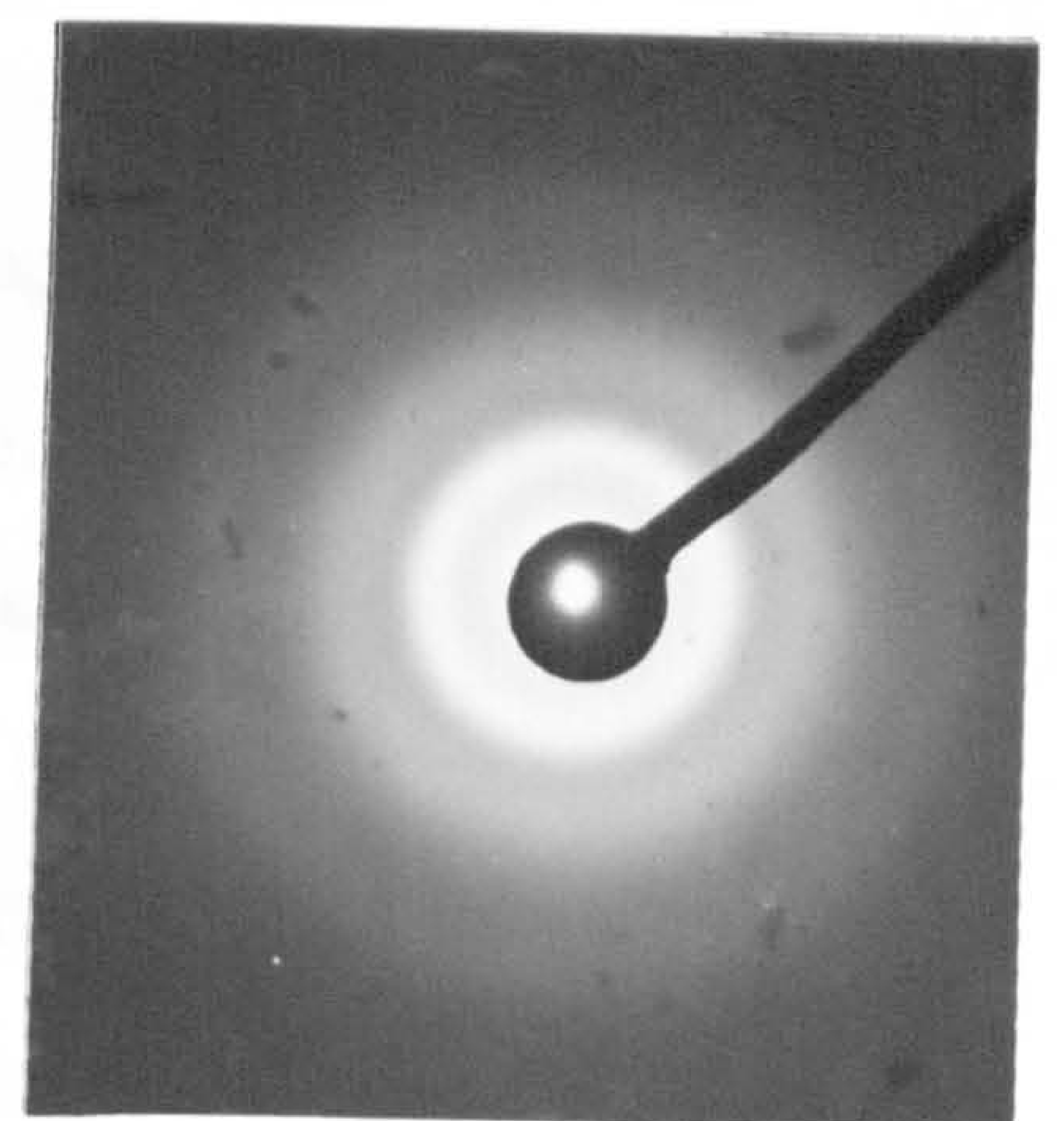

Micrograph Diffraction pattern

Fig. 6.13. Electron micrograph and diffraction patterns of WO_3/CeO_2 thin film after annealing

CHAPTER 7. RESULTS AND DISCUSSION OF SiO/TeO_2 THIN FILMS.

7-1. INTRODUCTION.

In recent years, the d.c and a.c conductivities in a number of thin oxide films have been investigated. Much experimental data has been gathered, but the conduction mechanism itself in these oxide films, is not yet completely understood [Jonscher(1967)]. The purpose of this study is to describe the electrical and optical properties of thin co-evaporated SiO/TeO_2 oxide films for various compositions and to try to compare these results with those of V_2O_5/TeO_2 and WO_3/CeO_2 thin films. The films studied in this Chapter with different compositions and thicknesses are listed in table(7.2)

7-2. A.C AND D.C ELECTRICAL CONDUCTIONS OF SiO/TeO_2

Figures (7.9), (7.10), (7.11) and (7.12) show the capacitance dispersions at various tempertures and different thicknesses of SiO/TeO_2 thin films. Over the frequency range of 0.1kHz to 400kHz and at reduced temperatures the capacitance remains constant, and at high temperatures and low frequencies it shows a slight increase as the frequency is decreased. This could be due to a space charge at the metal-insulator interface.

The conductance shown in figure (7.3) shows two distinct dispersive regions. There is a frequency region below 10^2kHz

where the log conductance shows a linear dependence on log frequency and a slight dependence on temperature. This region is also observed in figures (7.6) and (7.8). This mechanism of conduction is due to hopping of carriers between localized states [Pollak and Geballe(1961)], and the other region is observed above 10^2kHz (fig(7.3)) where the conductance shows a square-law dependence on frequency and it is insensitive to temperature. This mechanism of conduction is also due to hopping of carriers and it is supposed to be confined to immediate neighbouring sites, giving rise to the square law frequency dependence and conductance almost independent of the temperature. These results are very similar to those obtained on silicon oxide by Argall and Jonscher(1968). This square law behaviour is different from that shown in figures (7.6) and (7.8). It is seen in these figures that at frequencies above 10kHz and at elevated temperatures the conductivity increases quickly as the temperature is increased. Thus, the carriers are thermally assisted to overcome potential barriers which may be caused by structural inhomogeneities in the sample or may be due to the presence of high concentrations of metal ions in the stucture.

In all samples at low frequencies, it was found that the a.c conductivity varies as ω^s, where ω is the angular frequency and s is a quantity whose value is close to, but less than, unity. This frequency dependence of the a.c conductivity has been observed experimentally in many amorphous semiconductors and it is interpreted in terms of model that considers conduction to occur by means of thermally assisted transport between localized

states in the gap. The theory to describe this frequency dependence was first proposed by Pollak and Geballe(1961) and it was later modified by Austin and Mott(1969) and further by Pollak(1971) and many others. According to this model, Austin and Mott(1969) derived a formula for the a.c conductivity given by

$$\sigma(\omega)=(\pi/3)[N(E_F)]^2kTe^2\alpha^{-5}\omega[\ln(\nu_{ph}/\omega)]^4 \qquad (7.1).$$

where $N(E_F)$ is the density of states at the Fermi level, α^{-1} is the spatial extension of the electron wave function $\exp(-\alpha r)$ associated with the localized states and ν_{ph} is a characteristic phonon frequency.

Equation(7.1) of the a.c conductivity is applied to tunnelling through a potential barrier. Pike(1972) has considered a case in which hopping between localized sites is over potential barriers with a height distribution caused by the random spatial distribution of these sites. This leads to ω^s behaviour at high frequencies with s decreasing linearly with temperature. Thus, he has given a model according to which the temperature variation of the exponent s can be approximated by the following equation.

$$1-s=6kT/W \qquad (7.2)$$

where W is a potential barrier, k is the Boltzmann constant and T is the absolute temperature.

The equation(7.2) suggests that a plot of (1-s) versus T should be

linear and pass through the origin. This model may be applied to 87%SiO/13%TeO_2 where the effect of inhomogeneities may be neglected and a gradual increase in the value of s with the decrease in temperature has been observed. Figure(7.6) shows the plot of log conductance versus log frequency for an 56%SiO/44%TeO_2 amorphous thin film. It is observed that the exponent s is independent of temperature at least up to 373K. Thus, the model given by Pike(1972) may be not applied to this sample (fig(7.6)).

Elliott(1977) proposed a theory which is an extension of that developed by Pike(1972). In this theory, hopping of carriers between two sites is over a barrier separating them, rather than tunnelling through this barrier. In this case the expression of the a.c conductivity is slightly different from that given by eq.(7.1) and it is expressed [Elliott(1977)] as

$$\sigma(\omega)=(\pi^2N^2\varepsilon_e/24)\,(8e^2/\varepsilon_e w)^6\omega^s/\tau_0^{(1-s)}. \qquad (7.3).$$

where N is the concentration of localized sites, ε_e is an effective dielectric constant and it can be taken as the bulk dielectric constant if the distance between the two localized sites is sufficiently large. The exponent s is given by Pike's equation(7.2), τ_0 is of the order of an atomic vibration period and W is given by equation(7.2) and it is approximately equal to the band gap of the material.

The Elliott model was applied by Islam and Hogarth(1987) to SiO/SnO_2 amorphous thin film to explain their a.c results.

According to Mott *et al* (1975) the energy W given by equation(7.2) can be expressed as

$$W=B+W_2-W_1. \qquad (7.4).$$

where B is the band gap of the material, and W_1 and W_2 are approximately the distortion energies associated with the neutral D and the charged D^+ dangling bonds. The nature of these bonds was discussed by Mott *et al* (1975).

If we assume that these two quantities W_1 and W_2 are equal, then the energy given by equation(7.2) will be equal to the band gap B.

By substituting the optical energy gap of $87\%/SiO/13\%TeO_2$ which is about 2.25eV, in equation(7.2) at T=298K, we obtained a value of the exponent s equal to 0.9 which is quite close to the experimental value 0.87 of the slope (at T=298K) of figure (7.3).

It seems that the model of Pike as well as of Elliott can be applied to SiO/TeO_2 if the sample is homogeneous and if the content of TeO_2 is low in the structure.

Figures (7.1) and (7.7) show the plots of log(I) versus log(V) for various compositions and different temperatures. It is seen that the I-V characteristic of $87\%SiO/13\%TeO_2$ is linear in the voltage range 0.1-2V with a slope equal to 1 indicating that ohmic conduction is dominant. On the other hand, in the same voltage range, it is seen that the I-V characteristic of a $56\%SiO/44\%TeO_2$

sample shown in figure (7.7) is roughly exponential, suggesting that the slope is not constant and thus, the power law dependence of current upon voltage due to space charge at the interface, may be ruled out. In fact it has been pointed out by Mead (1962) that, provided the dielectric sample is sufficiently thick, the I-V characteristic should be limited by the bulk properties rather than by conditions at the interfaces. The same idea had already been proposed theoretically by Rose (1955) and there are various experimental results which support this point of view. Therefore, the I-V characteristic of SiO/TeO_2 with a thickness in the range 1.5-5μm, is not affected by any effect which is due to interfaces such as space charge or Schottky effects. By comparing the I-V characteristics of 87%SiO/13%TeO_2 shown in figure (7.1) to that of 56%SiO/44%TeO_2 in figure (7.7) we may suggest that the exponential increase of the current with the voltage is caused by the presence of the high content of TeO_2 in the structure. This type of behaviour is also observed in amorphous V_2O_5/TeO_2 thin films (Chapter 5). It is thought that it may be associated with a type of conduction dominated by the Poole-Frenkel effect, that is, the electrons in the trapping centres are thermally excited into the conduction band due the high fields and high temperatures. Therefore, we have plotted log(I) versus $V^{1/2}$ in figures (7.2) and (7.4). These plots show straight lines at high fields indicating that an equation of the form

$$I \propto \exp(\beta V^{1/2}) \qquad (7.5)$$

is obeyed. β is a constant depending on temperature and in the case of Poole-Frenkel effect it is given by

$$\beta=\beta_{PF}/kTd^{1/2}. \qquad (7.6)$$

where k is the Boltzmann constant, T the absolute temperature, d the thickness of the film and $\beta_{P.F}$ is the barrier lowering coefficient and it is given theoretically by the following relation.

$$\beta_{PF}=(e^3/\pi\varepsilon_0\varepsilon_r)^{1/2} \qquad (7.7)$$

where e is the electron charge and ε_r is the relative dielectric constant which can be calculated from the capacitance at high frequencies as follows

$$\varepsilon_r=Cd/\varepsilon_0 s \qquad (7.8)$$

where d and s are the thickness and the surface area respectively of the specimen.

The experimental values of the field-lowering coefficient were calculated from the slope of the log(I) versus $V^{1/2}$ plots and the theoretical values were calculated by substituting in equation(7.6) the value of ε_r given by equation(7.7). The experimental and the theoretical values of β_{PF} are listed in table(7.1) for comparison.

Table (7.1). Experimental values of β_{exp} given by eq.(7.6) at different temperatures for 87%SiO/13%TeO_2 thin film (356nm thick).

The value of $\beta_{P.Fth}$ calculated from eq.(7.7) is weakly dependent on temperature and is approximately equal to $29X10^{-5}$(eV $V^{-1/2}cm^{1/2}$).

T(K)	$\beta_{exp}(10^{-5}eV\ V^{-1/2}\ cm^{1/2})$.
298	32
318	35
335	41
361	61

Table (7.2). Experimental values of the optical gap E_{opt} and the constant B given by eq.(7.9) for various compositions of SiO/TeO_2 thin films with different thicknesses.

%mol.SiO	Thickness(nm)	E_{opt}(eV)	$B(10^5eV^{-1}cm^{-1})$
30	199	1.95	1.10
56	199	2.10	0.97
79	328	2.70	0.85
80	183	2.40	4.44
87	356	2.25	1.40
93	252	2.30	2.50

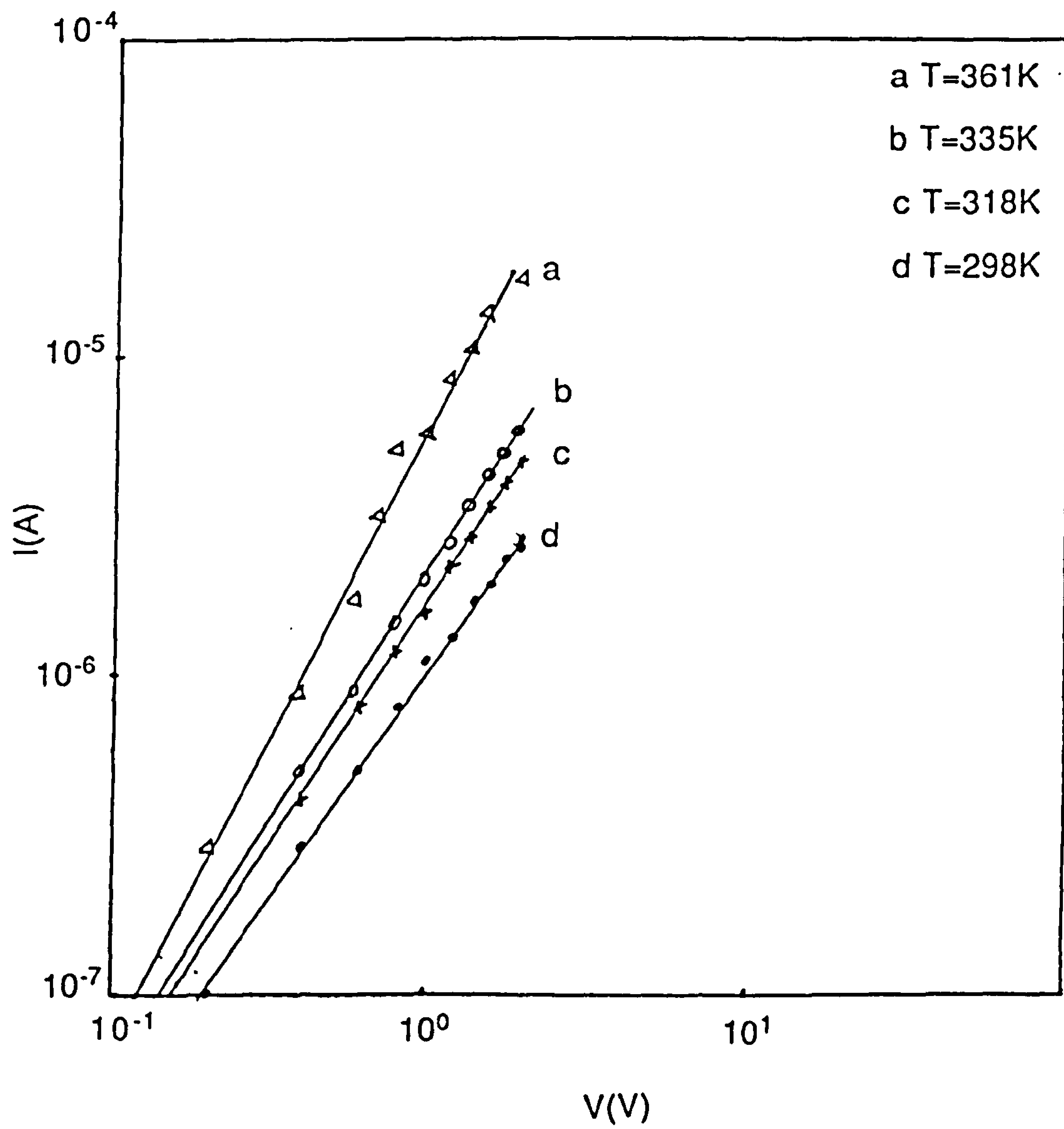

Fig. 7.1. I-V characteristics of 87%SiO/13%TeO_2 thin film.

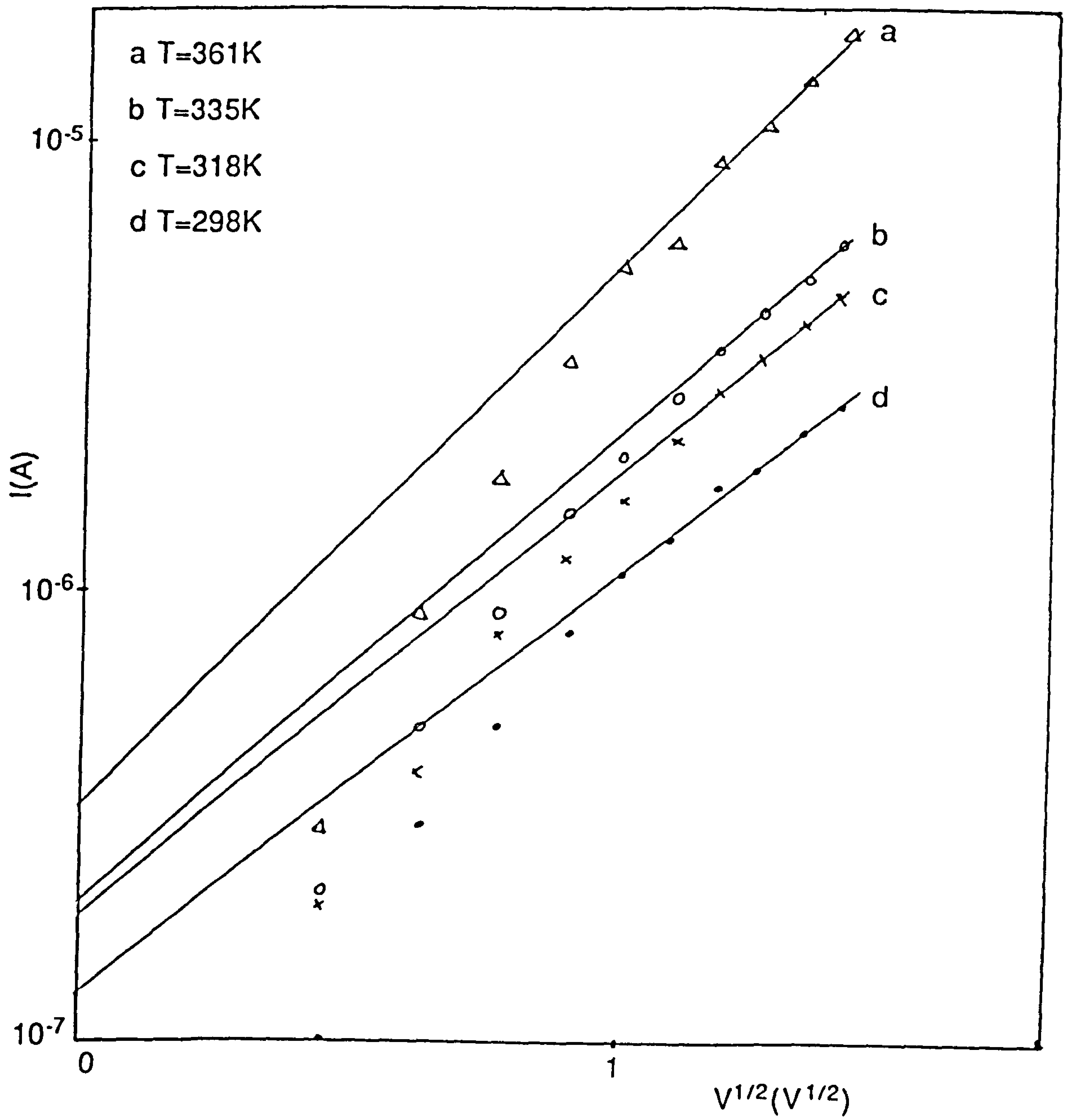

Fig. 7.2. log(I) versus $V^{1/2}$ for 87%SiO/13%TeO_2 thin film.

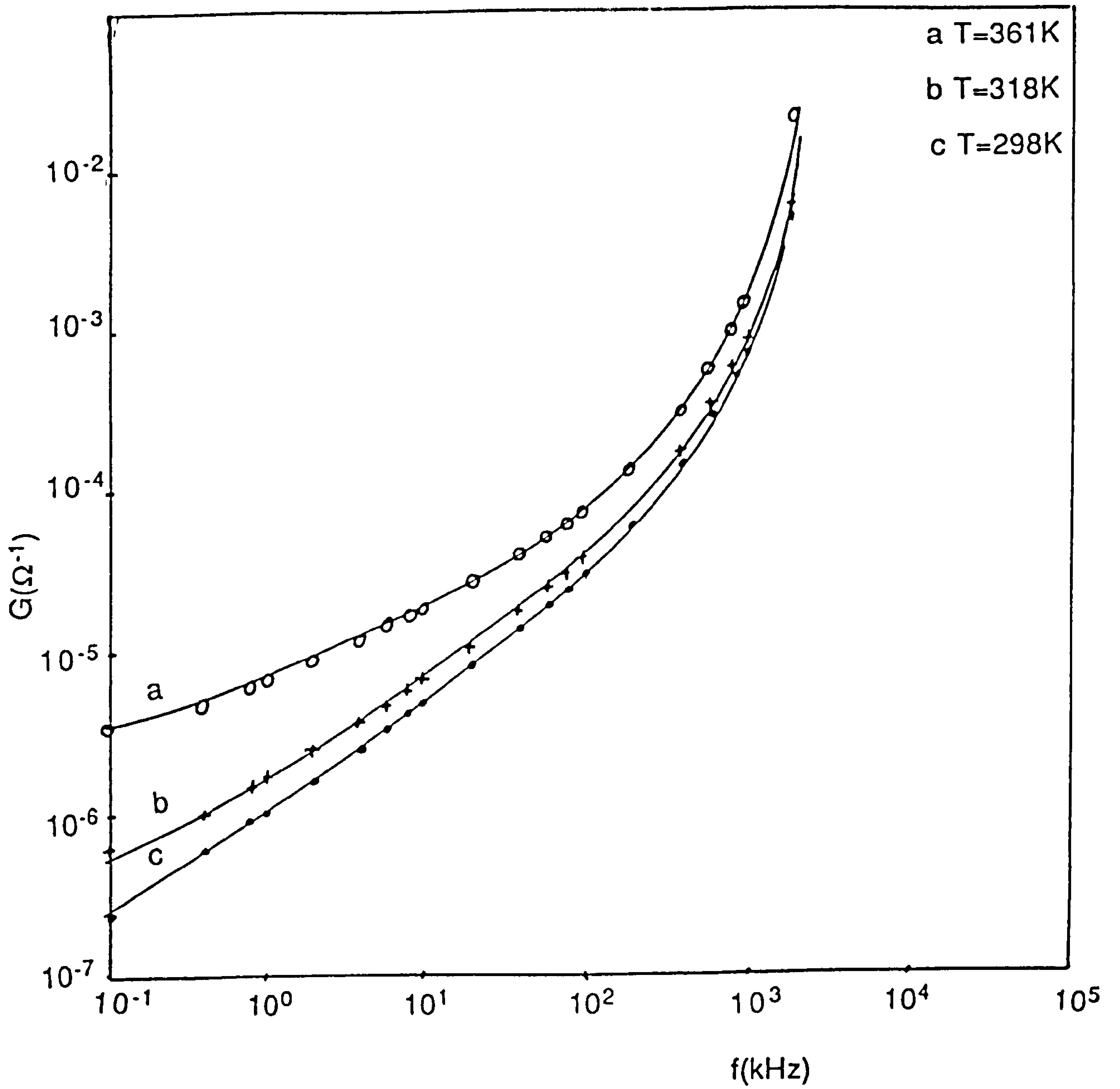

Fig. 7.3. A.C conductance versus frequency for 87%SiO/13%TeO_2 thin film.

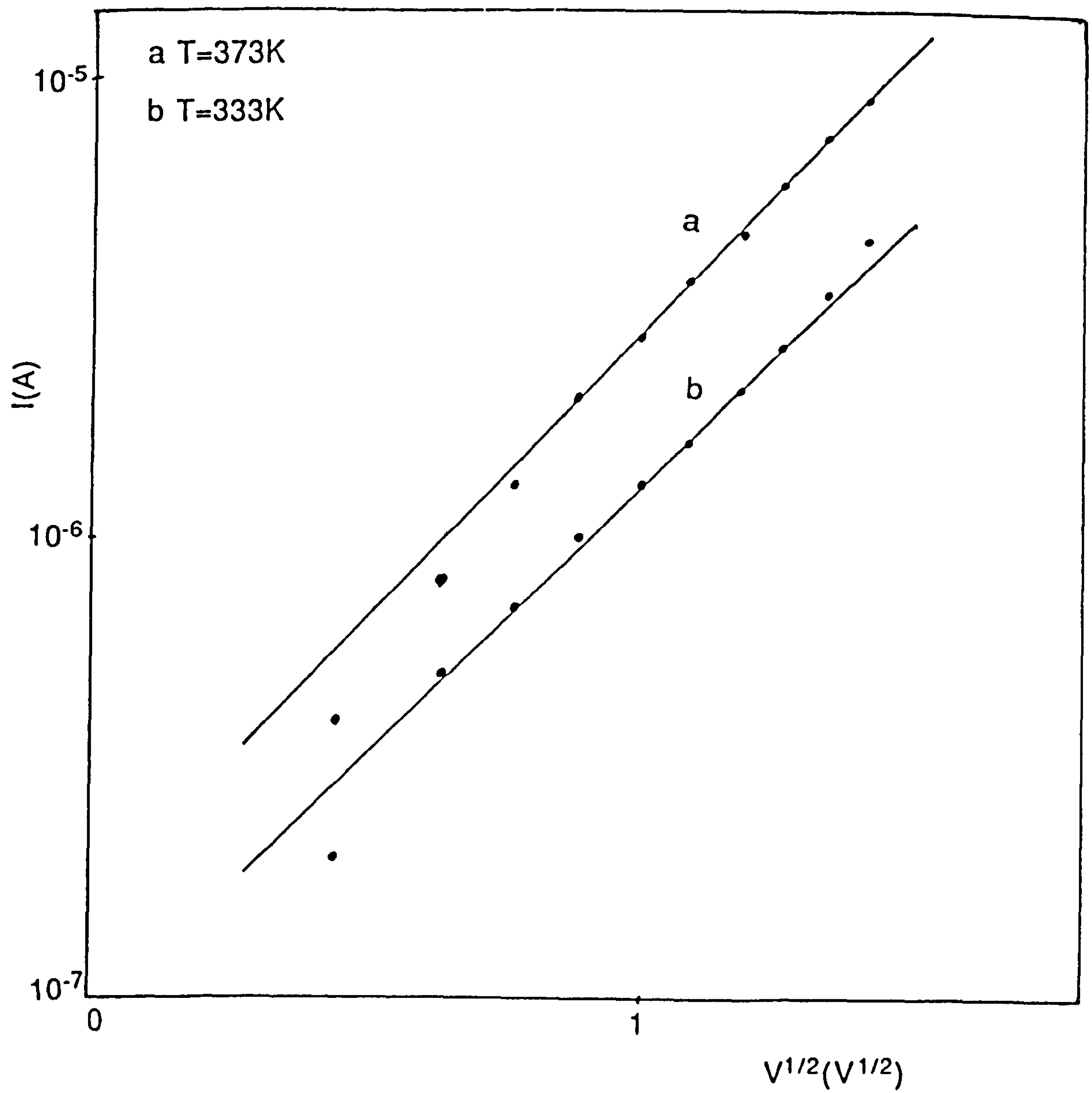

Fig. 7.4. log(I) versus $V^{1/2}$ for 56%SiO/44%TeO_2 thin film.

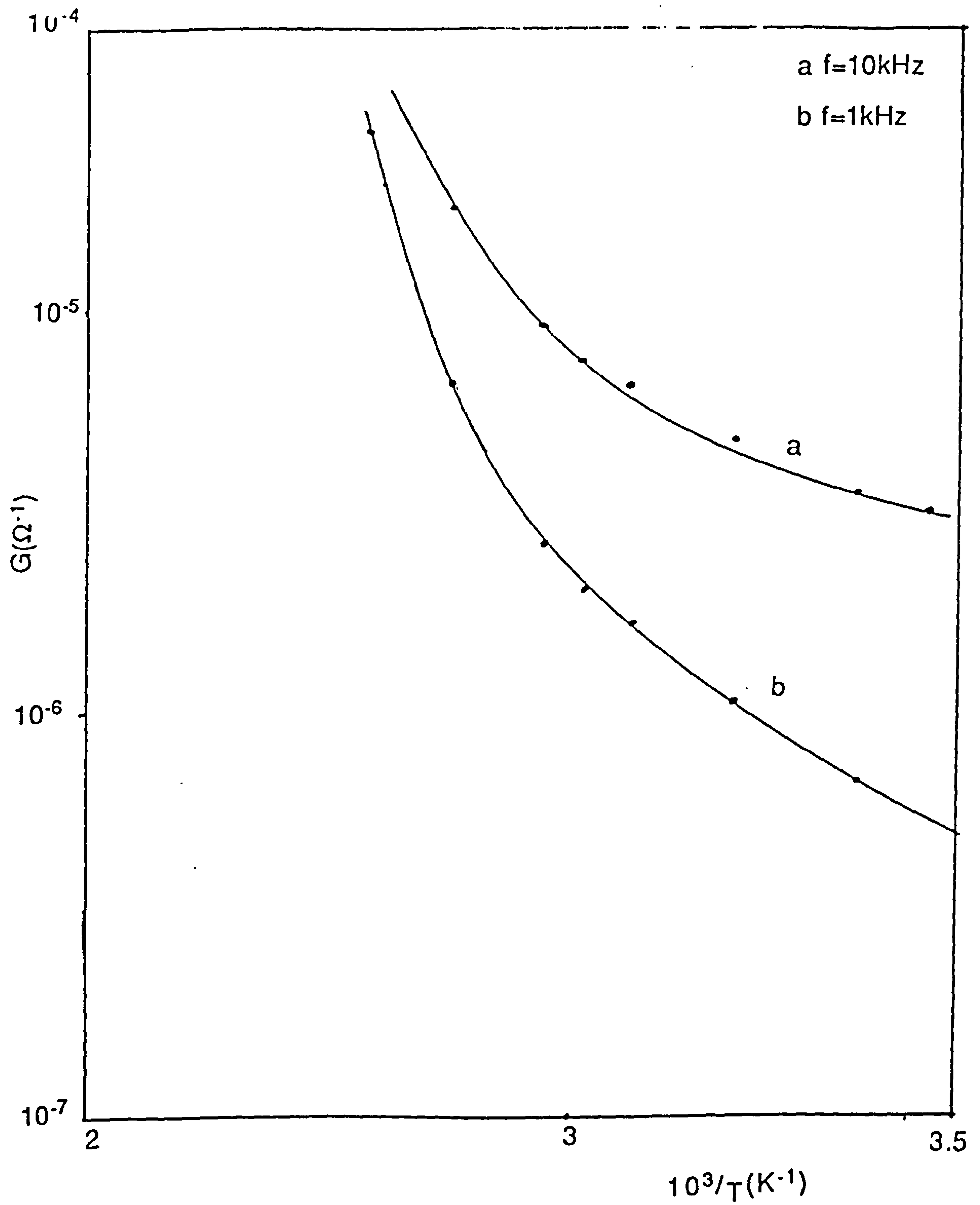

Fig. 7.5. log(G) versus 1/T for 87%SiO/13%TeO_2 thin film.

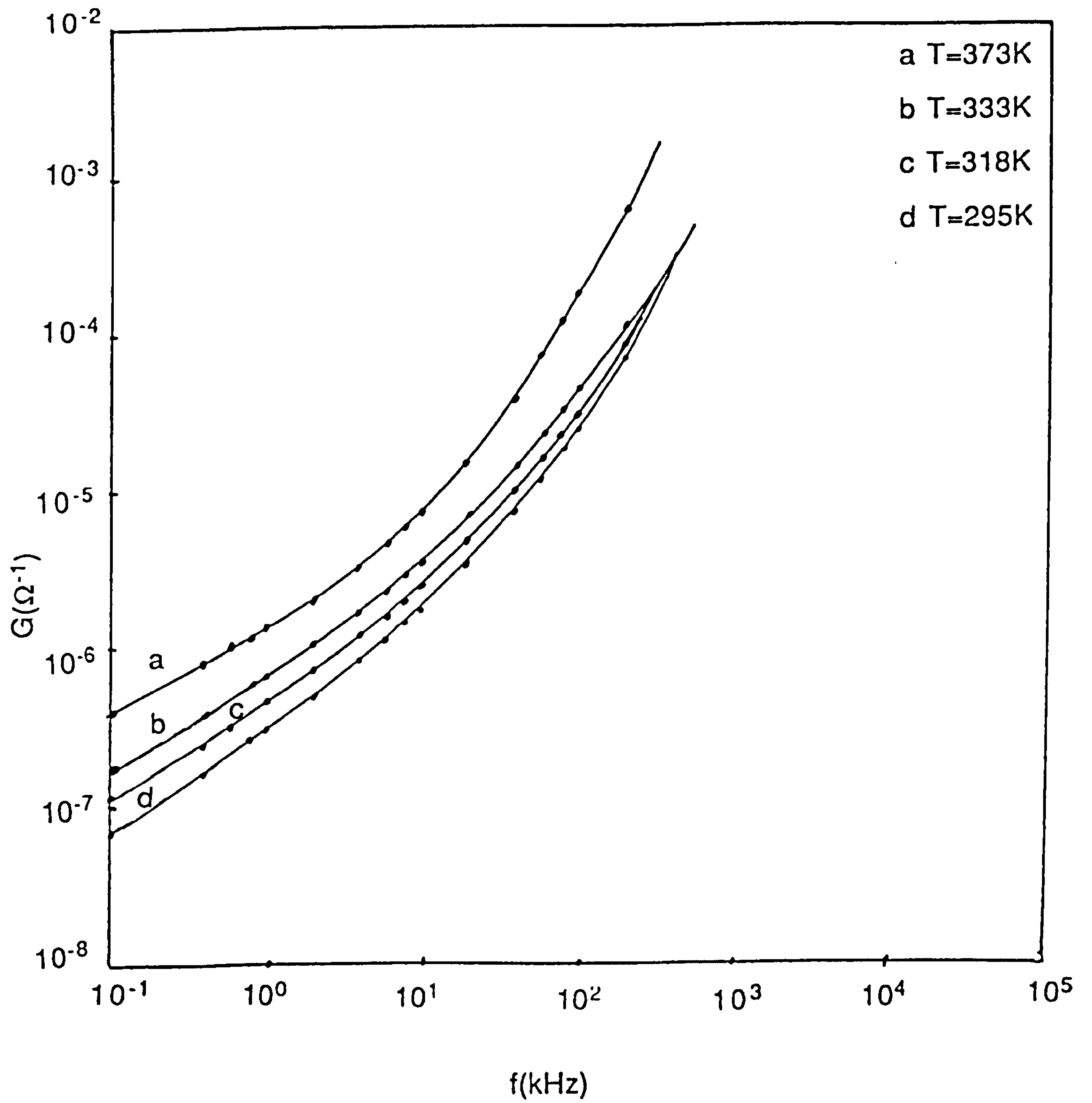

Fig. 7.6. A.C conductance versus frequency for 56%SiO/44%TeO_2 thin film.

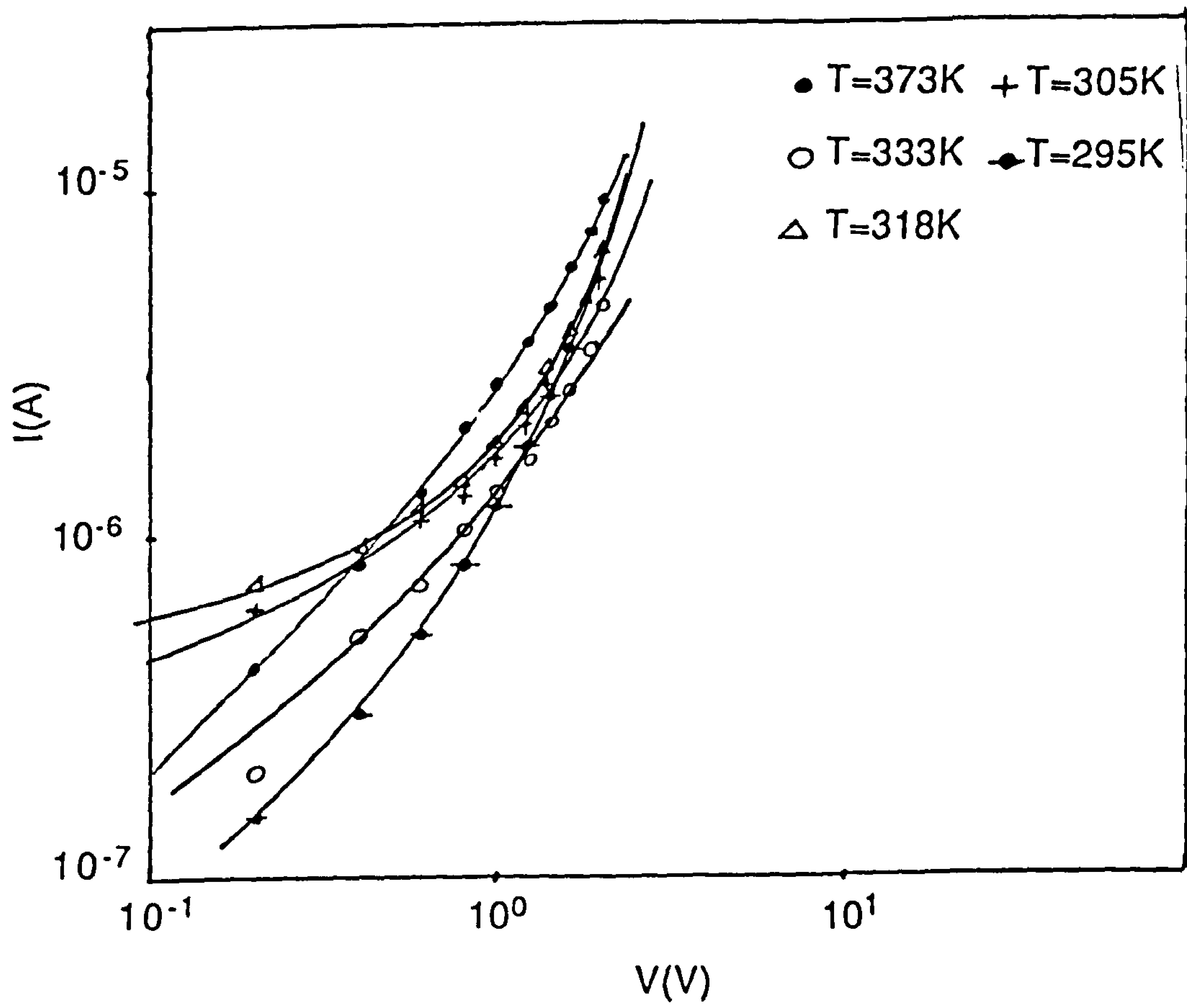

Fig. 7.7. I-V characteristics of 56%SiO/44%TeO_2 thin film.

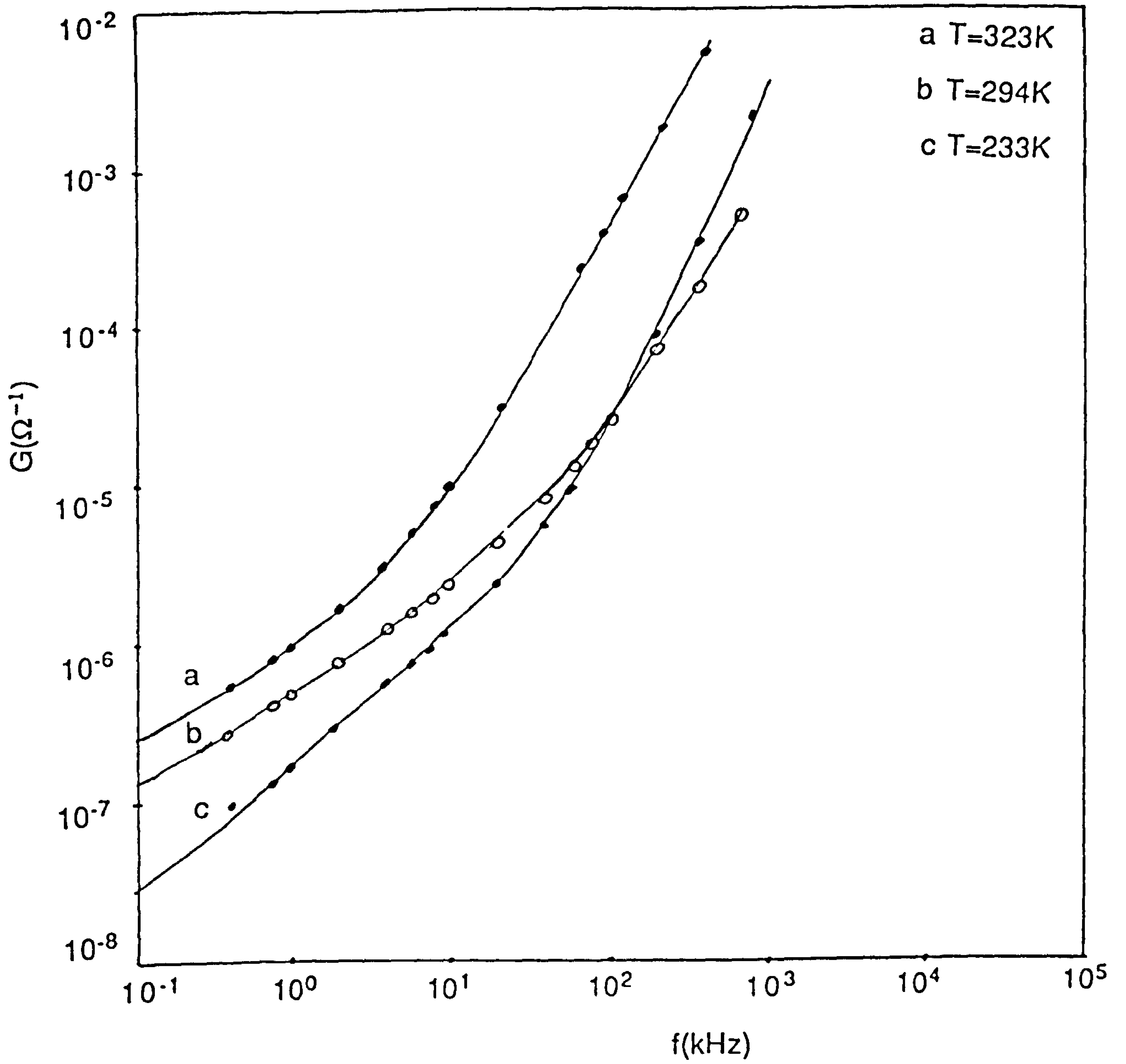

Fig. 7.8. A.C conductance versus frequency for 30%SiO/70%TeO_2 thin film.

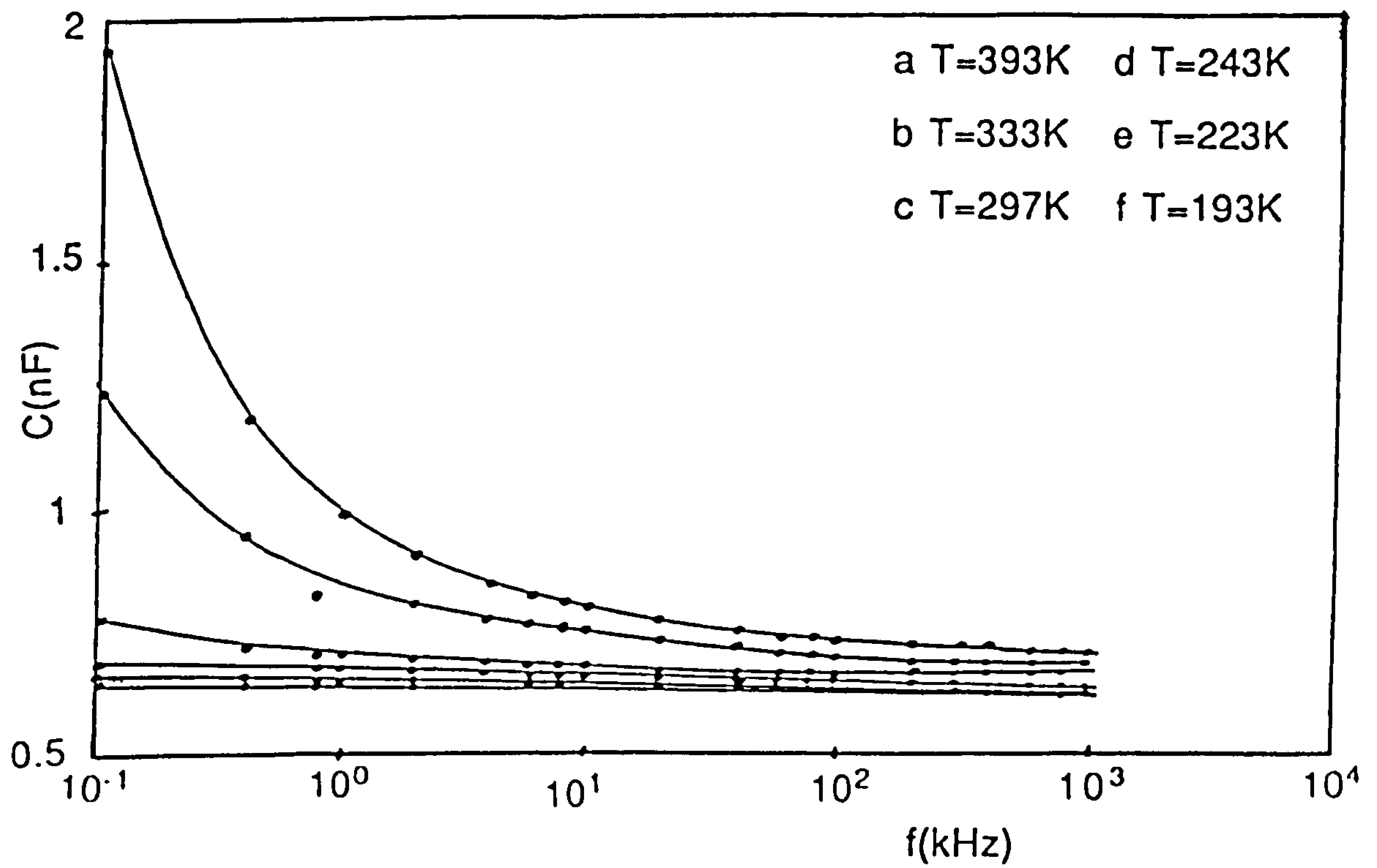

Fig. 7.9. Capacitance versus frequency for 93%SiO/7%TeO_2 thin film.

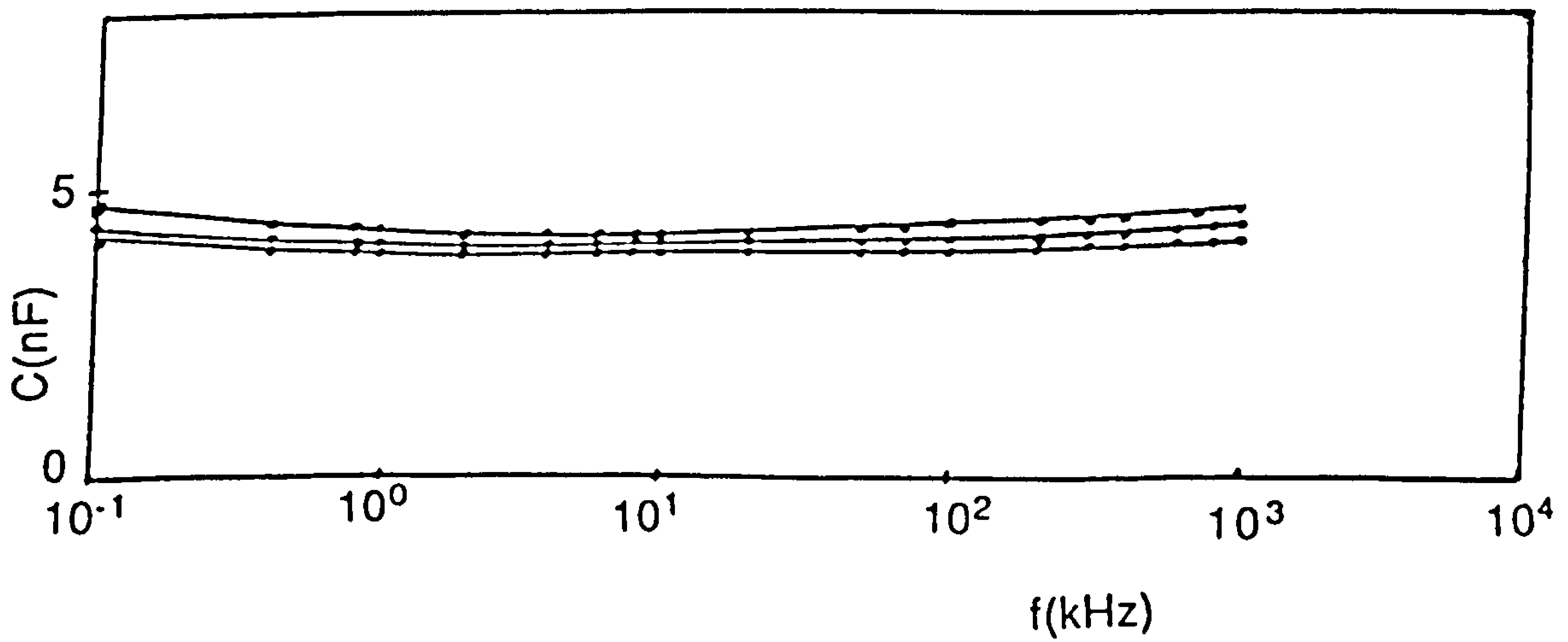

Fig. 7.10. Capacitance versus frequency for 30%SiO/70%TeO_2 thin film.

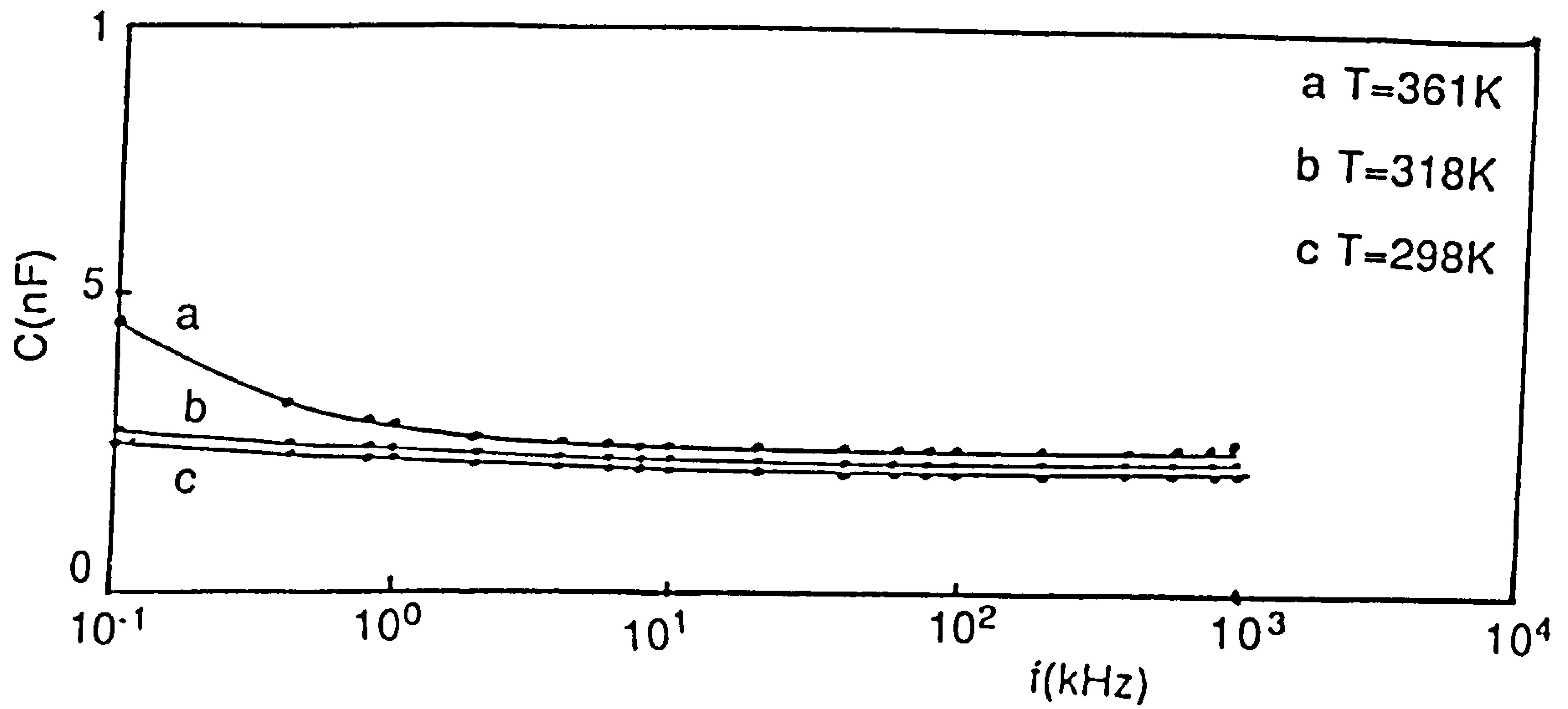

Fig. 7.11. Capacitance versus frequency for 87%SiO/13%TeO_2 thin film.

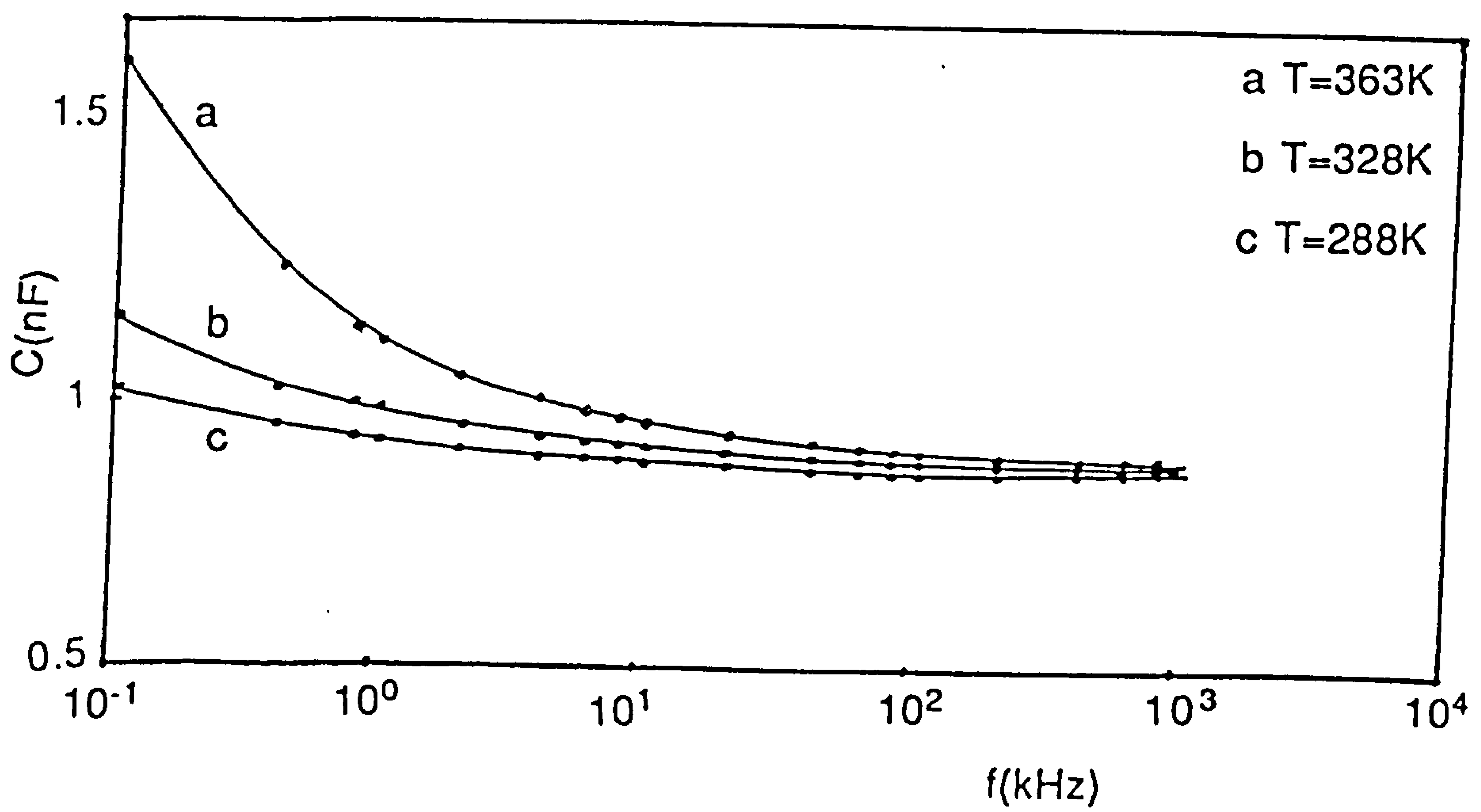

Fig. 7.12. Capacitance versus frequency for 82%SiO/18%TeO_2 thin film.

7-3 OPTICAL ABSORPTION EDGE OF SiO/TeO_2 THIN FILMS.

7-3-1 INTRODUCTION.

Al-Ani and Hogarth(1984) have studied the optical absorption edges of vacuum-evaporated silicon monoxide and tellurium oxide TeO_2 thin films and a general equation [Davis and Mott(1970)] based on the absorption being due to indirect transitions in k-space was found to be compatible with their experimental results. They have also shown experimentally how the values of the optical energy gap depend on the conditions of preparation, thickness and annealing. They explained their results in terms of atomic disorder which is the main cause of the localised states in the gap.

In the present work we have concentrated on the optical absorption edge of the co-evaporated SiO/TeO_2 thin film only.

7-3-2 RESULTS AND DISCUSSION OF THE ABSORPTION EDGE OF SiO/TeO_2 THIN FILM.

Davis and Mott(1970) neglected all transitions in which both the initial and the final states are localized. This assumption is based on the arguments that in the same region of space there is little chance of finding a localized state derived from both the valence and conduction bands. In this case they found the following formula which has already been applied in this thesis to WO_3/CeO_2 amorphous thin films (Chapter 6).

$$(\alpha\hbar\omega)^{1/2}=B(\hbar\omega-E_{opt}) \qquad (7.9)$$

where E_{opt} is the optical energy gap, ω is the angular frequency, α is the optical absorption coefficient and B is a constant of the order of $10^5 cm^{-1}eV^{-1}$.

Figure(7.13) shows the absorption spectra near the fundamental edge for a series of co-evaporated SiO/TeO_2 samples of different thicknesses and compositions. The optical absorption coefficient α is given by

$$\alpha=(1/t)\ \ln(I_0/I) \qquad (7.10)$$

where t is the thickness of the sample, I_0 and I are the intensities of the incident and transmitted lights respectively.

The high absorption region may be analysed by plotting $(\alpha\hbar\omega)^{1/2}$ against $\hbar\omega$ in accordance with equation (7.9). These results are shown in figure(7.14) and are of linear form in the high absorption region. The values of E_{opt} obtained from extrapolation of the linear regions and of B obtained from the slops of these linear regions are given in table (7.2). It is seen that the optical energy gap is systematic only in a certain range of compositions and in some other compositions the systematic change is not respected. This could be due to the change of the optical energy gap of SiO from 2.25eV to 2.73eV at rapid and slow evaporations respectively [Al-Ani *et al* (1984)].

The density of the localized states near the forbidden gap is of particular concern mainly because of its contribution to the optical transitions and to the conductivity at low temperatures (thermally-activated hopping). It has been suggested that these localized states are due to the lack of the long-range order (atomic disorder). Most workers believe that the role of these localized states may be seen at low energies corresponding to low absorption ($\alpha << 10^4 cm^{-1}$). It has been suggested that the Urbach tail could be interpreted as arising from transitions between these localized states [Tauc(1966)]. In fact, the optical absorption edge at low energies ($\alpha < 10^4 cm^{-1}$) of nearly all amorphous semiconductors is characterized by an absorption coefficient which rises exponentially with photon energy. However, the absorption edge of amorphous SiO/TeO_2 thin films shown in figure(7.15) are rather sharp. These results are similar to those of amorphous silicon [Fischer and Donovan(1972)] and amorphous germanium [Donovan *et al* (1969)]. In these materials it is seen that the absorption edge, is about as sharp as the direct edge in their corresponding crystalline materials. The results found in amorphous SiO/TeO_2, Si and Ge made strong support as evidence against the interpretation that the localized states in the gap are responsible for the following exponential relation

$$\alpha \propto \exp(\hbar\omega/E_t) \qquad (7.11)$$

which is known as Urbach rule. Moreover, we think that E_t may not

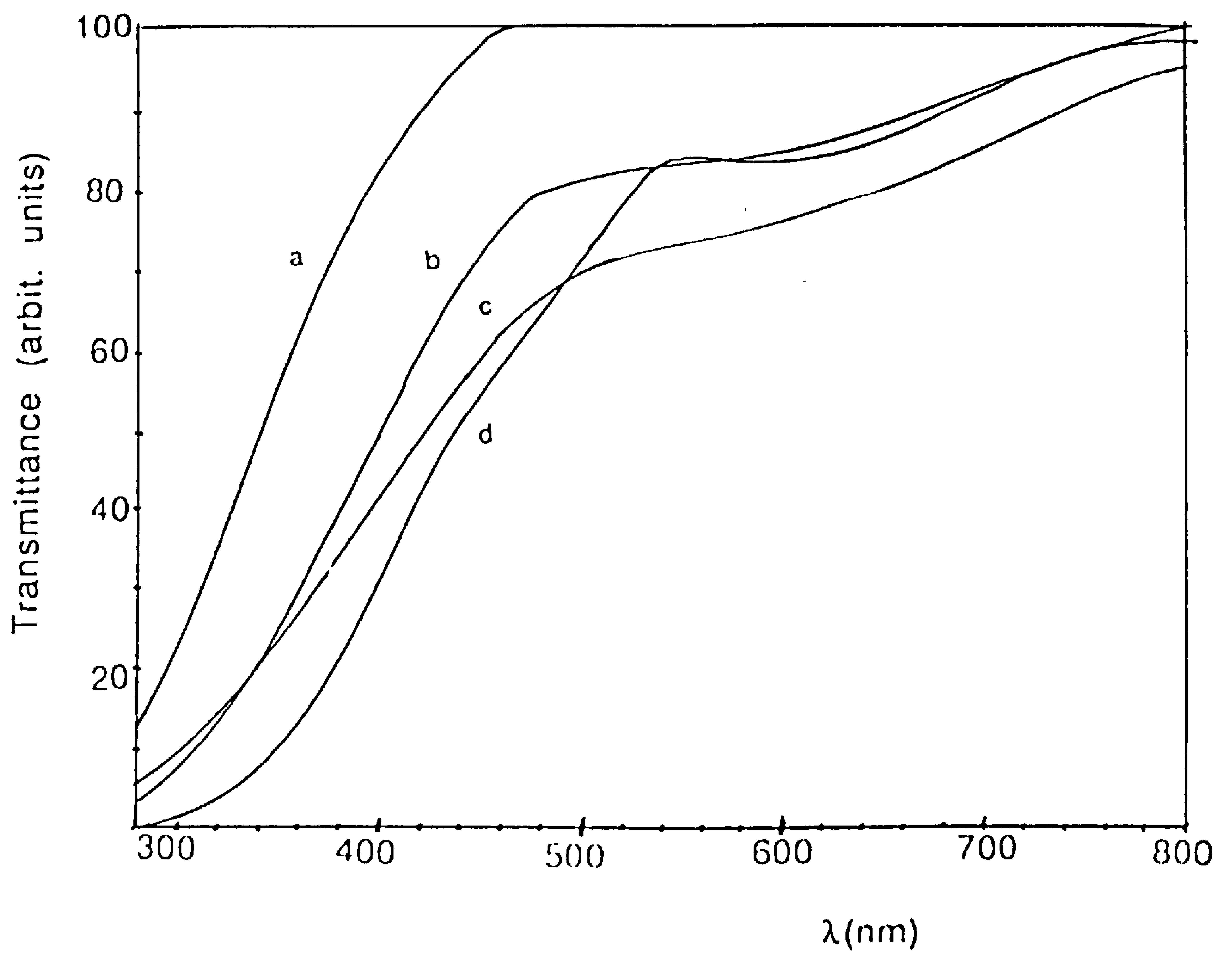

Fig.7.13 Optical transmittance as function of wavelength for SiO/TeO_2 thin films.

a) 79%SiO (328nm thick)

b) 56%-- (199nm thick)

c) 30%-- (199nm thick)

d) 87%-- (356nm thick).

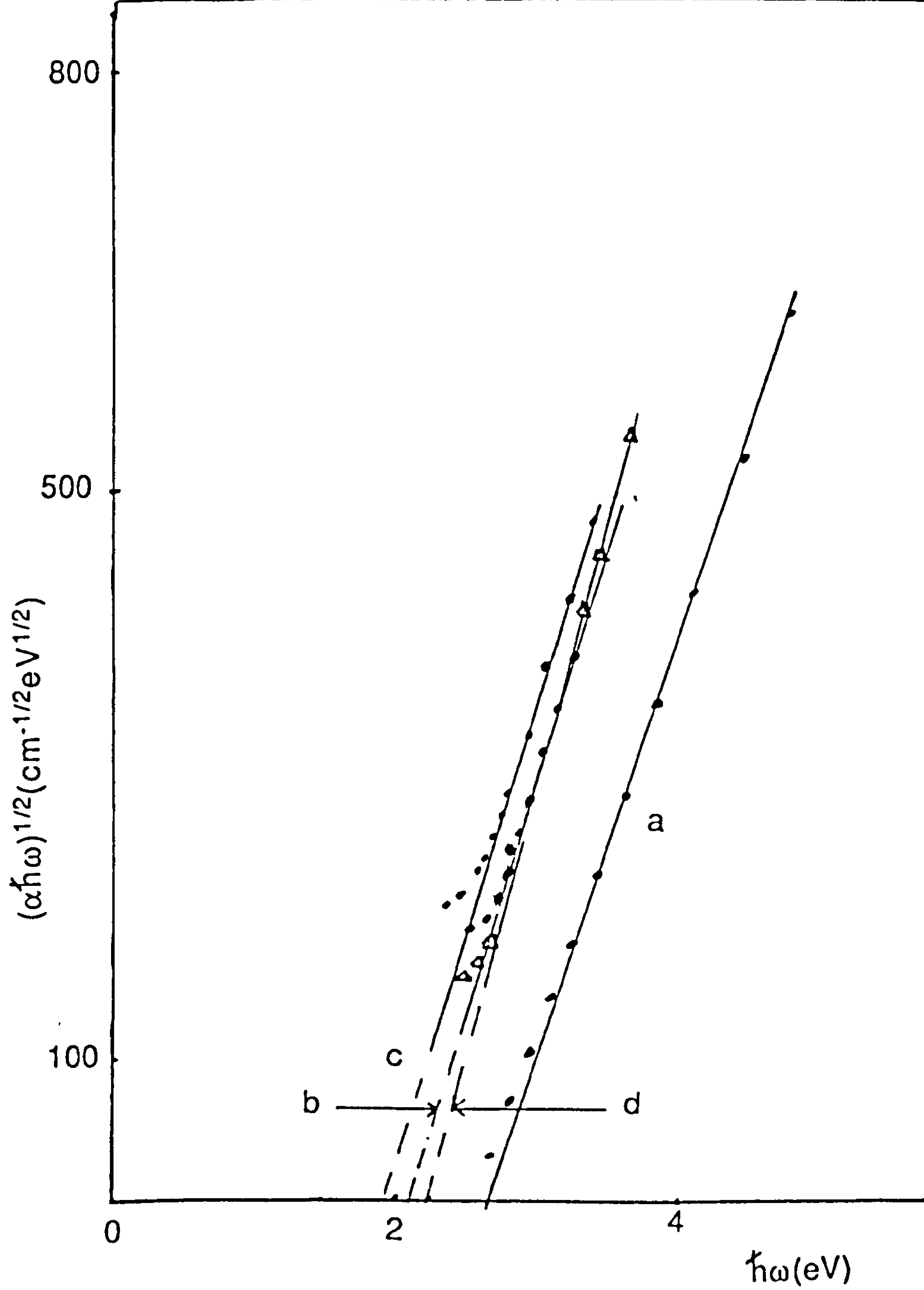

Fig.7.14. $(\alpha\hbar\omega)^{1/2}$ versus photon energy for the same samples as in figure(7.13).

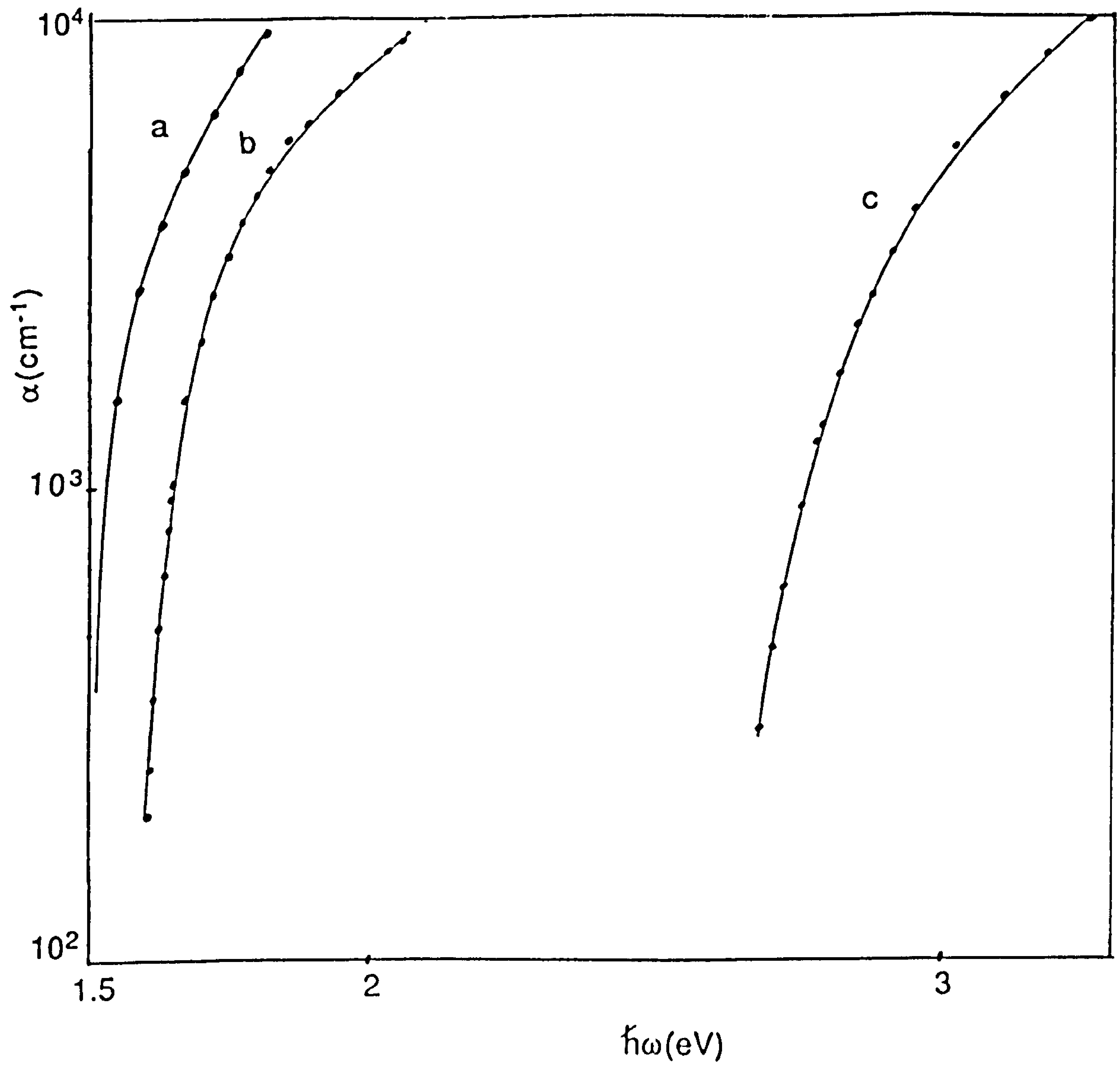

Fig. 7.15. log(α) versus photon energy for various compositions of SiO/TeO_2 thin films. a) 30%SiO, b) 56%SiO and c) 79%SiO.

depend on the lack of the long-range order because of the above arguments and because the Urbach rule is also obeyed in some crystalline materials. Dow and Redfield(1970) suggested that the Urbach rule arises from an electric field broadening of an exciton. We think that this theory could be the solution to this problem or at least is one of the closest theories for its solution because excitons can also exist in both crystalline and non-crystalline materials.

7-4 ELECTRON MICROSCOPE STUDY OF SiO/TeO_2

The film of SiO/TeO_2 has also been prepared on a carbon-coated mica substrate held at room temperature and was studied in the transmission electron microscope. The electron diffraction patterns and the electron micrographs were obtained at room and high temperatures.

The results of the diffraction pattern as well as those of the electron micrograph shown in figure (7.16) at room temperature indicate that the structure of SiO/TeO_2 thin film is amorphous, while at high temperature, the electron diffraction pattern shown in figure (7.17) for the same sample shows that the amorphous structure tends to become polycrystalline as indicated by the appearance of the sharp rings. Thus we would suggest that the structure of the small islands shown by the electron micrograph in figure(7.17) could be chains of metallic crystallites. Therefore we may suggest that the SiO/TeO_2 amorphous structure is thermally unstable and this could be the cause of the decrease of

the conductivity as the temperature is increased in certain films of SiO/TeO_2, that is, the decrease in the conductivity could be due to the formation of crystalline states in the structure.

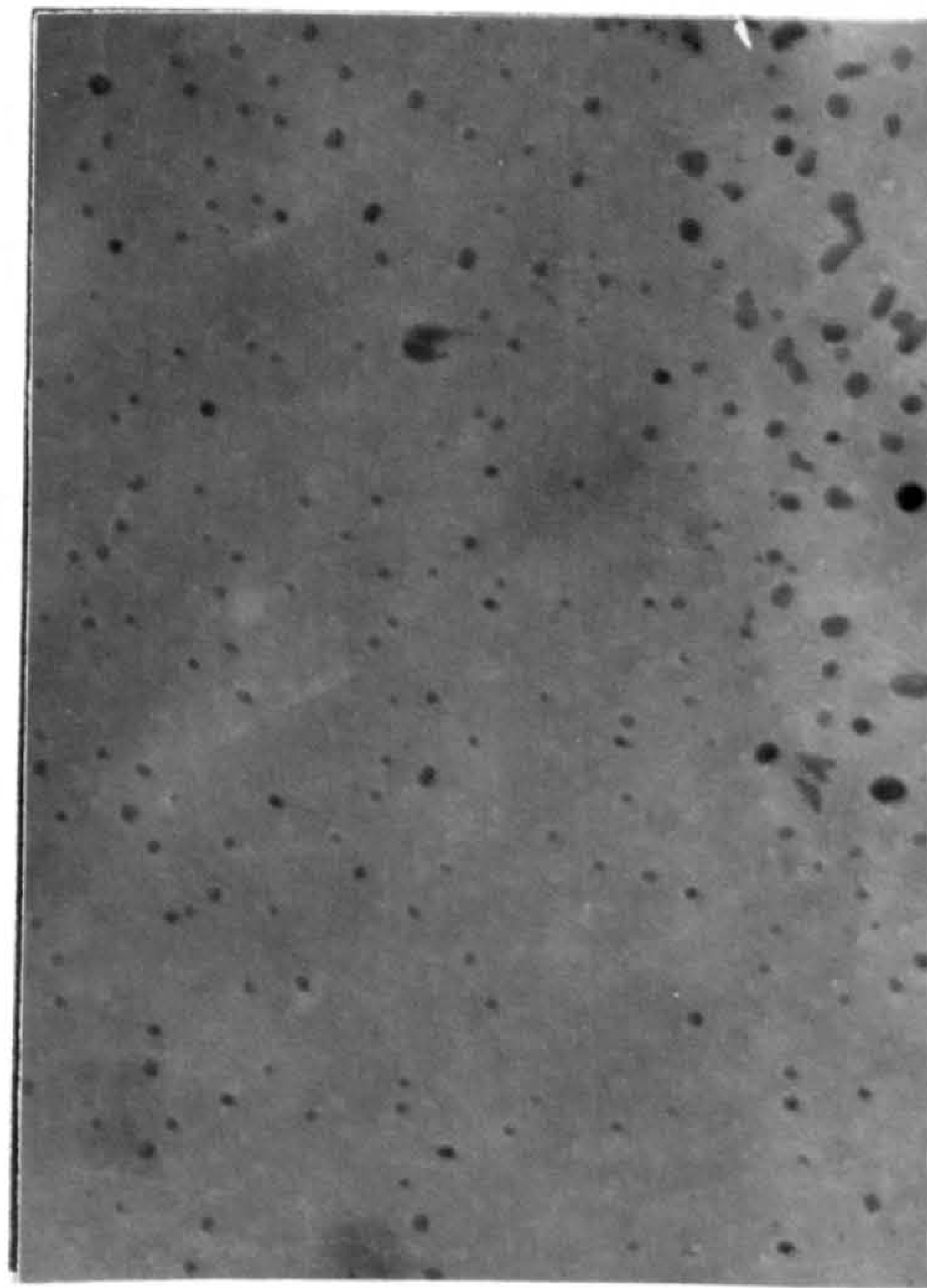

Micrograph

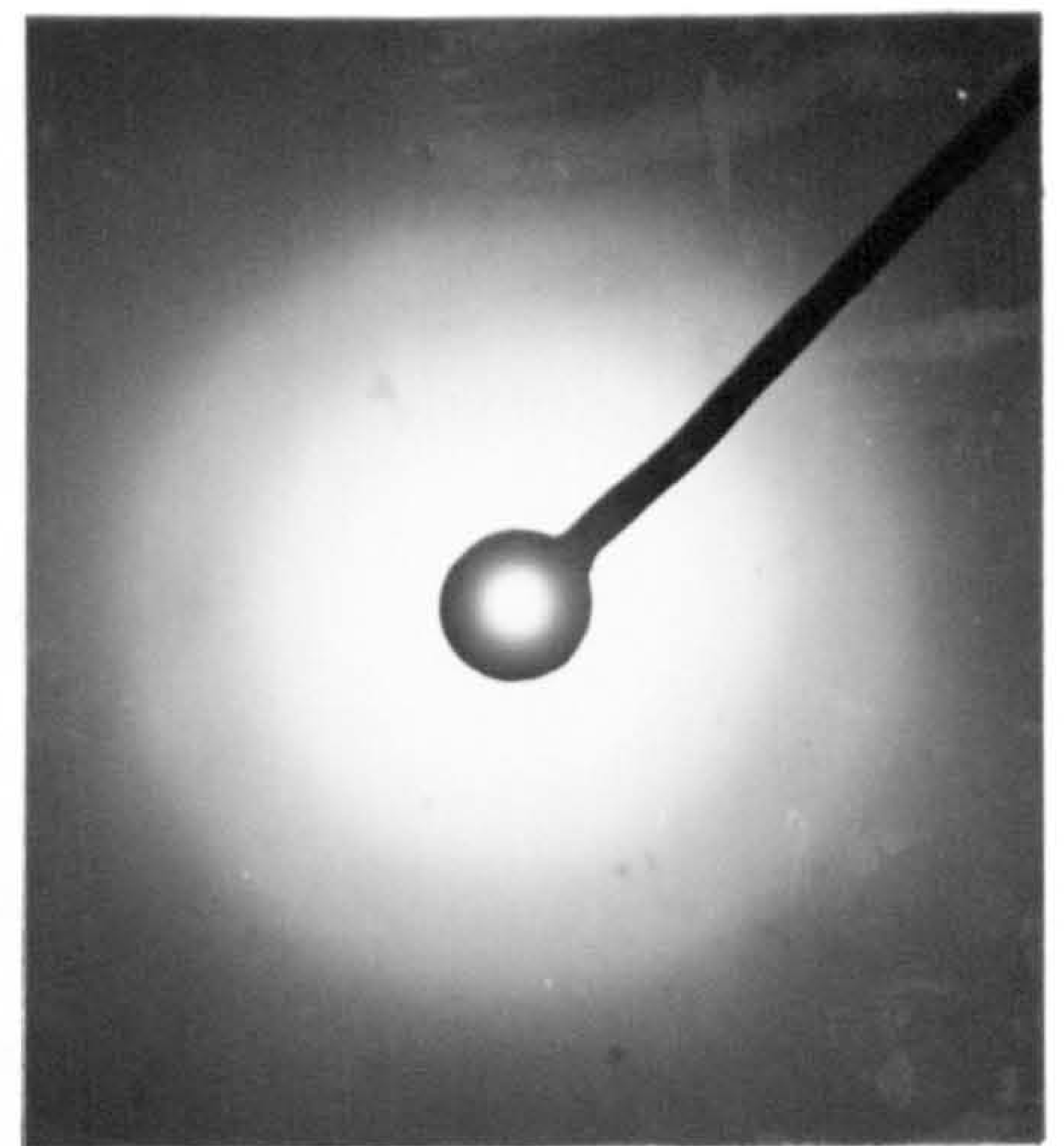

Diffraction pattern

Fig. 7.16. Electron micrograph and diffraction patterns of SiO/TeO_2 thin film at room temperature.

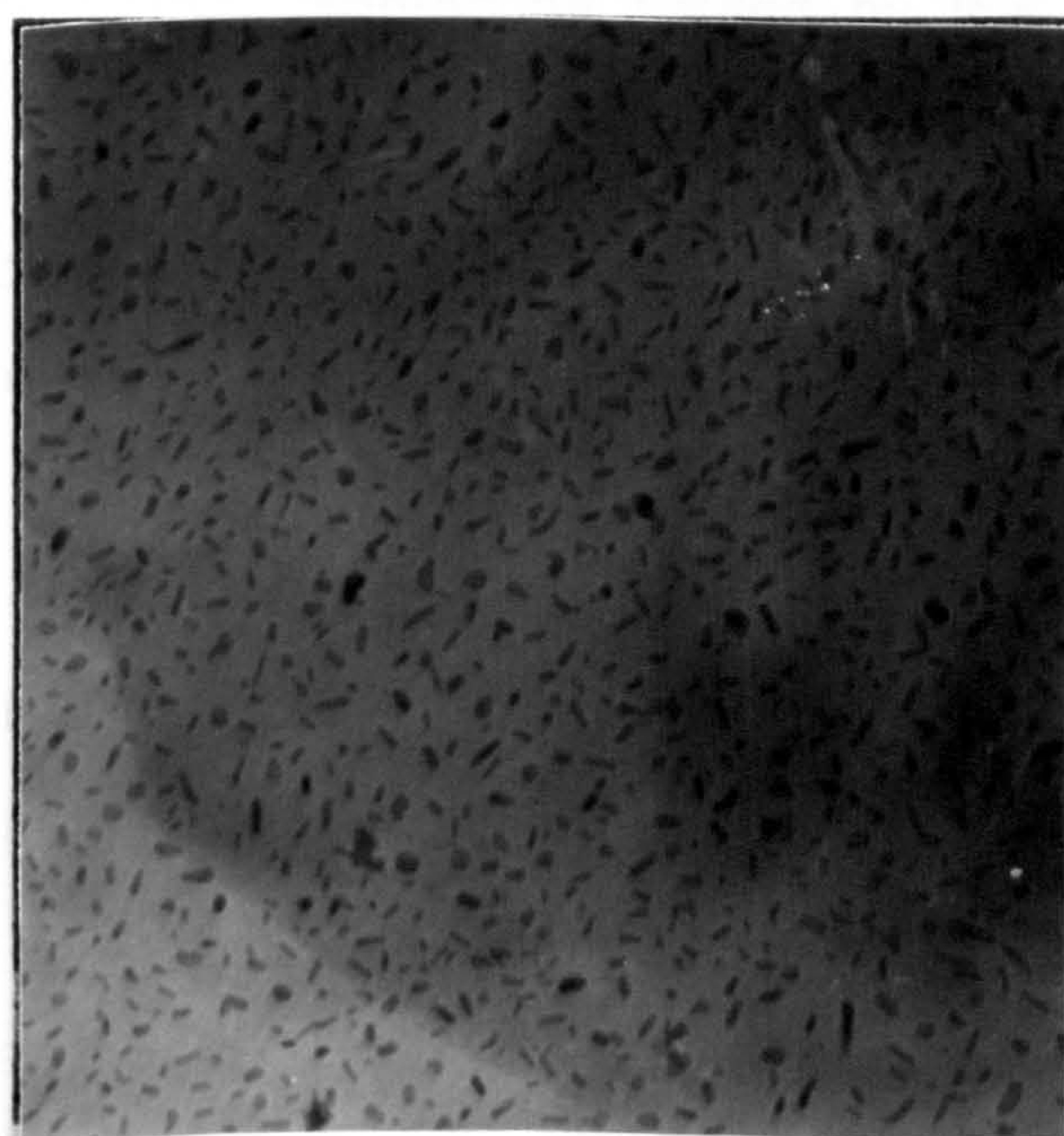

Micrograph

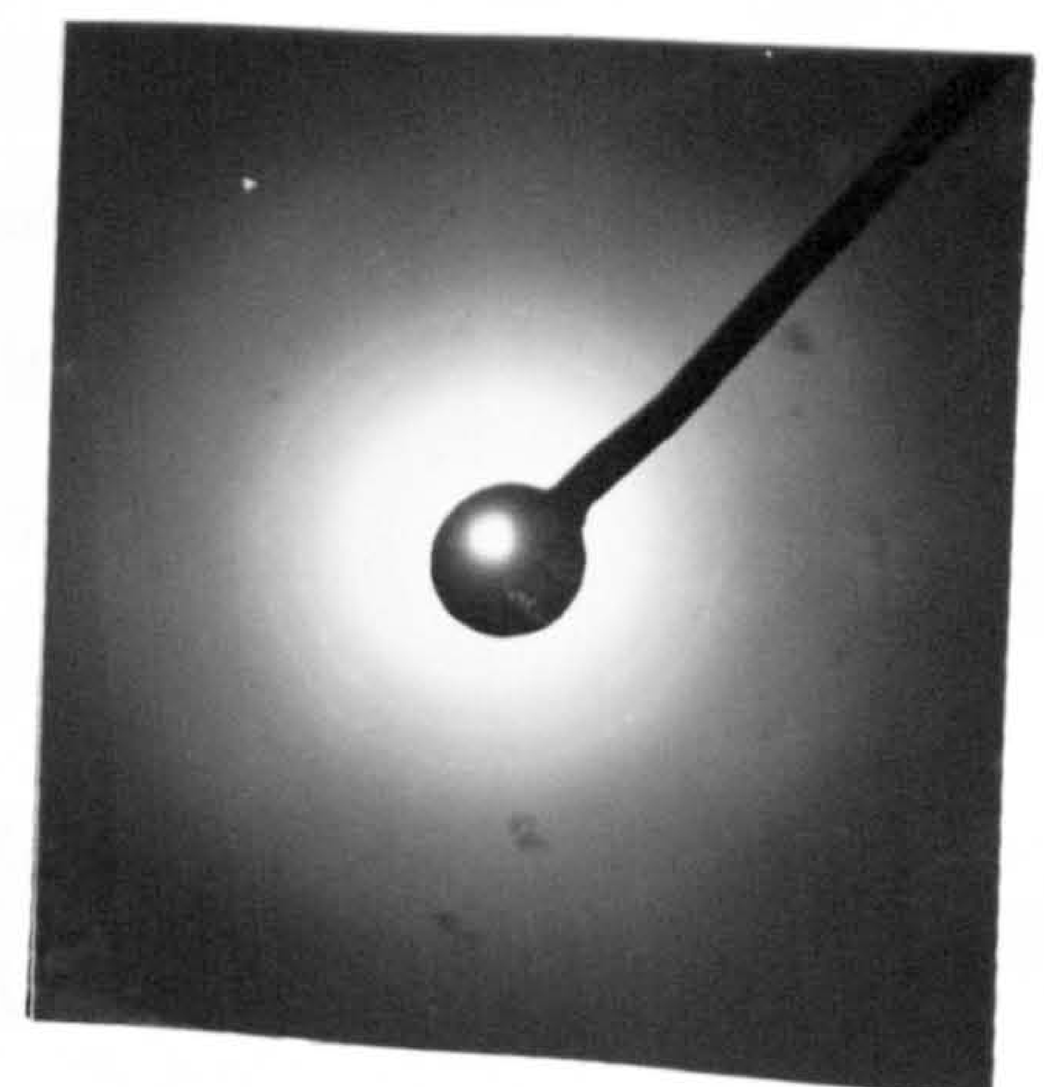

Diffraction pattern

Fig. 7.17. Electron micrograph and diffraction patterns of SiO/TeO_2 thin film after annealing

CHAPTER 8. RESULTS AND DISCUSSION OF WO_3/TeO_2 THIN FILMS

8-1 A.C CONDUCTION MECHANISM IN WO_3/TeO_2 THIN FILMS.

Figures(8.2) and (8.4) show the capacitance variation with log frequency. It is seen that the capacitance increases very rapidly with decreasing frequency. This is thought to be due to an ionic build up at the interfaces which means that the aluminium electrodes influence the electrical properties of WO_3/TeO_2. These results are very similar to those of 68%V_2O_5/32%TeO_2 but different from those of SiO/TeO_2 thin film. The capacitance of the latter is almost independent of frequency in the range 0.1kHz to 10^3kHz indicating that the effects of the electrodes can be neglected. These results are in good agreement with Mead (1962) who first pointed out that the electrical conduction in dielectrics such as SiO/TeO_2, should be limited by the bulk properties if the sample is sufficiently thick. However in transition metal oxides such as V_2O_5 or WO_3 there is a possibility that the metal ions may migrate for some distance under the influence of an electric field, and because of the presence of the potential barrier at the interfaces these ions will be blocked leading to a formation of space charges at the electrodes which is indicated by the large increase of the capacitance at low frequencies.

Figure (8.5) shows the plots of the dielectric loss and the capacitance as function of frequency of Al-83%WO_3/17%TeO_2-Al

thin film (252nm thick). It is seen that the dielectric loss and the capacitance have the same slope in the frequency range 2kHz-10^2kHz and at T=238K, hence, the dielectric loss ε'' is proportional to the capacitance.

$$\varepsilon'' \propto C \qquad (8.1)$$

Figure (8.1) shows the plots of a.c conductance and loss $\tan\delta$ as function of frequency. It seen that at T=238K, the a.c conductivity is proportional to ω^S in the frequency range 2kHz-10^2kHz.

$$\sigma \propto \omega^S \qquad (8.2)$$

where s is approximately equal to 0.8.

The dielectric loss ε'' was calculated from the conductance and its expression can be given by

$$\varepsilon'' \propto \sigma/\omega \qquad (8.3)$$

or

$$\sigma \propto \varepsilon''\omega \qquad (8.4)$$

Inserting equation (8.1) in (8.4) we obtain

$$\sigma \propto C\ \omega \qquad (8.5)$$

where C is the capacitance.

Equation (8.5) means the conductivity and the capacitance are related to the same mechanism of conduction at low temperatures and in the frequency range 2kHz-10^2kHz. According to equation (8.2) with s=0.8, this mechanism of conduction is by hopping of carriers from site to site, that is, from W^{5+} to W^{6+}. The slope calculated from figure (8.5) at T=238K is approximately equal to -0.2, thus the capacitance is given by

$$C \propto \omega^{-0.2} \qquad (8.6)$$

Inserting this equation in (8.5) we obtain equation (8.2) with s=0.8.

Equations (8.2) and (8.6) of the conductivity and the capacitance respectively can be written in the forms

$$\sigma_{a.c}=\sigma_{d.c}+A_o\omega^S \qquad (8.7)$$

and

$$C_{a.c}=C_{in}+A_1\omega^{S-1} \qquad (8.8)$$

where $\sigma_{d.c}$ is the d-c conductivity, A_o and A_1 are constants depending on temperature, and C_{in} is the high frequency capacitance from which the high frequency dielectric constant ε_{in} is given by

$$\varepsilon_{in}=C_{in}d/\varepsilon_o a \qquad (8.9)$$

where d is the thickness, a is the active area of the sample and ε_o is the permittivity of the free space.

The value of ε_{in} calculated from equation (8.9) at T=238K is equal to 19.

Equations (8.7) and (8.8) may suggest that the carriers which contribute to the conductivity may be treated as polarons, and this yields an expression for the index s in terms of temperature [Pike (1972)]. Pike's model assumes an electron transferring from one polarisable site to another. Thus, the hopping mechanism involves two sites, and is over a potential barrier whose height is given by W_o separating the two metal ions W^{5+} and W^{6+} at which the electron is localized. Hence, each pair of these sites contributes a dipole moment to the material. Similar equations to (8.7) and (8.8) of the a.c conductivity and capacitance were found by Springett (1974) in $4.5TiO_{2-x}/2P_2O_5$ glass and he suggested that the behaviour is similar in all respect to other transition metal oxide glasses.

The fact that a dipole exists would suggest that the binding energy of the electron is so high that the coulombic interaction is not strong enough to bring back the electron to the initial ion. Thus an electron is in a potential well of site (say) W^{5+} corresponding to the polarization energy W_p. Therefore, in order that an electron jumps to another site (say) W^{6+}, thermal fluctuations should produce a potential well depth in this site and at the same time reduce the depth of the potential well of the site W^{5+} by the same amount so that an electron can jump when

both wells have the same depth which corresponds to half of the polarization energy. Therefore the hopping energy W_{po} of a polaron is half of the polarization energy W_p [Austin and Mott(1969)].

In the case of $83\%WO_3/17\%TeO_2$ we assume that the concentrations of W^{5+} and W^{6+} are high so that the polarization clouds overlap which is the characteristic of the adiabatic regime. If we assume that the distance r through which the electron must be transferred from site to the other is not large compared to the polaron radius r_s then the hopping energy of the polaron W_{po} is given [Killias(1966), Austin and Mott(1969)] by

$$W_{po}=(e^2/4\varepsilon_e)\ \{(1/r_s)-(1/r)\} \qquad (8.10)$$

where $1/\varepsilon_e=1/\varepsilon_{in} - 1/\varepsilon_s$ is the effective dielectric constant, ε_{in} is the high frequency dielectric constant, ε_s is the static dielectric constant, r_s is the polaron raduis and r is the distance between the centres. The total hopping energy is given by [Mott(1968)]

$$W_h=W_{po}+(1/2)W_D \qquad (8.11)$$

where W_D is the Miller and Abrahams(1960) term. The case in which $W_D=0$ has been investigated by Holstein(1959) and Emin and Holstein(1969). However electron diffraction examination shows that WO_3/TeO_2 thin films are amorphous and thus the energy W_D is different from zero. This latter case has been investigated by

Schnakenberg(1968).

The above arguments would suggest that the Elliott model (1977), which assumes hopping over a barrier, is applied in our case. Elliott(1977) has used Pike's expression given by

$$1\text{-}s=6kT/W \qquad (8.12)$$

where s is the index given by $\sigma \propto \omega^{s}$, k is the Boltzmann constant, T the absolute temperature and W is a potential barrier. However, the plot (1-s) versus T do not always pass through the origin. Therefore, Springett (1974) has attempted to improve the model of Pike(1972) and has given the following approximate expression of the temperature variation of s.

$$1\text{-}s=(6kT/W_o)[1-(1/2)(r_s/r_a)^3] + \theta(T) \qquad (8.13)$$

where r_s is the small polaron radius, r_a is the average site separation, W_o is a potential barrier, and $\theta(T)$ is a term which tends to zero as the temperature is reduced in order that the term (1-s) will be linear at low temperatures.

We may conclude that in WO_3/TeO_2 thin films with high concentration of WO_3, the Elliott model with Springett expression (eq;(8.13)) instead of Pike's expression (eq;(8.12)) may be applied

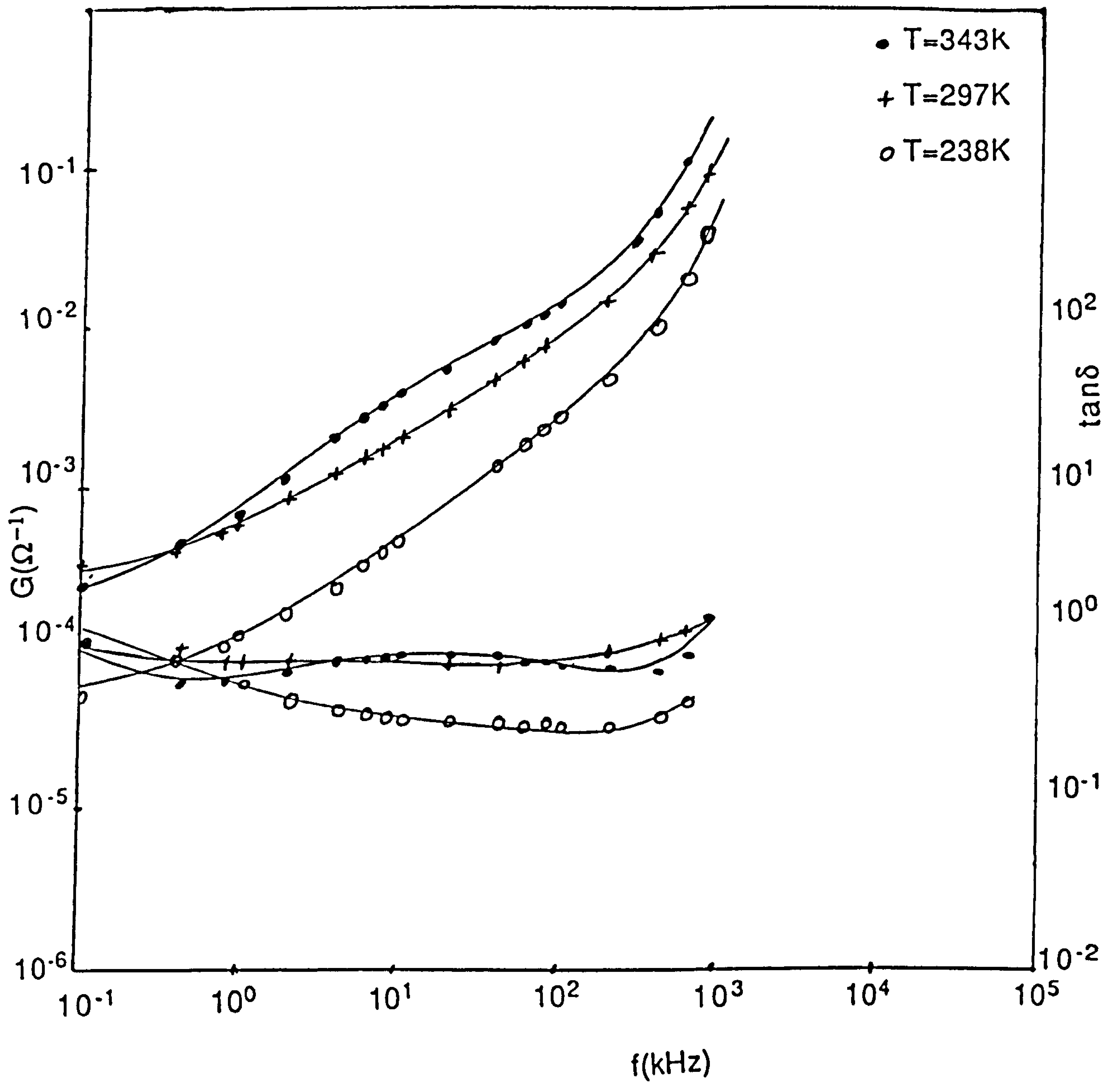

Fig. 8.1 Conductance G(three upper curves) and tanδ (three lower curves) versus frequency for 83%WO_3/17%TeO_2 thin film.

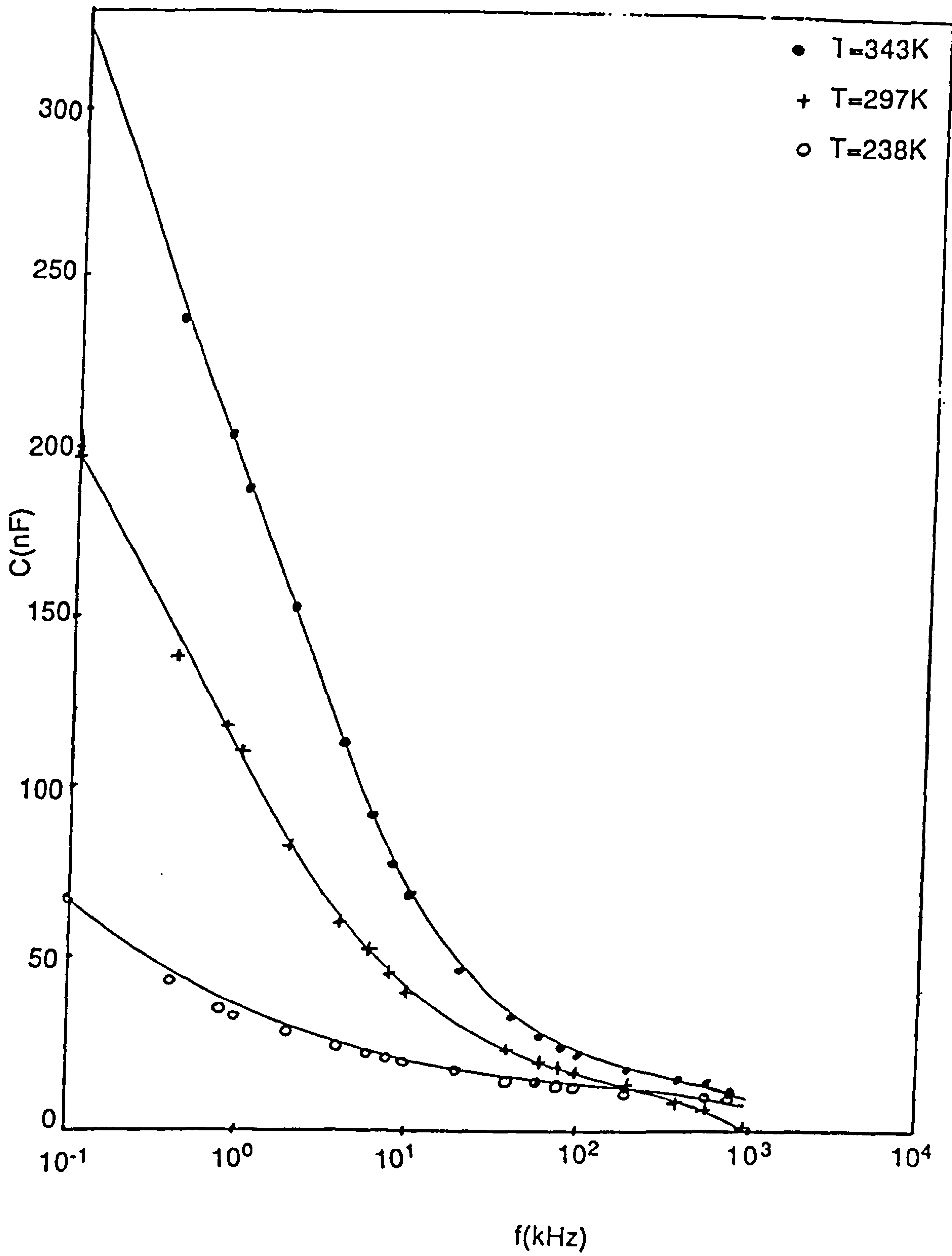

Fig. 8.2 Capacitance C versus frequency for 83%WO_3/17%TeO_2 thin film.

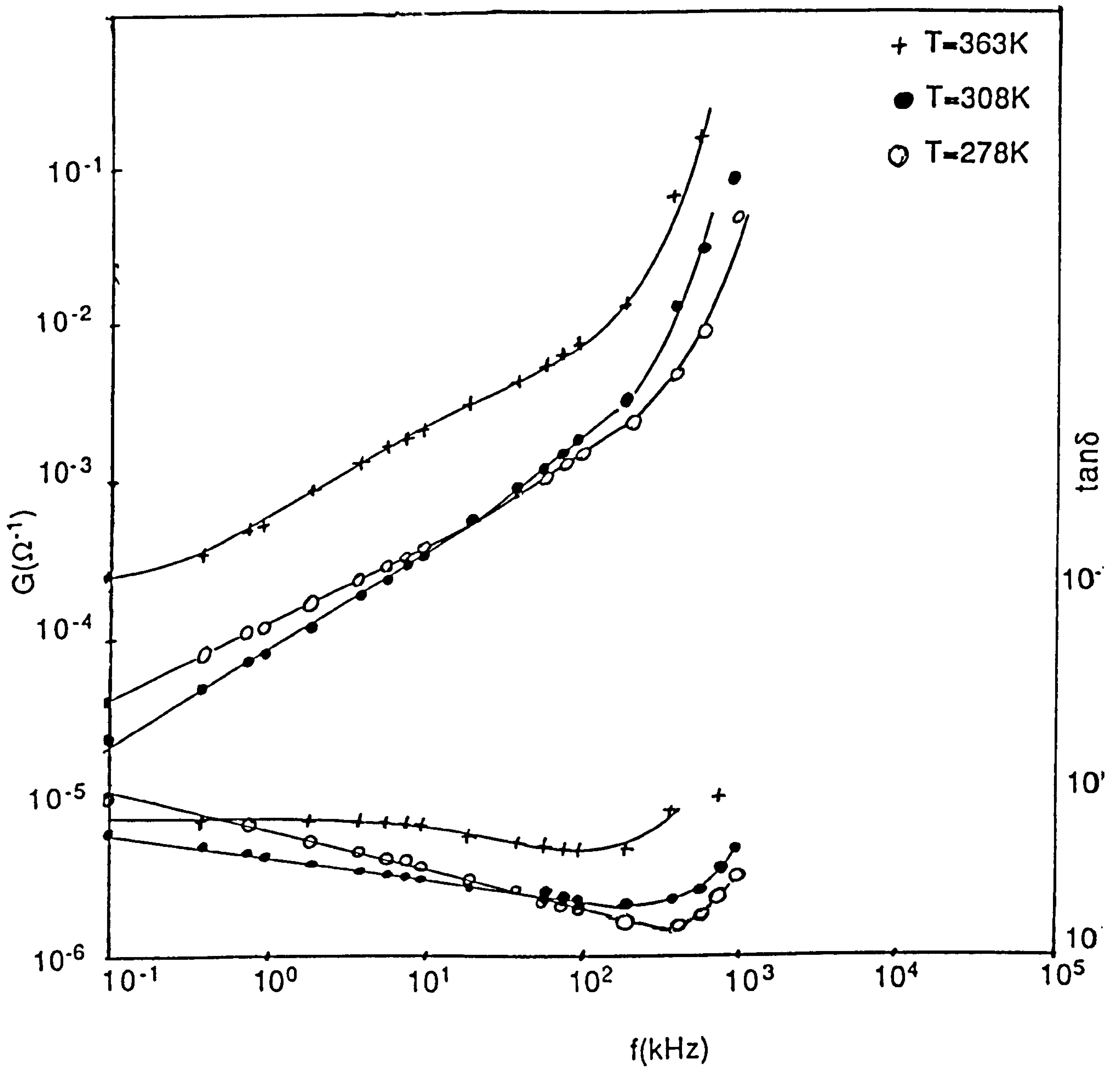

Fig. 8.3 Conductance G (three upper curves) and tanδ (three lower curves) versus frequency for 61%WO_3/39%TeO_2 thin film.

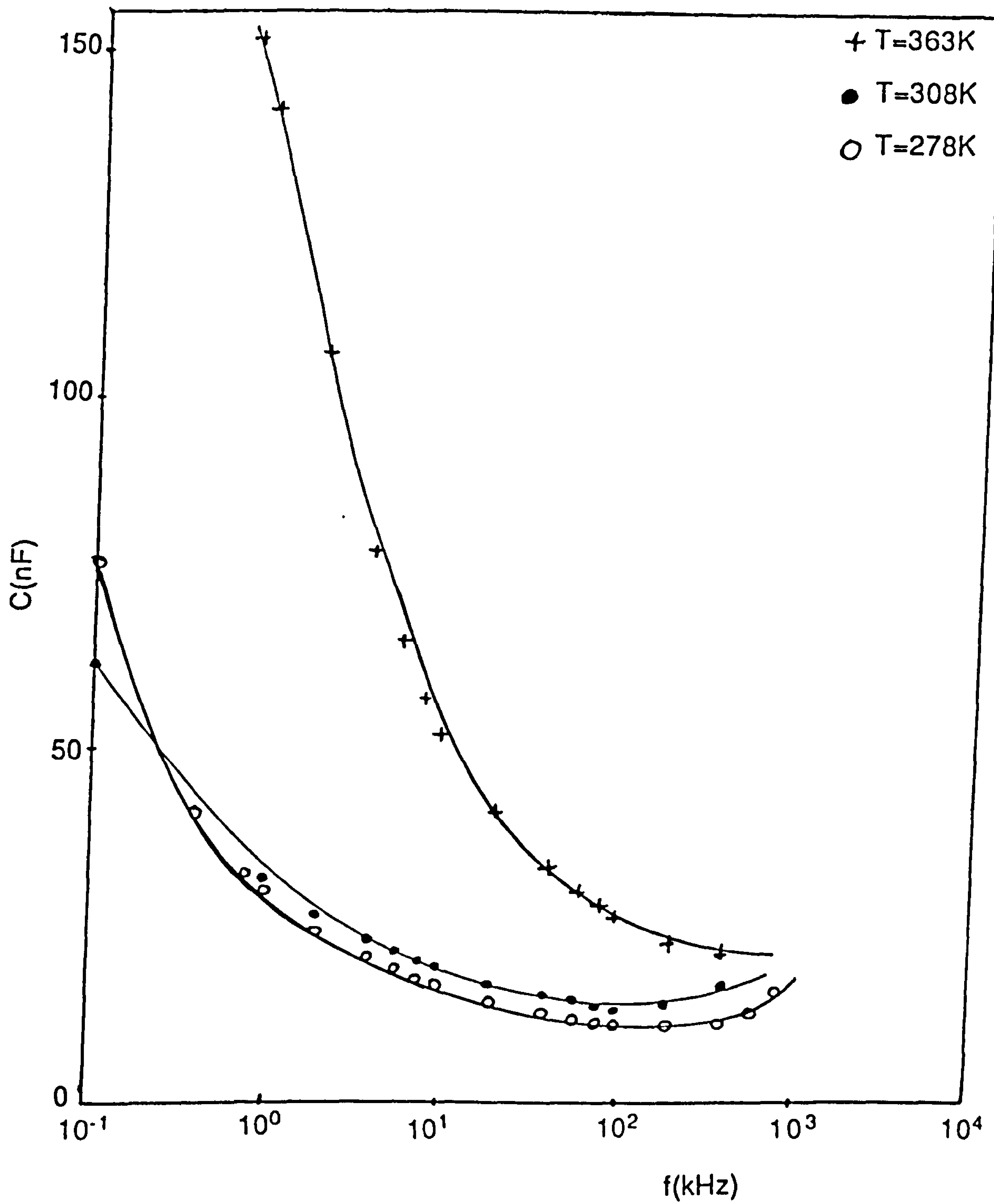

Fig. 8.4 Capacitance versus frequency for 61%WO_3/39%TeO_2 thin film.

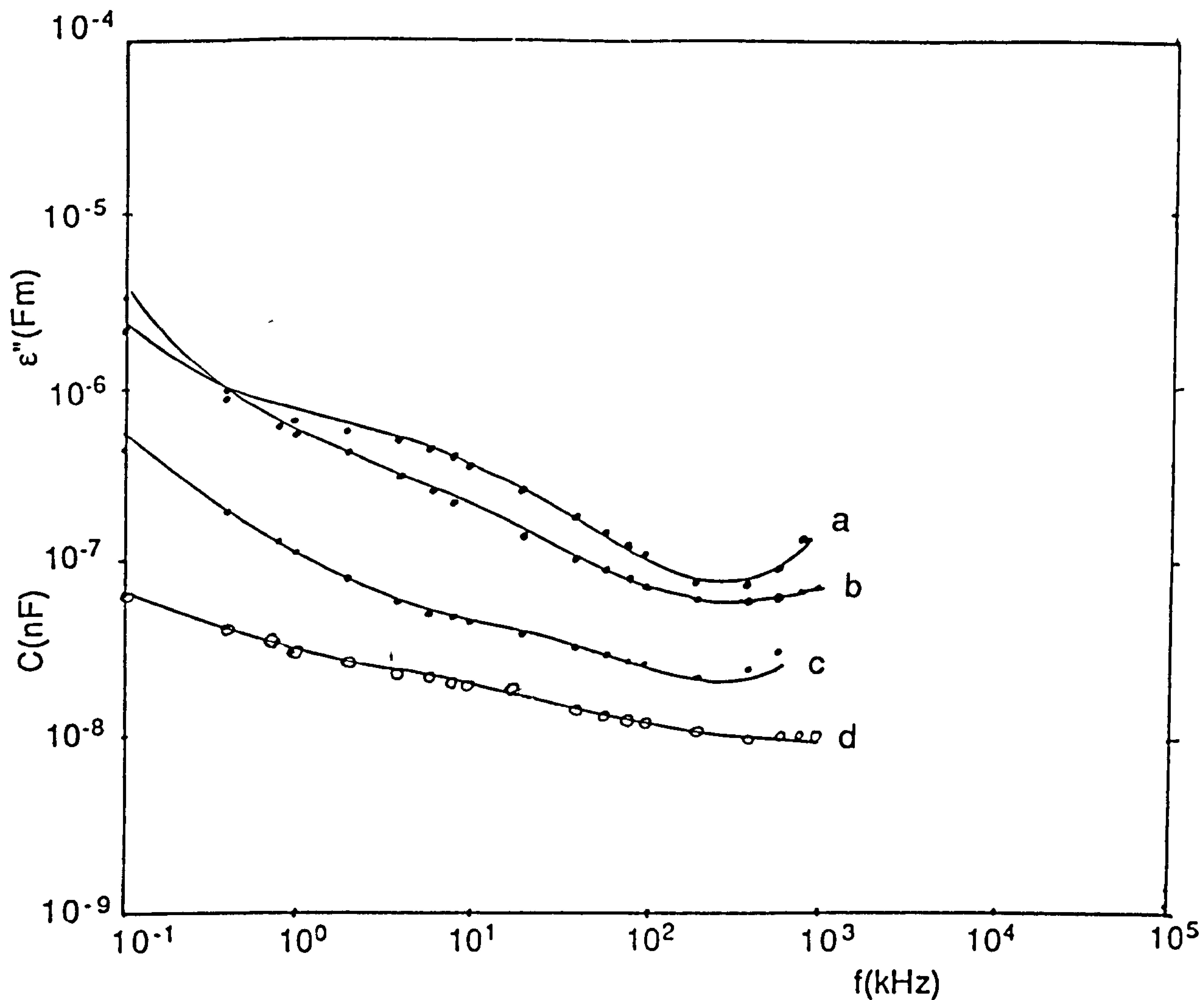

Fig. 8.5 Dielectric loss ε" (•) and capacitance (o) versus frequency for $83\%WO_3/17\%TeO_2$ thin film.

a) T=343K

b) T=297K

c) T=238K

d) T=238K.

8-2 OPTICAL ABSORPTION EDGES OF WO_3/TeO_2.

8-2-1. INTRODUCTION.

Tungstic oxide is one of the transition metal oxides and as a semiconducting oxide and because of its ferroelectric properties, has attracted attention over the years. Amorphous films of WO_3 have been studied and their optical and electrical properties have been reported by many authors [Deb (1973), Deb and Chopoorian(1966), and Mansingh *et al* (1978)]. The aim of the work presented here is to study the optical absorption edge of WO_3/TeO_2 amorphous thin films with various compositions.

Al-Ani and Hogarth (1984) have studied the WO_3/TeO_2 glass system based on TeO_2 in the composition range 70%-95% TeO_2. It was therefore of interest to study this mixture in thin film form with molar percentage of WO_3 higher than 50%. As was mentioned before, the presence of TeO_2 in the mixture will only increase the distance between metal ions and the amount of disorder.

To see the effect of TeO_2 on the optical absorption edge of WO_3, we have first studied the optical absorption of this latter.

8-2-2. OPTICAL ABSORPTION EDGE OF WO_3 THIN FILM.

The optical absorption spectra of thin films of WO_3 deposited on Corning 7059 glass were measured with a U.V visible spectrophotometer at room temperature .

Figure (8.6a) shows the transmission spectra of thin films of WO_3 at room temperature. Figure (8.8a) shows the plot of the logarithm of the absorption coefficient as a function of photon energy. The linear relationship clearly shows that the absorption edge follows the Urbach rule which states that the absorption coefficient is given by

$$\alpha(\omega) \propto \exp(\hbar\omega/E_t). \qquad (8.15)$$

where $\hbar\omega$ is the photon energy of the incident light and E_t is constant.

Figure (8.7a) shows the plot of $(\alpha\hbar\omega)^{1/2}$ as function of photon energy. It is clearly shown that the relation between $(\alpha\hbar\omega)^{1/2}$ and $\hbar\omega$ is linear and its intercept with the photon energy axis determines the optical energy gap which is about 3.25eV. These results are in good agreement with those reported by Deb (1973).

The results obtained on the optical absorption spectra of WO_3 thin films suggest that the absorption edge can be separated into two regions; a region where $\alpha \propto \exp(\hbar\omega/E_t)$ and the other region where $(\alpha\hbar\omega)^{1/2} = B(\hbar\omega - E_{opt})$. The low absorption region which is found in many amorphous solids is not calculated because of the small thickness of the film.

The exponential tail edges known as Urbach (1953) edges, have been observed in a number of amorphous as well as crystalline materials. Dexter(1967) suggested that the exponential tail could be due to the quadratic Stark effect. However, Dow and

Redfield(1970) showed that the Stark effect ceases to be quadratic at high fields. Instead they suggested that the Urbach rule arises from an electric field broadening of an exciton. We think that the latter suggestion could be possible and the reason for this is given in Chapter 7-3.

The formula which describes the high optical absorption was derived by Davis and Mott (1970) by assuming a linear dependence of the electronic density of states on energy.

The E_{opt} is the optical energy gap and it corresponds to transitions from localized states at the top of the valence band into the extended states in the conduction band or vice versa.

8-2-3. THE EFFECT OF INHOMOGENEITIES ON THE OPTICAL ABSORPTION EDGE OF WO_3/TeO_2 THIN FILMS.

The optical transmittance as a function of wavelength for WO_3/TeO_2 films of various compositions is shown in figure(8.6). Two knees are observed in the high absorption region for 61%WO_3/39%TeO_2 and 56%WO_3/44%TeO_2 samples. We have plotted this region in figure(8.7) in accordance with the Davis and Mott(1970) equation for the non-direct optical transitions. However, two linear regions in each curve are observed for the samples with 61% and 56% of WO_3 content. Each of them has two intercepts with the $\hbar\omega$ axis for the same sample. Therefore, this would suggest that these samples are inhomogeneous and thus Davis and Mott equation for the non-direct optical transitions

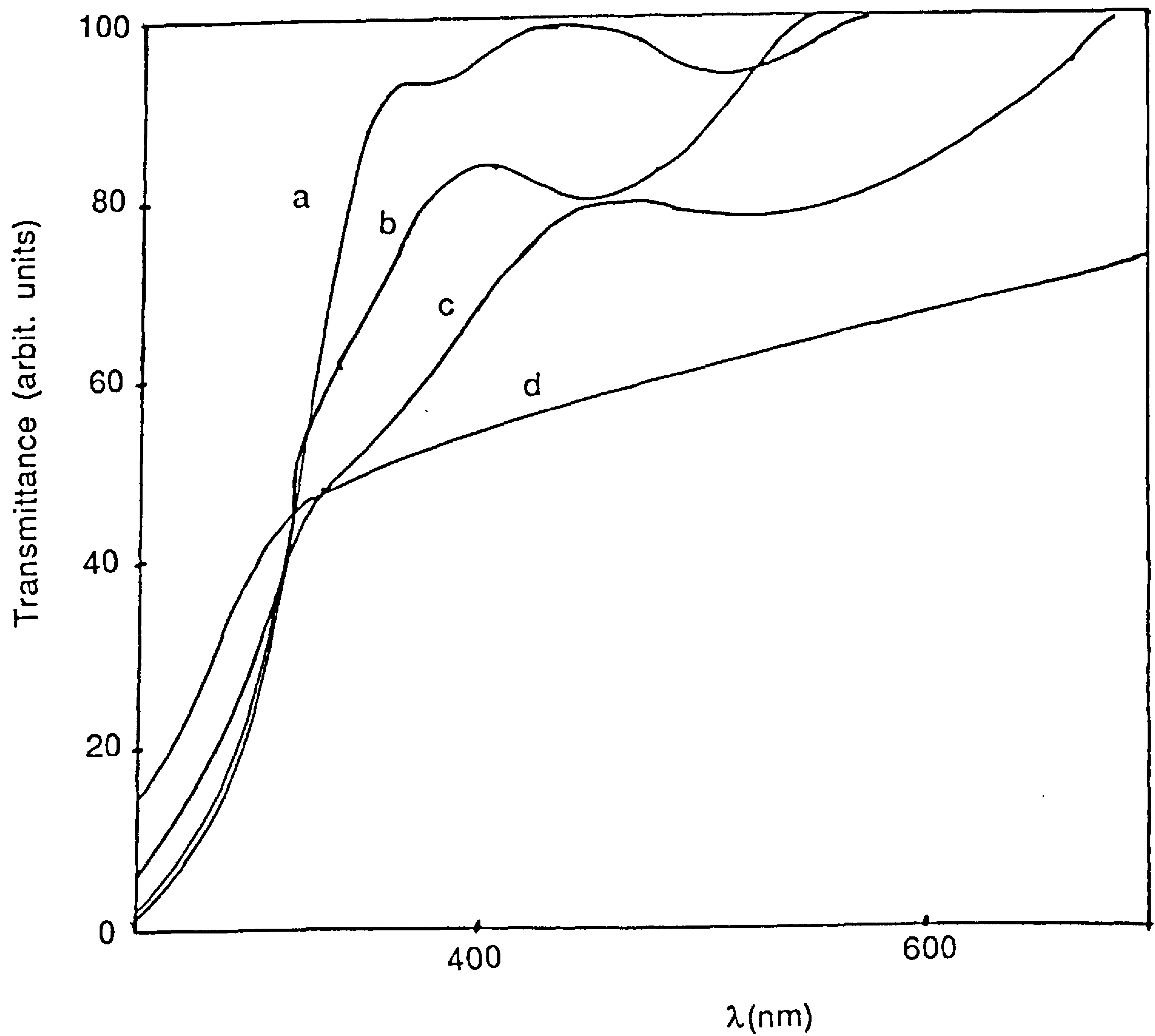

Fig. 8.6. Optical transmittance versus wavelength for different compositions of WO_3/TeO_2 thin films.

a) 100%WO3 (294nm thick)

b) 61%-- (245%nm thick)

c) 56%--(247nm thick)

d) 100%TeO2 (108nm thick)

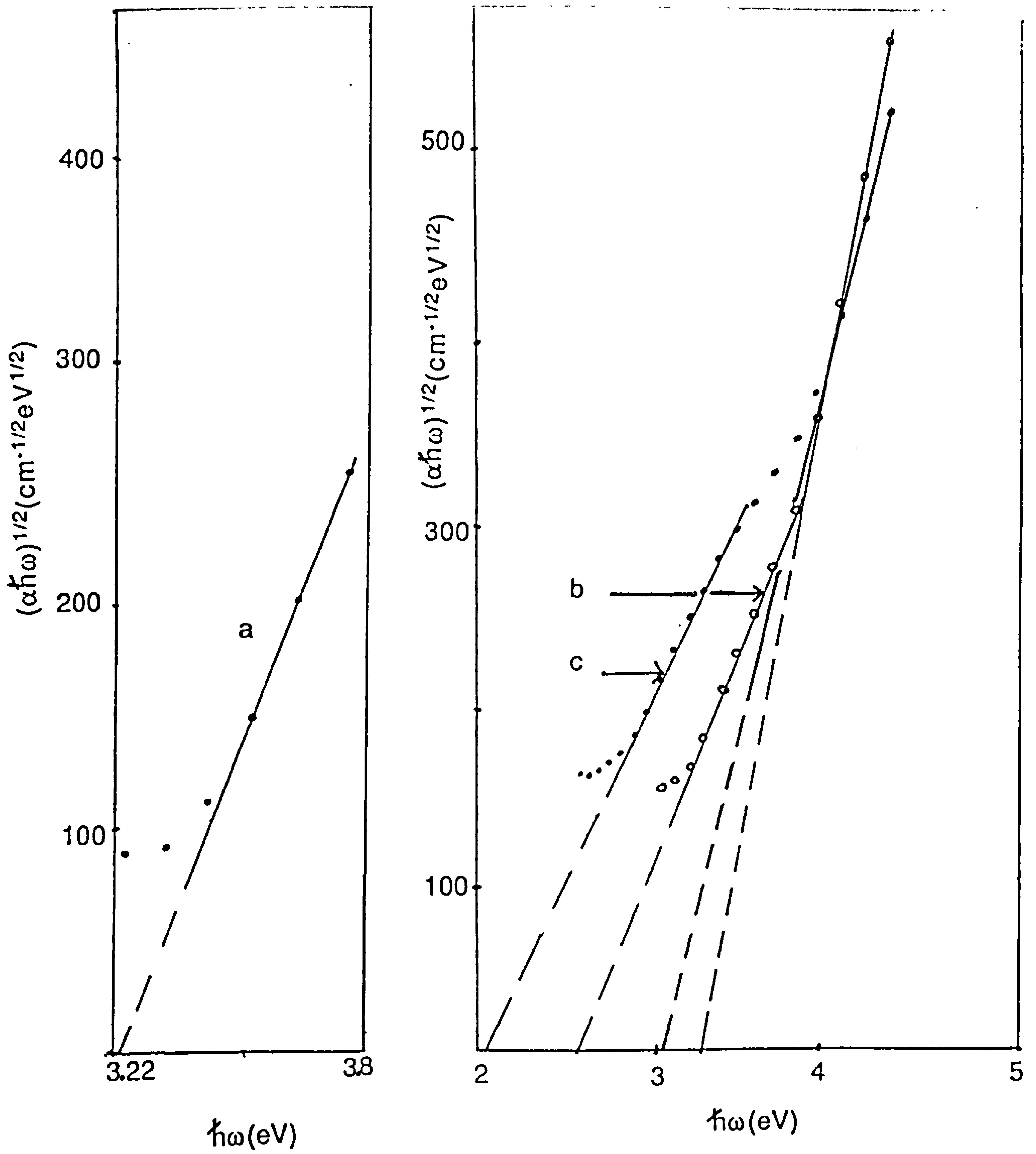

Fig. 8.7. $(\alpha\hbar\omega)^{1/2}$ as function of photon energy for the same samples as in figure (8.6).

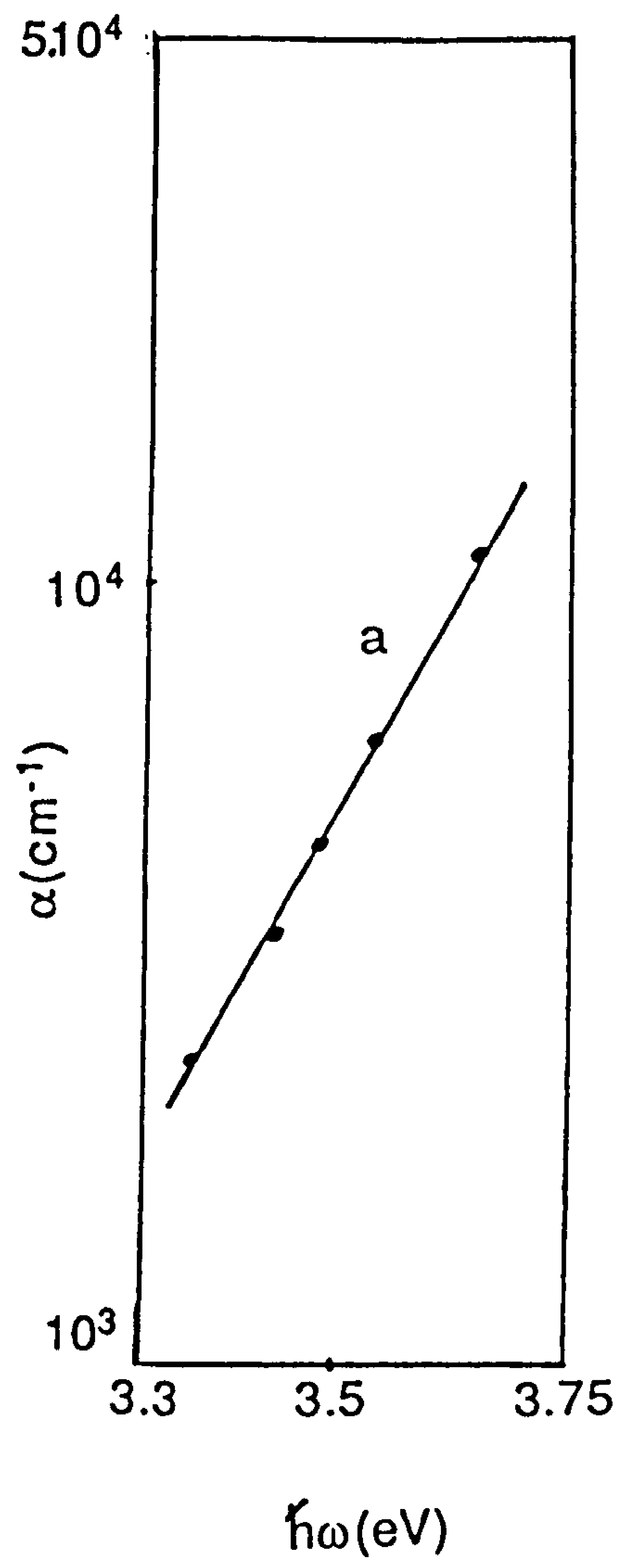

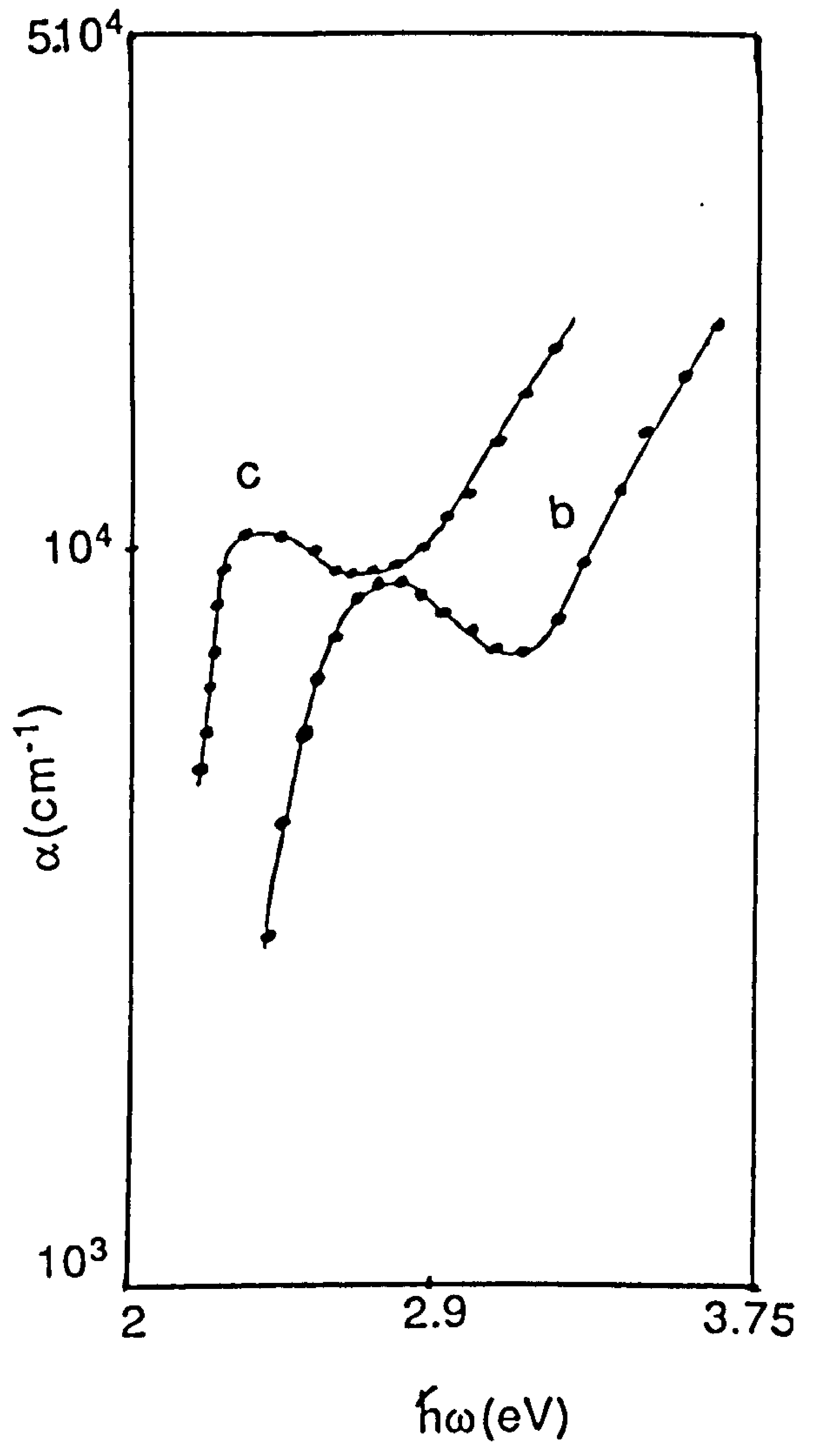

Fig. 8.8 log(α) versus ħω for the same samples as in figure (8.6).

cannot be applied. As a result of inhomogeneities we would not expect the average of the magnitudes of the internal fields which are random due to the structural disorder to give a constant uniform field. Thus the exponential tail which is derived from uniform fields [Dow and Redfield(1972)] can not be obtained, that is the pronounced peak and the sharpness of the exciton line may be observed in the curve of log(α) versus photon energy. In fact this is well illustrated in figure(8.8) which is in good agreement with the arguments above. Many experimental results have been obtained for exponential broadening of absorption edges [Olley(1973) and Alfromowitz and Redfield(1968)]. We believe that these experiments do not affect the homogeneity of the material according to the present arguments. Moreover, we think that the effect of inhomogeneities on the optical absorption edge may be important in a mixed structure of two oxides one with very high optical transmittance such as WO_3 [Fig(8.6a)] and the other with very low transmittance such as TeO_2 [Fig(8.6d)].

8-3. ELECTRON MICROSCOPE STUDY OF WO_3/TeO_2 THIN FILMS.

Thin films of WO_3/TeO_2 have been deposited on carbon-coated mica substrates held at room temperature and were studied in the transmission electron microscope. The electron micrographs and diffraction patterns were obtained at room and high temperatures. Figure(8.9) shows the electron micrograph and

diffraction pattern at room temperature for a WO_3/TeO_2 thin film. The diffraction pattern shows broad haloes suggesting that the film is amophous. The electron micrograph shows some kind of defects or inhomogeneities which disappear as the temperature is raised. The diffraction pattern at high temperature is shown in figure (8.10). It may be seen that the rings are slightly more pronounced than those shown in figure (8.9). This suggests that the structure of the film tends to become more ordered or more stable as the temperature is increased.

Micrograph

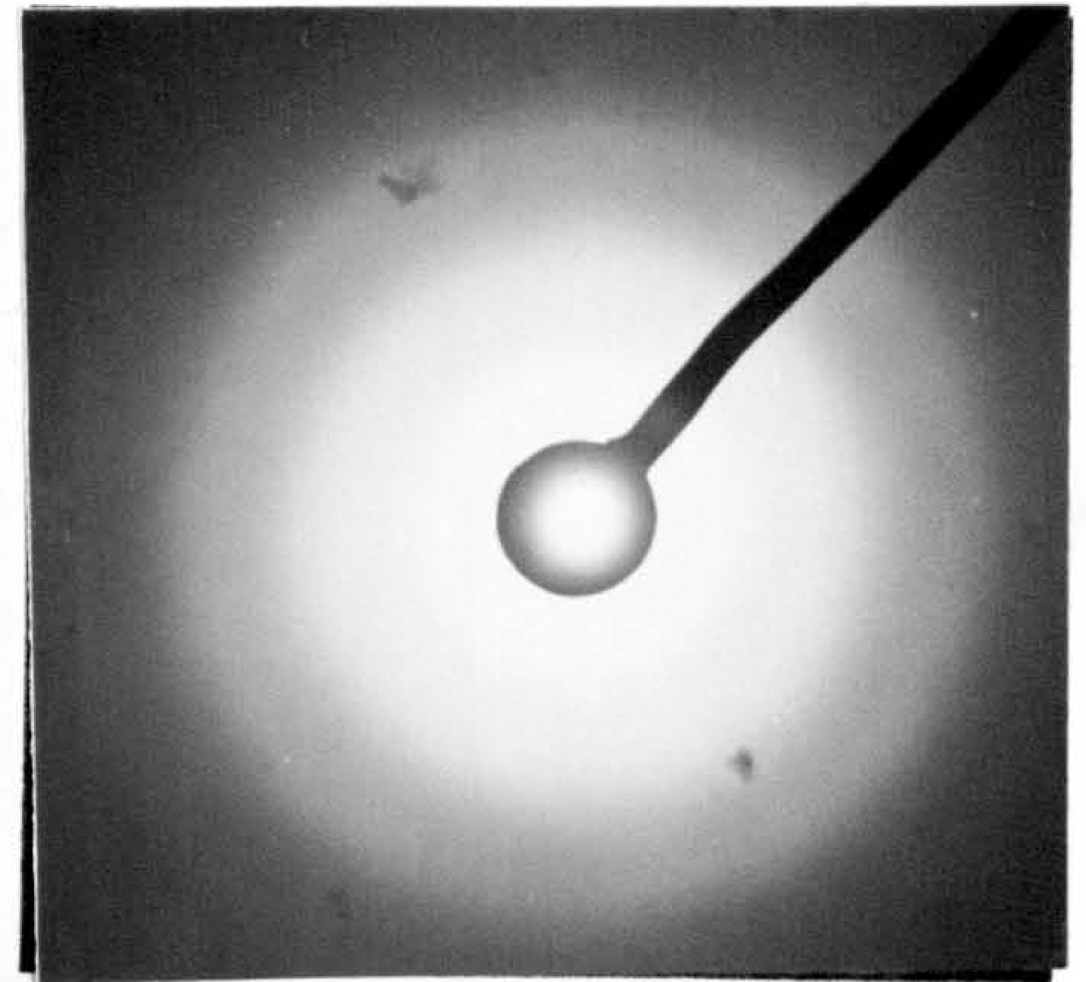

Diffraction pattern

Fig. 8.9. Electron micrograph and diffraction patterns of WO_3/TeO_2 thin film at room temperature.

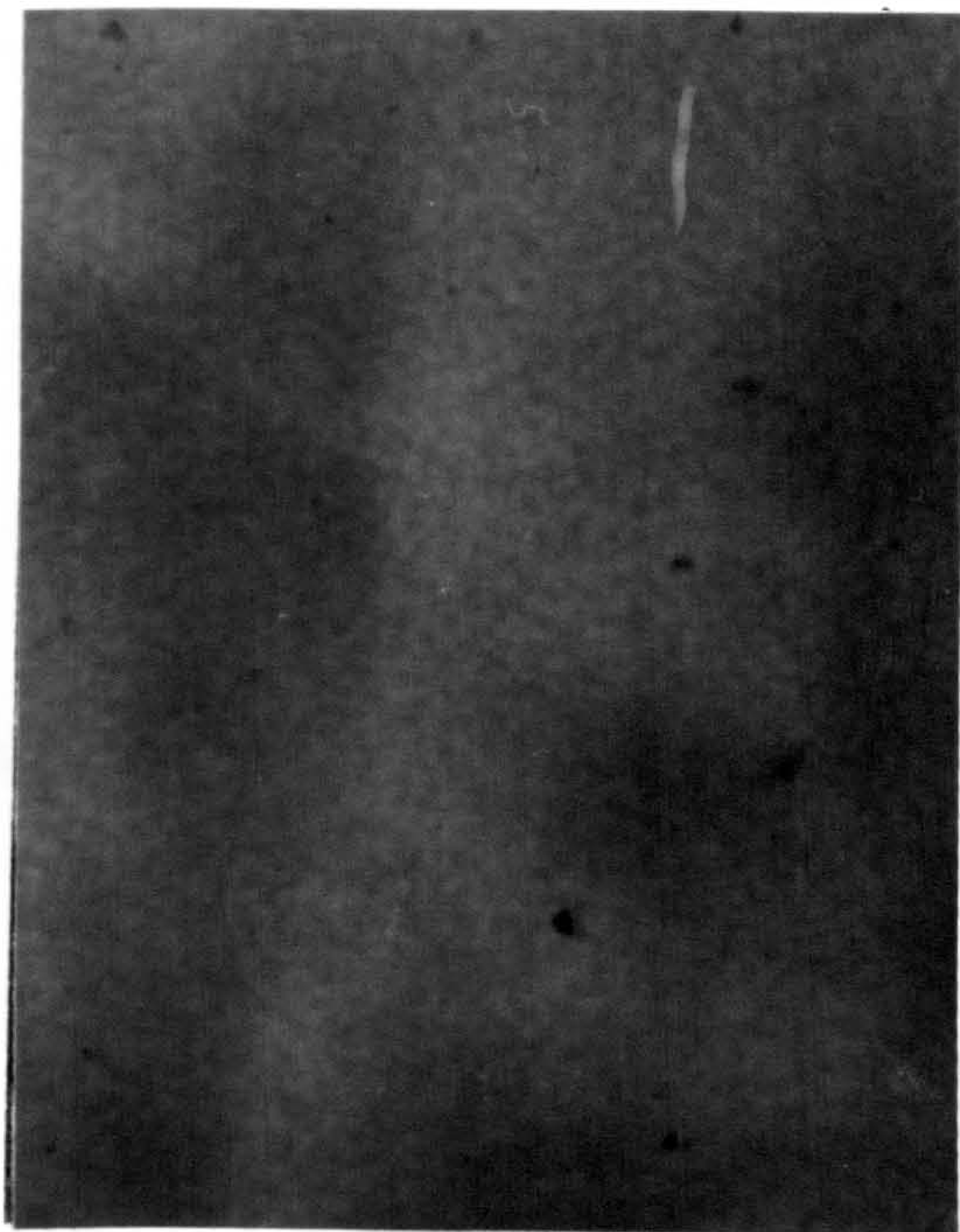

Micrograph

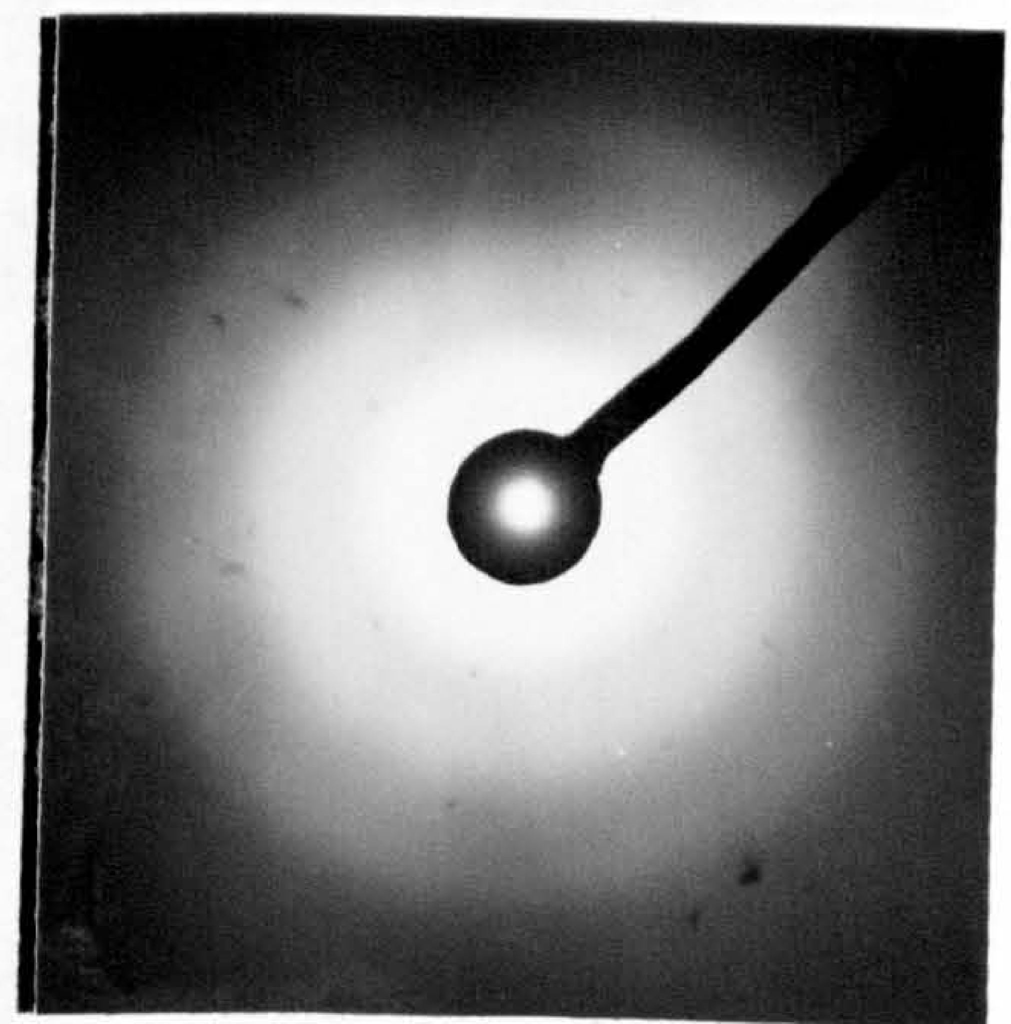

Diffraction pattern

Fig. 8.10. Electron micrograph and diffraction patterns of WO_3/TeO_2 thin film after annealing

CHAPTER 9 SUMMARY AND CONCLUSION .

In Chapter 5 we have discussed the electrical and optical properties of V_2O_5/TeO_2 co-evaporated thin films. The electron microscope diffraction patterns show that these films prepared by co-evaporation are amorphous.

TeO_2 is one of oxide glass formers which have strong ionic bonds and are usually good insulators. A transition from an insulating to a semiconducting state can be made by the addition of transition metal ions in different valence states (V^{4+},V^{5+}).

We have suggested that at low temperatures, in films where the concentration of V_2O_5 is very low the conduction is of the Miller and Abrahams type, that is the total activation energy may consist only of one term which is due to the disorder. If the concentration of V_2O_5 is high enough for the non-adiabatic regime to be effective, the conduction has been discussed in terms of polarons and thus the total activation energy should contain the hopping energy of the polaron.

We have suggested that in the voltage range 0.2-2V which may be considered as an intermediate range between low and high fields, three types of conduction are possible and they are either due to (a) Schottky or (b) Poole-Frenkel effects or (c) most probably due to impurities that are embedded in the material.

The relation $\sigma \propto \omega^{s}$ where $0.5<s<1$, has been found in V_2O_5/TeO_2 thin films and it has been suggested that it is due to hopping conduction between localized states.

The curves of the optical transmittance for V_2O_5/TeO_2 thin films show that they are more absorbing than SiO/TeO_2, WO_3/CeO_2 and WO_3/TeO_2 thin films and thus an absorption coefficient less than $10^3 cm^{-1}$ is impossible to obtain in V_2O_5/TeO_2 thin films of thickness less than, say 300nm. Therefore the exponential tail is not as deep as it is usually in amorphous semiconductors.

We have found that in the high absorption region the absorption coefficient of V_2O_5/TeO_2 thin films fits the condition for the direct forbidden transitions. The reason for that is that the site symmetry of the vanadium ions during the transition from crystalline to amorphous states is conserved.

In Chapter 6 we have discussed the electrical and optical properties of WO_3/CeO_2 thin films. Their electron diffraction patterns are very similar to those of V_2O_5/TeO_2 but their amorphous structure is more stable than that of V_2O_5/TeO_2.

In films where the concentration of WO_3 is very high the d.c current is not steady because of the polarization effects in the specimen. As the content of CeO_2 is increased the current becomes more steady and d.c measurements were possible. In this case ohmic behaviour has been observed at low fields and non-ohmic behaviour at high fields.

The capacitance of WO_3/CeO_2 shows very different behaviour from that of V_2O_5/TeO_2, WO_3/TeO_2 and SiO/TeO_2 thin films. We have suggested that in films where the content of WO_3 is high,

the a.c properties are those of the sample. However, as the content of CeO_2 is increased a phenomenon such as that described by Street *et al* (1970) due to the lead resistance and capacitance could cause the square law frequency dependence of the conductivity.

The optical transmittance of WO_3/CeO_2 thin films is very similar to that of crystalline materials. In the high absorption region we have found that the optical absorption coefficient fits the well known relation of the non-direct optical transition [Davis and Mott(1970)]. The optical energy gap shifts systematically towards lower energies as the content of CeO_2 is increased up to a certain amount, then starts shifting back to higher energies as the content of CeO_2 is farther increased. We have described this behaviour of the optical energy gap in a similar way as for doped crystalline semiconductors by making an analogy between localized states in the amorphous structure and the impurity states in crystalline semiconductor.

The values of the constant B given by equation (6.8) of the non-direct transitions are in good agreement with those found by Davis and Mott (1970).

In Chapter 7 we have studied the electrical and optical properties of SiO/TeO_2 dielectric thin films. Their structures shown by electron diffraction patterns indicate that these films prepared by thermal co-evaporation are amorphous. However this structure is not as stable as that of WO_3/CeO_2 thin films.

The capacitance of SiO/TeO_2 dielectric thin films at low frequencies and high temperatures increases with increasing frequency but by very much less than that of V_2O_5/TeO_2, WO_3/CeO_2 and WO_3/TeO_2 thin films. This is in good agreement with Mead(1962) who first pointed out that electrical properties of dielectrics such as SiO/TeO_2 of sufficient thicknesses are not influenced by the electrodes. This could also mean that the ionic bonds of the dielectric are very strong and thus the ions could not migrate towards the electrodes. Therefore the increase of the capacitance at low frequencies is not as large as in the case of transition metal oxides such as V_2O_5 and WO_3.

The ω^s-law has been found in SiO/TeO_2 thin films with the index s varying in the range 0.5 to 2. The mechanism of conduction at low frequencies with s in the range 0.5 to 1 is attributed to hopping of carriers between localized states. At high frequencies the square law frequency dependence of the conductivity has been observed and the mechanism of conduction is also attributed to hopping but confined only to immediate neighbouring sites. This hopping conduction may be described by the Elliott(1977) model which states that hopping is over the potential barrier not tunnelling through it.

Ohmic conduction has been observed at low fields and at slightly higher fields a mechanism of conduction due to Schottky or space-charge effects is ruled out according to Mead(1962). Instead it could be due to either Poole-Frenkel effect or impurities [Hill(1967)]. In fact Table(7.1) shows that even the

Poole-Frenkel effect may be ruled out in the voltage range 0.2-2V The optical absorption edge of SiO/TeO_2 in the low absorption region is sharp and as a result we have suggested that the localized states could not be responsible for the exponential tail, instead we have chosen the Dow and Redfield (1970) interpretation for the Urbach rule.

The addition of TeO_2 content clearly shows that the optical energy gap tends to higher energies. However we have observed that there is no systematic change as in the case of WO_3/CeO_2 and we have attributed this to the change of the optical energy gap of SiO from 2.25eV to 2.73eV at rapid and slow evaporations respectively [Al-Ani *et al* (1984)].

In Chapter 8 we have studied the a.c electrical and optical properties of WO_3/TeO_2 thin films. Their electron diffraction pattern shows that these are amorphous. We have shown that at low temperatures the capacitance is proportional to the dielectric loss. This leads to a.c conductivity and capacitance equations of the forms similar to those found by Springett(1974) in TiO_{2-x}/P_2O_5 glasses. Therefore, we have used the Springett as well as the Elliott(1977) models to describe the mechanism of conduction in WO_3/TeO_2 thin films at low temperatures.

The optical absorption edge of WO_3/TeO_2 thin films is clearly influenced by the effects of heterogeneities. As a result, the Davis and Mott (1970) as well as the Tauc *et al* (1966) equations for the non-direct optical transitions and the Urbach rules are not

obeyed in samples which are not homogeneous. As a consequence, in order to obtain an exponential tail with no exciton absorption peak, we have suggested that in addition to the structural disorder the material should be homogeneous or at least not affected by the inhomogeneities.

REFERENCES

-Al-Ani, S. K. J., Ph.D Thesis (1984). Brunel University, Uxbridge

-Al-Ani, S. K. J., and Hogarth, C. A., J. Materials Science., 20, 1185, (1985).

-Al-Ani, S. K. J., Arshak, K. I., and Hogarth, C. A., J. Materials Science., 19, 1737, (1984).

-Alfromowitz. M. A., and Redfield, D., Proc. 9th Int. Conf. on the Physics of Semiconductors, Moscow, p.98, Nauka, Leningrad, (1968).

-Anderson, P. W., Phys. Rev., 109, 1492, (1958).

-Anderson, G. W., and Compton, W. D., J. Chem. Phys., 52, 6166, (1970).

-Anderson, J. C., "The Use of Thin Films in Physical Investigations", (Academic Press, London), (1966).

-Andriesh, A. M., and Kolomiets, B. T., Fiz. Tverd. Tela., 5, 1461, (1963). [Translation: Soviet Phys. Solid State., 5, 1063, (1963)]

-Argall, F., and Jonscher, A. K., Thin Solid Films., 2, 185, (1968).

-Arshak, K. I., and Hogarth, C. A., Thin Solid films., 137, 281, (1986).

-Austin, I. G., and Mott, N. F., Adv. Phys., 18, 41, (1969).

-Bardeen, J., Blatt, F. J., and Hall, L. H., " In Photoconductivity Conference., Ed. By Beckenridge, R. G., Russell, B. R., and Hahn, E.E., (wiley, New York), p. 146, (1956).

-Bidadi, H., and Hogarth, C. A., Thin Solid Films., 27, 319, (1975).

-Bodo', Z., and Hevesi, I., Phys. Status Solid., 20, K45, (1967).

-Cohen, M. H., Fritzsche, H., and Ovshinsky, S. R., Phys. Rev. Letters., 22, 1065, (1969).

-Coutts, T. J., "Active and Passive Thin Film Devices", (Academic Press, London), (1978).

-Crowder, B. L., and Sienko, M. J., J. Chem. Phys., 38, 1576, (1963).

-Cutler, M., and Mott, N. F., Phys. Rev. 181, 1336, (1969).

-Davis, E. A., and Mott, N. F., Phil. Mag., 22, 903, (1970).

-Davydov, A. S., Phys. Stat. Sol., 27, 51, (1968).

-Deb, S. K., and Chopoorian, J. A., J. Appl. Phys., 37, 4818, (1966).

-Deb, S. K., Phil. Mag., 27, 801, (1973).

-Denton, E. P., Rawson, H., and Stanworth, J. E., Nature., 173, 1030, (1954)

-Dexter, D L., Phys. Rev. Lett., 19, 1383, (1967)

-Dhawan, V. K., Mansingh, A., and Sayer, M., J. Non-cryst. Solids., 51, 87, (1982).

-Donovan, T. M., Spicer, W. E., and Bennett, J. M., Phys. Rev. Lett., 22, 1058, (1969).

-Dow, J. D., and Redfield, D., Phys. Rev., 1B, 3358, (1970).

-Dupuy, C. H. S., and Cachard, A., "Physics of Nonmetallic Thin Films", (Plenum Press. N. Y.), (1976).

-Elliott, S. R., Phil. Mag., 36, 1291, (1977).

-Elliott, S. R., Phil. Mag., 37B, 553, (1978).

-Emin, D., and Holstein, T., Ann. Phys., 53, 439, (1969).

-Fagen, E. A., and Fritzsche, H., J. Non-cryst. Solids., 2, 170, (1970a).

-Fagen, E. A., and Fritzsche, H., J. Non-cryst. Solids., 4, 180, (1970b).

-Fischer, J. E., and Donovan, T.M, J. Non-cryst. Solids, 202, 8110 (1972).

-Flynn, B. W., and Owen, A. E., J. Phys. Colloq (France), 42, c4, pt.2, p.1005-8, (Oct.1981).

-France, P. W., and Hooper, H. O., Bull. Am. Phys. Soc., 13, 90, (1968).

-Frenkel, J., Phys. Rev., 54, 647, (1938).

-Frerichs, R., J. Opt. Soc. Am., 43, 1153, (1953).

-Hartke, J. L., Phys. Rev., 125 1177, (1962).

-Hill, R. M., Thin Solid Films., 1, 39, (1967-68).

-Hirsch, P. B., Howie, A., Nicholson, R. B., Pashley, D. W., and Whelan, M. J., "Electron Microscopy of Thin Crystals" (Butterworths London), (1965).

-Hogarth, C. A., and Ilyas, M., J. Mater. Sci. Letters., 2, 535, (1983).

-Holstein, T., Ann. Phys. (N.Y), 8, 343, (1959).

-Hung, C. S., and Gliessman, J. R., Phys. Rev., 79, 726, (1950).

-Hung, C.S., Phys. Rev., 79, 727, (1950).

-Janakirama-RaO, BH. V., J. Am. Ceram. Soc., 49, 605, (1966).

-Jonscher, A. K., Thin Solid Films., 1, 213, (1967).

-Killias, H. R., Phys. Letter., 20, 5, (1966).

-Kolomiets, B. T., Phys. Status Solidi., 7, 359, 713, (1964).

-Kolomiets, B. T., Manontova, T. N., and Negreskul., Phys. Status. Solidi., 27, K15, (1968).

-Landsberger, F. R., and Bray, P. J., Bull. Am. Phys. Soc., 14, 30, (1969).

-Lanyon, H. P. D., Phys. Rev., 130, 134, (1963).

-Lamb, D, R., "Electrical conduction mechanisms in thin insulating films.", (1967).

-Lampert, M, A., Rep. Prog. Phys., 27, 329, (1964).

-Linsley, G. s., Owen, A. E., and Hayatee, F. M., J. Non-cryst.Solids, 4, 208, (1970).

-Mackenzie, J. D., "Modern Aspects of the Vitrous State., Vol.3, (Butterorth, Washington), p.126, (1964).

-Mansingh, A., Sayer, M., and Webb, J. B., J. Non-cryst. Solids., 28, 123, (1978).

-Marshall, J. M., and Owen, A.E., Phil. Mag., 24, 1281, (1971).

-Mead, G. A., Phys. Rev., 128, 2088, (1962).

-Miller, A., and Abrahams, E., Phys. Rev., 120, 745, (1960).

-Morey, C. W., "The Properties of Glass, 2nd ed. p. 28. Reinhold Publ. Co. New York. (1954).

-Mott, N. F., and Gurney, R. W., "Electronic Processes in Ionic Crystals", Oxford Univ. Press, London, (1940).

-Mott, N. F., and Twose, W. D., Adv. Phys., 10, 107, (1961).

-Mott, N. F., and Gurney, R. N., "Electronic Processes in Ionic Crystals", (Dover, Inc, N. Y.), (1964).

-Mott, N. F., Adv. Phys., 16, 49, (1967).

-Mott, N. F., J. Non-cryst. Solids., 1, 1, (1968-69).

-Mott, N. F., Phil. Mag., 19, 835, (1969).

-Mott, N. F., J. Non-cryst. Solids., 22, 7, (1970).

-Mott, N. F., Phil. Mag., 26, 1015, (1972a).

-Mott, N. F., J. Non-Cryst. Solids., 8-10, 1, (1972b).

-Mott, N. F., Davis, E. A., and Street, R, A., Phil. Mag., 32, 961, (1975).

-Mott, N. F., and Davis, E. A., Electronic Processes in Non-Crystalline Materials, Clarendon, Oxford, (1979).7

-O'Dwyer, J. J., "The Theory of Electrical Conduction and Breakdown in Solid Dielecrtics", (Clarendon Press Oxford, (1973).

-Olley, J. A., Solid State Commun., 13, 1437, (1973).

-Owen, A. E., Glass Ind., p.632, p.695. (1967).

-Owen, A. E., and Robertson, J. M., J. Non-cryst. Solids., 2, 40, (1970).

-Pike, G. E., Phys. Rev., B6, 1572, (1972).

-Pollak, M., Phil. Mag., 23, 519, (1971).

-Pollak, M., Int. Conf. Phys. Semicond., Exeter, p.76, (1962).

-Pollak, M., and Geballe, T. H., Phys. Rev., 122A, 1742, (1961).

-Razzaq, M, Ph.D thesis Brunel University Uxbridge, England, (1988)

-Redfield, D., Phys. Rev., 140, A2056, (1965).

-Roberts, G. G., and Macginnity, T. M., Thin Solid Films., 68, 223, (1980).

-Rockstad, H. K., J. Non-cryst. Solids., 2, 192, (1970).

-Rose, A., Phys. Rev., 97, 1538, (1955).

-Swada, S., and Danielson, G. C., Phys. Rev., 113, 803, (1959).

-Sayer, M., and Lynch, G. F., J. Phys. C Solid State., 6, 3674, (1973).

-Schmid, A. P., J. Appl. Phys., 39, 3140, (1968).

-Schnakenberg, J., Phys. Status Solidi, 28, 623, (1968).

-Simmons, J. G., J. Phys. Chem.Solids., 32, 1987, and 2581, (1971).

-Spear, W. E., Proc. Phys. Soc., 70B, 669, (1957).

-Spear, W. E., Proc. Phys. Soc., 76, 826, (1960).

-Springett, B. E., J. Non-cryst. Solids., 15, 179, (1974).

-Street, R. A., Davis, G., and Yoffe, A. D., J. Non-cryst. Solids., 5, 276, (1971).

-Street, R. A., and Mott, N. F., Phys. Rev. Lett., 35, 1293, (1975).

-Tauc, J., Grigorovici, R., and Vancu, A., Phys. Stat. Sol., 15, 627, (1966)

-Urbach, F., Phys. Rev., 92, 1324, (1953).